Investigations on Neural Activity Source Identification and Connectivity of EEG data using Particle Filter

A Thesis

Submitted in partial fulfillment of the requirements

for the award of the degree of

DOCTOR OF PHILOSOPHY

by

SANTHOSH KUMAR VEERAMALLA

(Roll No: 715048)

Supervisor:

Dr. T.V.K. Hanumantha Rao
Associate Professor

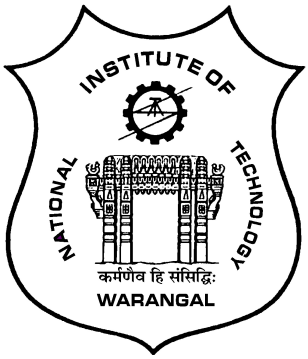

DEPARTMENT OF ELECTRONICS AND COMMUNICATION ENGINEERING
NATIONAL INSTITUTE OF TECHNOLOGY WARANGAL
TELANGANA STATE-506004, INDIA

2021

Dedicated to

My family

DECLARATION

This is to certify that the work presented in the thesis entitled " **Investigations on Neural Activity Source Identification and Connectivity of EEG data using Particle Filter**" is a bonafide work done by me under the supervision of **Dr. T.V.K. Hanumantha Rao**, Associate Professor, Department of Electronics and Communication Engineering, National Institute of Technology Warangal, India and was not submitted elsewhere for the award of any degree.

I declare that this written submission represents my ideas in my own words and where others' ideas or words have been included, I have adequately cited and referenced the original sources. I also declare that I have adhered to all principles of academic honesty and integrity and have not misrepresented or fabricated or falsified any idea / data / fact / source in my submission. I understand that any violation of the above will be a cause for disciplinary action by the Institute and can also evoke penal action from the sources which have thus not been properly cited or from whom proper permission has not been taken when needed.

Santhosh Kumar Veeramalla

(Roll No: 715048)

Date: 16 December, 2020

DEPARTMENT OF ELECTRONICS AND COMMUNICATION ENGINEERING

NATIONAL INSTITUTE OF TECHNOLOGY WARANGAL

TELANGANA STATE-506004, INDIA

CERTIFICATE

This is to certify that the thesis entitled " **Investigations on Neural Activity Source Identification and Connectivity of EEG data using Particle Filter**", which is being submitted by **Mr. Santhosh Kumar Veeramalla (Roll No: 715048)**, in partial fulfillment for the award of the degree of Doctor of Philosophy to the Department of Electronics and Communication Engineering of National Institute of Technology Warangal, is a record of bonafide research work carried out by him under my supervision and has not been submitted elsewhere for any degree.

Dr. T.V.K. Hanumantha Rao
(Supervisor)
Associate Professor
Department of E.C.E.
N.I.T. Warangal
Warangal - 506004, India

ACKNOWLEDGEMENTS

Firstly, I would like to express my sincere gratitude to my supervisor Dr. T.V.K. Hanumantha Rao for the continuous support of my Ph.D study and related research, for his patience, motivation, and guidance. My sincere thanks to him for providing me an opportunity to join the institute as a Ph.D research scholar and giving me access to the research facilities. I find words inadequate to thank him for enabling me to complete this work in spite of all obstacles. The thesis would not have seen the light of the day without his insistent support and cooperation.

I am also grateful to Prof. L. Anjaneyulu, Head of the department, Department of Electronics and Communication Engineering, NIT Warangal for his valuable suggestions and support that he shared during my research tenure.

Besides my supervisor, I take this privilege to thank Doctoral Scrutiny Committee members, Prof. C.B. Rama Rao, Professor, Department of Electronics and Communication Engineering, Prof. L. Anjaneyulu, Professor, Department of Electronics and Communication Engineering, and Dr. P. Muthu, Associate Professor, Department of Mathematics, NIT Warangal for their continuous support, suggestions and advice's during my research period whenever required.

I would like to thank Dr. K. Aditya, Assistant Professor, Department of Physiology, Apollo Institutes of Medical Sciences & Research, Hyderabad, for his feedback, cooperation during the review of results and helped me to get results of better quality.

It is my pleasure to show my indebtedness to my co-scholars at NIT for their help during the course of this work. I find no words inadequate to express any form of acknowledgment to my family members for their love, support and patience for making my dream come true.

Finally, I thank God, for filling me every day with new hopes, strength, purpose and faith.

ABSTRACT

In human brain mapping, connectivity is one of the main concerns. Connectivity enables connections through the nervous system across different brain regions. Based on the interactive time series, the causal connectivity between scalp sensors has been studied until now. The result acquired through the application of causal connectivity between the sensor time-series measurements does not permit an interpretation of interacting brain sources. Sensors are placed outside the head in electroencephalography (EEG) recording, and the volume conduction problem arises. This means that each sensor collects a linear superposition of signals from across the brain instead of measuring activity at only one brain site. This superposition of signals creates immediate associations in the data and can detect improper connectivity. It is because the locations of the channel cannot be seen as a physiological location of sources. This thesis proposes an analysis methodology that partially overcomes this limitation.

Source localization is essential for the visualization, surveillance, and comprehension of brain activity. Electromagnetic signals are generated by groups of firing neurons at the scalp surface detected in the cerebral cortex by electroencephalography (EEG). EEG thus represents the strength as well as the location of the brain activated areas.Several issues complicate the localization of neural sources from measured fields based on the solution of an inverse problem. The problem is ill-posed: there are an infinite number of current distributions which also describe a given measurement. The main focus of this thesis is on finding the source of brain activity. Although specific methods demonstrate the flow of scalp sources, prior assumption in active brain regions is still necessary. Here is a new approach to describe the brain sources in their respective position, amplitudes based on particle filters. For this procedure, the current dipole is taken as the hidden state, and the EEG records as the observation state for a state-space model. Then, by using the particle filter, estimate the unknown state i.e., location of the sources.

To alleviate particle degeneracy of the particle filter, some improvements have been suggested by developing resampling techniques in particle filters for EEG applications. In this thesis, a new approach based on partial stratified resampling (PSR), branching, and minimum sampling variance (MSV) resampling methods in the particle filter for localization of the neural source of EEG data is proposed.

The connectivity methods used to assess statistically significant functional relationships between the temporal dynamics of sources. EEG source space connectivity can be used to identify the connectivity among the brain sources. EEG localization techniques and connectivity methods have been developed considerably over the past decades separately. In this thesis, we

propose a framework which combines both localization and conectivity methods. The particle filter was applied to extract the sources and their amplitudes. Multivariate (MVAR) model is applied to the time courses of estimated sources, and by using the Granger causality techniques to obtain the connectivity measures of the given data.

The objective and scope are clear: automatic and reliable localization and connectivity of the sources could be practical in several fields, including clinical applications (pre-surgical evaluation, focal epilepsy), brain-computer interfaces, and analysis of large datasets.

Contents

List of Figures

List of Tables

List of Abbreviations

3D	Three Dimensional
2D	Two Dimensional
BCI	Brain Computer Interface
BEM	Boundary Element Method
FEM	Finite Element Method
EEG	Electroencephalogram
MEG	Magnetoencephalogram
MRI	Magnetic Resonance Imaging
fMRI	functional Magnetic Resonance Imaging
CNS	Central Nervous System
PNS	Peripheral Nervous System
AP	Action Potential
EPSP	Excitatory postsynaptic potential
IPSP	Inhibitory Postsynaptic Potential
EMG	Electromyography
EOG	Electrooculography
GCI	Granger Causal Index
DTF	Directed Transfer function
PDC	Partial Directed Coherence
MVAR	Multivariate Autoregressive
PF	Particle Filter
PSR	Partial Stratified Resampling
MSV	Minimum sampling variance
SP	Signal Processing
PCA	Principal Component Analysis
BSS	Blind Source Separation
ICA	Independent Component Analysis
MUSIC	MUltiple Signal Classification
RAP-MUSIC	Recursively Applied and Projected MUSIC

dSPM	dynamical Statistical Parametric Mapping
MNE	Minimum Norm Estimation
sLORETA	Statistical low resolution electromagnetic tomography
KF	Kalman Filter
LLF	Local Linearization Filter
RBF	Radial Basis Functions
UKF	Unscented Kalman Filter
RBPF	Rao-Blackwellized Particle Filter
APF	Auxiliary Particle Filter
NuPF	Nudged Particle Filter
RSR	Residual Systematic Resampling
RMSE	Root Mean Square Error
RA	Relative Accuracy
MSE	Mean Square Error
DTI	Diffusion Tensor Imaging
MSC	Magnitude Squared Coherence
DCM	Dynamic Causal Modeling
GCM	Granger Causal Modeling
BESA	Brain Electrical Source Analysis
SEM	Structural Equation Modeling
ECG	Electrocardiogram
CT	Computer Tomography
ROI	Region of Intrest

Chapter 1

Introduction

1.1 Overview

The brain is a highly complex and interrelated network of billions of neurons. The neural activity starts from the early stages of prenatal development in the human brain. In this early stage and throughout life, electric signals produced by the brain believed to reflect not only the brain's activity but the state of the human body. We perceive the brain function as observers through the measurements or signals we get from it. Three methods can monitor functional and physiological changes within the brain neural activity with high temporal resolution: an electroencephalogram (EEG), a magnetoencephalogram (MEG), and a functional magnetic resonance imaging (fMRI), which have their advantages and drawbacks.

In this thesis, the EEG is taken as a signal acquisition measure. The EEG measures the time-evolving voltages caused by brain activity. To detect, diagnose, and treat brain disorders, it is vital to understand the neuronal functions and neurophysiological property of the brain and the mechanisms underlying the bio-signal generation and their recording. It means that sophisticated digital signal processing techniques will extend to electroencephalogram (EEG) signals obtained from the human brain. Electroencephalography allows physicians to observe and interpret the electrical fields of brain activity. The specialist tries to determine the existence and location of EEG patterns for each type of diagnosis and whether they represent normal or abnormal neuronal activity.

Hans Berger (1873–1941) was the discoverer of human EEG signals. In 1920 he started researching human EEGs [4]. In 1910, he began working with a string galvanometer, and after 1924 he switched to a smaller variant of Edelmann and a bigger Edelmann model. In 1926 Berger started using the Siemens double-coil galvanometer, which became more robust [5]. His first human EEG recording on picture paper was in 1929, lasting between one and three minutes.

In this recording, he only used a one-channel bipolar technique with the front-occipital leads. EEG recording became famous in 1924. The first Berger analysis was the alpha rhythm. He then reported the impact of hypoxia on the human brain and the presence of several diffused and localized disorders in the brain that proposes epilepsy discharges occur [6]. Berger also had a keen interest in the location of brain tumors and cerebral localization. He also discovered some relationship between mental behaviors and EEG signal variations.

EEG has been used in routine development of clinical, trial, and computational studies to determine, identify, diagnose, and treat a wide range of human brain and central-nervous-system (CNS) neurological and physiology disorders. EEGs are invasively and without interference collected using computers. A selection of signal processing tools, delicate and sensitive electrodes, and enough memory for long-term recordings of several hours are needed for the EEG machines.

1.2 Outline of nervous systems

The nervous system consists of nerve cells located between neurons, which absorb, interact, and process body information and send it away rapidly and accurately, internally, and externally. Two elements of the nervous system include the Central Nervous System (CNS) and the Peripheral Nervous System (PNS). CNS consists of the brain, the spinal cord, and PNS consists of sensory neurons and nerve cells that are linked together and often associated with the CNS. All systems are closely connected as the sensory input of CNS is provided from PNS, and the PNS communicates responses to the organ system.

A neuron is composed of a cell body (also known as soma), dendrites, and an axon. The neuron must now make a decision based on the information given by dendrites from other neurons, which will then be forwarded to the dendrite of another neuron across the axon [7]. Figure 1.1 shows the scheme of the neuron. Nerve cells respond to stimuli and transmit information at long distances. The majority of the metabolism of nerve cells, especially those related to protein synthesis, is comprised of a single nucleus in the nerve cell body. Neurons transfer electrical potential to other cells through thin fibers known as axons. An axon is a long wire bearing an electrical pulse that can last for a few meters. Dendrites are connected to other nerve axons or dendrites that receive pulses from other nerves or transmit signals from them to other nerves. In the human brain, each nerve is connected mainly by dendritic connections to about 10,000 other nerves. The activities of CNS related to current between axons (synapses) and cell dendrites and the interactions between the dendrites. The synapse is a neural structure (or nerve

cell) allowing the transmission of an electric signal to another neuron. Such electrical signals referred to as Action Potentials (AP).

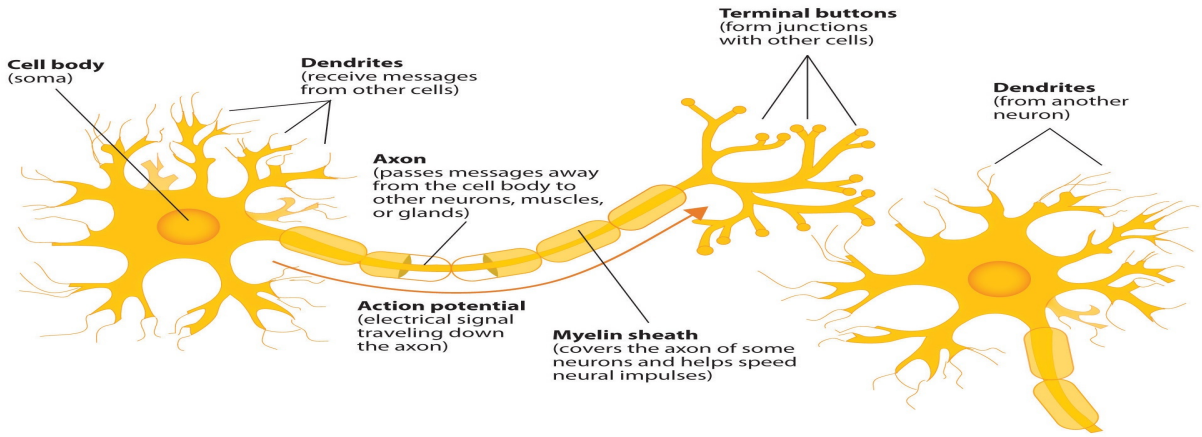

Figure 1.1: Scheme of the neuron

The cell membrane of the body may report a negative polarity of an AP of 60–70 mV. This potential varies with differences in the synaptic process. Within such sequences, the first cell to generate action potentials are the presynaptic cell, and the second cell that addresses the first cell in the synapse is called the postsynaptic cell. The presynaptic cells typically consist of neurons and generally are postsynaptic cells in other neurons, muscle cells, or gland cells. A synaptic signal cell may be suppressed, activated, or modulated. The corresponding neuron produces an excitatory postsynaptic potential (EPSP). When an event potential flows through the fiber resulting in an excitatory synapse. The fiber ends in an inhibitory synapse when hyperpolarization occurs, indicating the inhibitory postsynaptic potential (IPSP).

The membrane keeps charged sodium (Na+) and potassium (K+) ions from floating in and out of the cell body that has a resting potential of -70mV negatively charged to the outside [7]. Figure 1.2 shows the synaptic activities schematically,

1. The electrical current coming from the dendrites increases the membrane potential.
2. When this depolarization hits -55mV, the cell membrane is opened entirely up to Na+ ions, which now enter the cell, creating a potential positive called action potential.
3. The cell membrane also opens up temporarily delayed for K+ ions in the cell that now exit the cell, allowing the membrane's ability to be repolarization.

4. The potential for the cell membrane is temporarily reduced to -70mV because the cells are slower to lose their permeability concerning the K+ ions (hyperpolarization) before it stabilizes at the resting potential.

The axon transfers the AP to the other neurons. To initiate AP, a stimulus must be above a threshold. Very low stimuli cause local electrical perturbation but do not create an AP which is transmitted. When the stimulus strength reaches the limit, an action potential will arise and flow down the nervous. The neuron activates and transfers the information (AP) to subsequent neurons when the electric current accumulated from all input axons reaches one certain threshold. The action potential velocity is 1 to 100 m/s. AP's are activated by different stimulus types; sensory nerves respond to a variety of stimuli including chemical, light, electricity, strain, touch, and stretching. The nerves within the CNS, on the other hand, are mostly activated by chemical processes at synapses (brain and spinal cord).

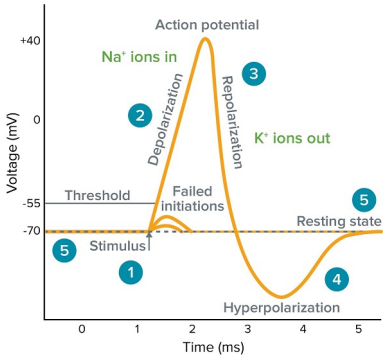

Figure 1.2: Action potential

1.2.1 Overview of EEG signals

Electroencephalography (EEG) is an electrophysiological monitoring tool for measuring brain electrical activity. The electrodes configured on the scalp usually are invasive, but sometimes invasive electrodes are used, as in electrocorticography. Clinically, EEG refers to the monitoring of spontaneous brain electrical activity in a period from several scalp electrodes [8].

The AP of a single neuron cannot be extracellularly measured since its amplitude is too low for the EEG to measure. The EEG signal is the measurement of currents flowing in dendrites of many pyramidal neurons of the cerebral cortex during synaptic excitation. When the brain cells (neurons) are activated, synaptic currents generated inside the dendrites. This current produces a magnetic field and secondary electric field; the magnetic field can be measured by electromyography machines (EMG) and a secondary electric field measured by EEG-systems

over the scalp. The electroencephalography describes the potential difference between two cortical positions over time [9].
For getting a good electric signal, the following conditions must be complied with:

- many neurons must fire synchronously.
- those neurons must be parallelly aligned, to summarize instead of canceling them [1] (see Figure 1.3)

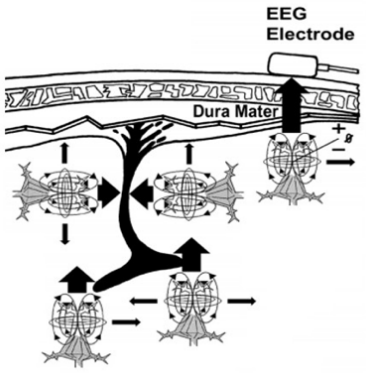

Figure 1.3: Cortical generators of electric currents. Thick arrows represent the propagation of electrical currents that can be picked up by the EEG electrode [1].

The combined postsynaptic potential of pyramid cells is responsible for the electric potential differences, which create electric dipoles between the soma (neuronal body) and the apical dendrites attached to the neurons shown in Figure 1.1. Currents in the brain are produced mostly through the neuronal membrane in the direction controlled by membrane potential through the positive ions of Na+, K+, Ca+, or the negative ion of chlorine, Cl- [10].

The human head consists of different layers, including the scalp, the skull, the brain, and several other thin layers. The skull attenuates the signals about 100 times more than the soft tissue. Also, most noise is produced either inside the brain (internal noise) or through the scalp. Only large populations of active neurons can thus provide sufficient potential for the scalp electrodes to be identified. Such signals are then substantially intensified for the monitoring of the EEG. When the central nervous system (CNS) is complete and functional at birth, about 10^{11} neurons are developed [11]. It generates 10^{14} neurons per cubic mm on average—nerve cells connected to neural networks through synapses. There are about 5×10^{14} synapses for adults. Overage, the number of synapses per neuron is growing while with age, there is a decrease in neurons.

The brain divided into three parts from an anatomical point of view: the cerebrum or cortex, cerebellum, and brain stem (Figure 1.4). Cerebrum contains areas for initiation of move-

ment conscious sensational perception, conceptual interpretation, and emotional and behavioral signals. The cerebellum (small brain) has two tightly folded hemispheres. The cerebellum helps regulate and manage voluntary muscle movements, posture, balance and preserves equilibrium. This collects feedback from spinal cord sensory systems and other brain areas and incorporates them into motor activity. The Brain Stem is the brain's lower and oldest portion, consisting of the midbrain, pons, and medulla. It regulates autonomous functions of the body, such as heartbeat, breathing, bladder function and sense of balance. The brain stem basically regulates everything you want to function automatically without having to think about it consciously [2].

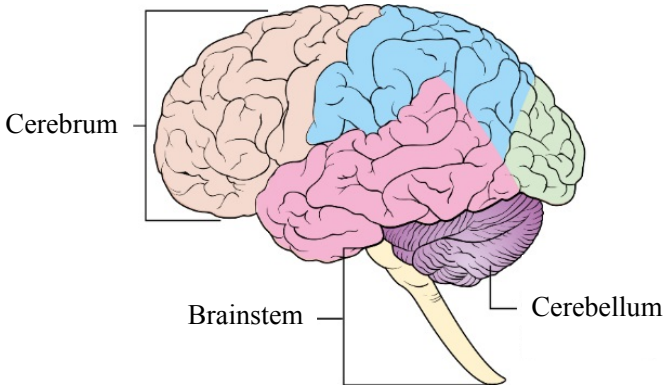

Figure 1.4: Diagrammatic representation of the brain [2].

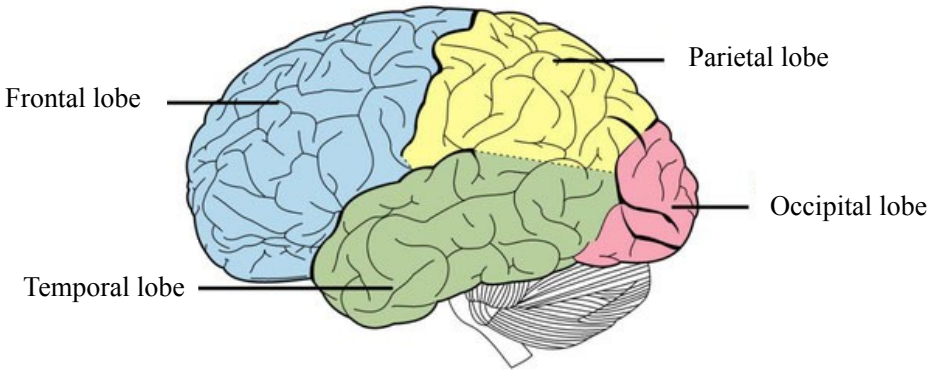

Figure 1.5: Cerebral cortex and its four lobes [2].

The cortex consists of two symmetric hemispheres, on the left and the right, separated by a deep longitudinal fissure. Every brain hemisphere categorized in lobes that are: the frontal lobe includes decision-making, problem-solving and timing; the temporal lobe involves perception, sensory language, and emotion; the parietal lobe engages in the processing and transmission of sensory information from the body, and occipital lobe involved in vision (Figure 1.5).

Table 1.1: EEG frequency bands

Frequency band	Range	Brain activity
Gamma	30 Hz	Conscious perception, cross-modal sensory processing
Beta	13-30 Hz	Active thinking, focus, high alert, anxious
Alpha	8-13 Hz	Relaxed, focused mind, closing the eyes
Theta	4-7 Hz	Normal sign of sleep, drowsiness, meditation
delta	up to 4 Hz	Deep and non dream sleep

1.2.2 Brain rhythms

EEG typically characterized by rhythmic activity. Rhythmic activity generally divided into frequency bands. Such frequency bands originate from a notion that rhythmic movement has a specific scalp distribution or biological significance within a certain frequency range (1.1). Spectral methods typically determine frequency ranges. These frequency ranges are classified as alpha, beta, theta, gamma, and delta [12] to represent most EEGs used in clinical practice. Figure 1.6 shows some of the EEG bands.

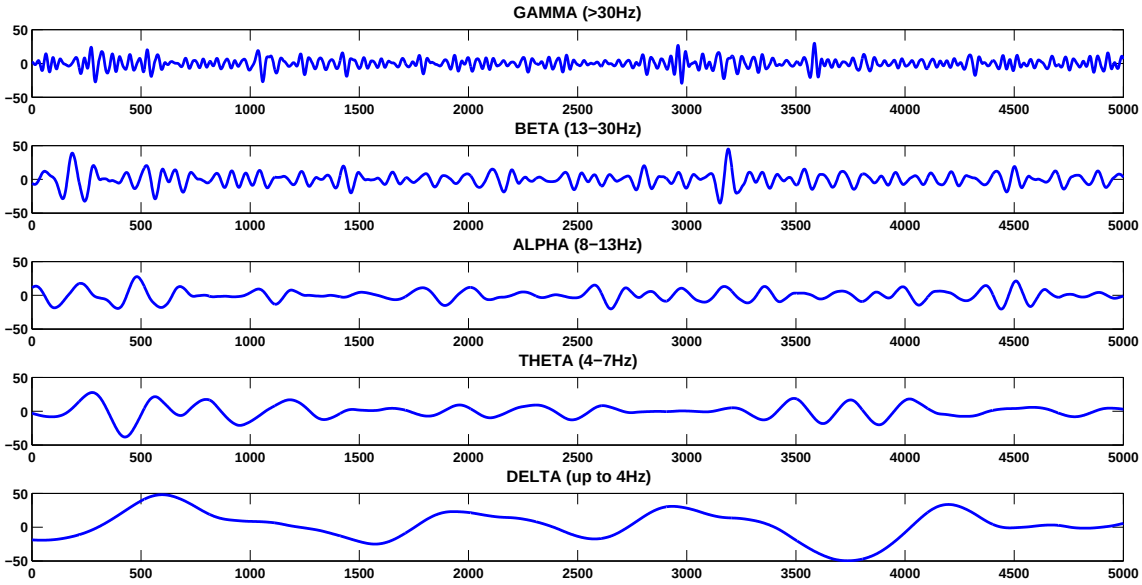

Figure 1.6: Some examples of EEG waves.

1.2.3 EEG bands

The Delta band has a frequency of up to 4 Hz. Such waves are associated mainly with deep sleep and can be present in the waking state. Artifact signals due to large muscles of the

neck and jaw can easily be confused with the true delta reaction. It is because the muscles are close to the skin surface and generate a strong signal, while the useful signal comes from deep inside the brain and severely attenuated throughout the skull. It is nevertheless easy to see when the response is caused by excessive movement by applying simple methods for the EEG signal analysis.

Theta is between 4 Hz and 7 Hz in the frequency range. The Theta band usually has seen In young children. It can be found in drowsiness or agitation in adults and can also see in meditation [13]. A theta wave also comes with other frequencies and tends to be related to the arousal level. It is called a focal disruption in superficial subcortical injuries; this can see in general distribution in diffuse or metabolic disorder or deep mid-line disturbances. In contrast, this spectrum has related to relaxed, meditative, and innovative reports [14].

The frequency for alpha waves is 8–13 Hz and typically shown as a circular or sinusoidal shaped signal. Alpha waves are found in the back of the head and usually located in the occipital brain region and in the posterior lobes of any brain region. They represent both a relaxed, focused mind. These waves are the most common pattern for brain activity.

An electric brain pulse that is between 14 and 30 Hz is a beta wave. A beta wave is the usual pattern of positive thought, close exposure to external problems, which found in healthy adults. A high-level beta wave can be obtained if a person is in panic. Rhythmic beta activity is observed primarily in frontal and central regions [8].

Gamma range is above 30 Hz frequencies and mostly up to 45 Hz. Gamma rhythms intended to connect various neural populations in a network to achieve a specific cognitive or motor function. While the amplitudes of these rhythms are very small and unusual, these rhythms can be used to confirm other brain disorders [15].

Several wave frequencies were much higher than the usual EEG activity range between 200 and 300 Hz. Such frequencies are found in animal brain structures but play no role in clinical neurophysiology. The majority of rhythms above could last for a few minutes, while others like gamma rhythm take just a few seconds.

1.2.4 Artifacts

Generally, an EEG activity study poses the question of the difference between real EEG activity and activity applied through several external factors. Such artifacts can affect the impact

of EEG recording. The artifacts come from many sources, including eye motion, heart, and muscle and power line interference. It is the EEG expert's primary responsibility to recognize, classify, and eventually remove the artifacts. The experienced neurophysiologist himself is unable to extract all artifacts from EEG data often. It is, however, always a significant objective for artifacts to be classified to ensure that they are not from the brain and should not be confused.

Usually, the artifacts divided into two groups, according to [16, 17] physiological and non-physiological. Physiological artifacts normally originate from sources inside the body that generate them and not necessarily from the brain, such as eye movement; electrocardiographic artifacts and electromyography, etc. Non-physiological artifacts come from many sources, including appliances (electrode artifacts) and digital devices (electronic materials, power lines, inductance, etc.).

Through rising technology and the creation and use of additional equipment in the clinic, new artifacts will arise. The appropriate filtering strategy for artifacts should remove the unnecessary amount of artifacts and, on the other hand, ensure that undetectable artifacts do not affect the resulting data. For situations where the EEG experts are relatively easy to detect the objects, visual inspections may be a good alternative.

1.2.5 Abnormal EEG

In certain subjects, some difference in EEG patterns suggests an abnormality. It can be caused by many factors, such as distortion and loss of regular patterns, increased irregular patterns, or the failure of all patterns. Most abnormal EEGs do not replace a typical EEG pattern entirely. They occur intermittently, only in some head regions, or in the normal background only. An EEG considered abnormal when it includes: (a) systematic disturbances of irregular slow waves that are usually related to delta and brain dysfunction, (b) bilateral EEG, sometimes associated with loss of consciousness, and (c) chronic Focal EEG, typically linked to focal cortical disorders.

The categories described are not easy to classify and should be applied to a variety of neurological diseases and other details. Precise analysis of irregular patterns leads to more clearly defined neurodegeneration disorders such as epilepsy, Parkinson's, Alzheimer's, sleep- and dementia diseases, or other processes, described in [18]. Nevertheless, recent studies have shown that there is a correlation between irregular EEG patterns, general brain pathology, and certain neurological illnesses [17].

1.2.6 EEG recording and measurement

Simple galvanometers reported the first electric neural activity. The light projected to the galvanometer on the wall replicated using a mirror to maximize the very slight variations of the pointer. In 1903, Einthoven invented the string galvanometer, an extremely delicate and precise measurement device. For many decades, it became a regular instrument for photographic recording. Recent EEG systems include several sensitive electrodes, a set of differential amplifiers (one for each channel) [2].

Spontaneous EEGs typically recorded using a standardized international 10-20 system. The scalp surface has 21 electrodes, as shown in Figure 1.7. Which are the following: reference points are a nasion at the top of the nose, and a skull base inion at the back of the head. The skull perimeters determined from these points in the transverse and median planes. The electrode positions are determined by dividing these outlines into 10% and 20% intervals. Instead of defined lengths, the use of percentages allows the relation between the electrodes and the corresponding regions of the brain to be maintained irrespective of the head size. The letters and numbers are associated to each location site. The frontal polar, frontal, central, parietal and occipital areas are indicated by Fp, F, C, P, and O. The right hemisphere represents even numbers, the left is with odd numbers and the midline is defined as "z".

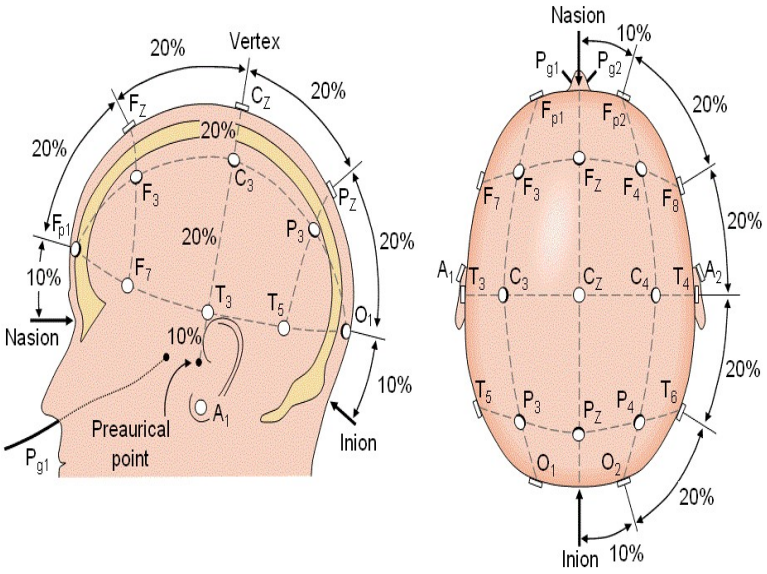

Figure 1.7: The international 10-20 system seen from left and above the head. A = Ear lobe, C = central, Pg = nasopharyngeal, P = parietal, F = frontal, Fp = frontal polar, O = occipital [3].

To use the conventional approach to set a more number of electrodes (more than 21 electrodes), the majority of the electrodes located at an equivalent distance between the electrodes,

respectively. For example, C1 is between C3 and Cz. Figure 1.8 indicates the larger scale for 81 electrodes (10-10 Electrode Placement system), including those based on the recommendations of the American EEG Society. With the use of 81 electrodes, the distances between interelectrodes are reduced to 10 percent, thus leading to a greater electrode density, which can in turn improve the source localization. For measuring EOG, ECG, and EMG of the underlying eye muscles, additional electrodes can be used. In addition to the international 10-20, 10-10 system, however, many other systems operate on the scalp [3, 19].

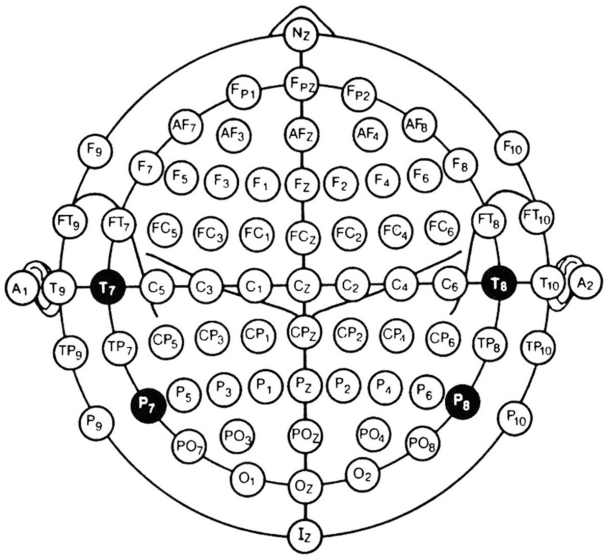

Figure 1.8: Electrodes in the 10-10 system of electrode placement, as standardized by the American Electroencephalographic Society [3].

EEG recordings are based on differential amplification principle with a rejection of noise in common mode. The EEG measurements dependent on the use of bipolar or unipolar electrodes Figure 1.9. The potential difference between electrodes pairs is measured in bipolar method. The potential of each electrode is comparable with the reference or average of all electrodes in a unipolar method [20].

1.3 Source localization

The brain divided into several parts, each producing a local magnetic field or electric synaptic current when active. The brain functions can see as a signal source either random or similar to natural brain activity, as a result of brain stimulation or as a result of physical movements.

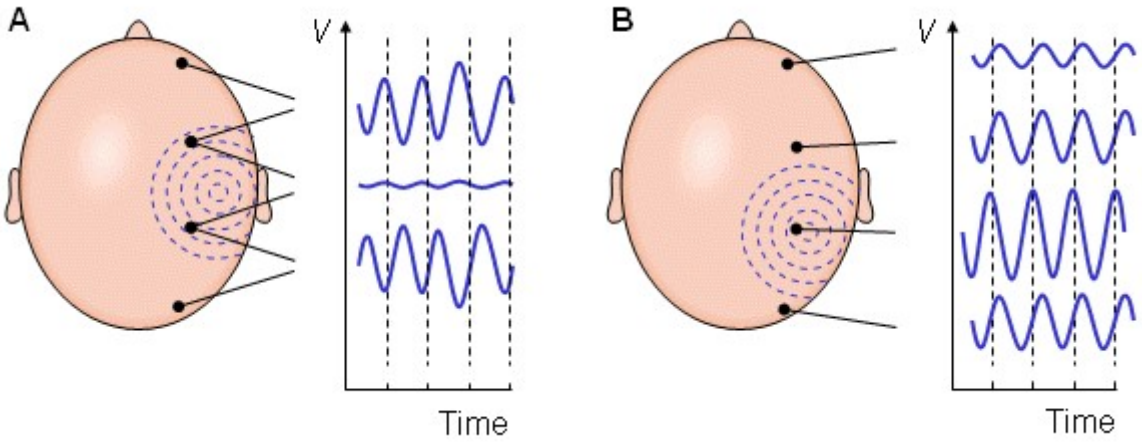

Figure 1.9: (A) Bipolar and (B) unipolar measurements.

EEG is a measurement of the large number of brain cell (neuron) potentials collected from scalp electrodes. While studying EEG, the focus always lies not with the potentials obtained on the scalp but with the possibility of the sources inside the brain. Direct measurements of the various regions in the brain allow electrodes to positioned inside the head, which implies surgery. It is undesirable, mainly because it causes pain and danger. A better solution would be if the desired signals from EEG collected on the scalp could be measured. Signals obtained are weighted cell potential quantities, where the weights depend on the signal path from the neurons to the electrodes.

Over the last two decades, identifying brain signal sources exclusively from EEGs has been an important field of study. This location of the source is needed to research the anatomical, pathological and functional anomalies of the brain and also body-related disorders and eventually to identify causes of abnormality such as tumors and epilepsy.

The difficulty of identifying the source locations responsible for the EEG electrode's measured potential considered as the inverse problem. There are infinite current sources in the brain which model the recorded data for any sets of measurements or sensors outside of the head. The estimation of scalp activity sources based on the concept of electrical activity propagation using different conductivity values of interfaces, including the brain, skull, and scalp, as the lead field matrix. Using sophisticated algorithms to inverse this matrix provides the so-called "source localization." That will mean that inverse solutions used to determine the position of the epileptic source within the solution space at each point in the spike-wave complex based on the voltage map for such a particular point in time.

There are currently two main fields of studies in neural source modeling. The first method of modeling involves the use of imaging models, which explain the data with a dense set of dipoles distributed at fixed locations. A second method is a parametric approach, which benefits from replacing these dense dipole sets with the help of a single equivalent current dipole [21]. The imaging technique can generate a detailed map of cerebral activity, but the parametric approach maps EEG measurements directly to a small number of parameters [22]. The parametric method can be used to provide more intuitive interpretations of the equivalent current dipole models, which explain the electrical activity of the brain. An essential task in the parametric approach is to evaluate the location of the equivalent current dipole sources within 3D brain volume through EEG scalp measurements. The majority of work previously done on locating EEG sources has two assumptions (1) that the number of dipoles is fixed and (2) that the source locations are fixed in time [23, 24, 25, 26, 27, 28, 29].

In general, the quantity and positions of neural dipoles vary dynamically over time. In [30], the number of neural dipoles and their locations are dynamically evaluated and updated at every step described from the measured data. The unknown source positions and moments have taken as the hidden state function, and EEG data taken as the state-space model's measurement function. The optimal estimation of the hidden state in a Bayesian context depends on the state's posterior density function (pdf) given in the observations [31].

Particle Filter (PF) is a sequential Monte Carlo procedure that uses Sequential Importance sampling to approximate the state's posterior distribution at each step [32]. Particle filter uses particle arrangement to sample the framework's state-space. These particles are then weighted utilizing the measurement model to give a measure of the state posterior density.

Several approaches for solving the inverse problem have been suggested, widely used for localization of brain sources. The most common algorithms include sLoreta (Standardized low-resolution electromagnetic tomography) [33] and MNE (Minimal Norm Estimation) [34] intended particularly for distributed brain sources [35]. The spatial maps from sLoreta and the MNE compared with inverse solutions. Since an accurate relationship among EEG activity, sLoreta, and MNE spatial maps is unclear, this approach gives only weak indications that it is located correctly.

1.4 Source connectivity

Neural connectivity analysis plays a crucial role in understanding the brain's overall functioning. Due to enormous advances in the areas of neuro-imaging and mathematical modeling, such analysis has become feasible over the past two centuries. The functionality of the imaging methods (Electroencephalography (EEG), Magnetoencephalography (MEG), functional magnetic resonance imaging (fMRI), etc.) used to improve the knowledge and diagnosis of neurological disorders such as epilepsy, autism, anxiety and Alzheimer's illnesses in clinical applications.

Electroencephalography (EEG)is the most commonly used method for studying brain connectivity because of its high temporal resolution. EEG based connectivity analysis is an estimation of interaction between neural sources based on EEG recordings. Connectivity used for identifying different forms of statistical interdependence among temporal waveforms of spatially separated brain regions, and those are anatomical (structural), functional (symmetric), and effective (asymmetric) [36]. Anatomic connectivity is at a given moment the anatomical brain connections and analyzed for determining of the physical composition of the brain. Symmetric or functional connectivity referred to the relationships during neuronal movement between brain fields. The links between neurons estimated on time domain or frequency domain. The effect of one region of the brain on another is examined in the effective or asymmetric connectivity. The objective is to determine which brain regions can induce the flow of neuronal data into other areas in the system [37]. Functional connectivity gives correlations (statistical dependencies) between neurons, and effective connectivity gives information flow between the neurons [38]. Statistical dependence is calculated using correlation or covariance measurement, spectral coherence, etc. Functional connectivity is not explicitly related to particular directional impacts or a structural model underpinned by it. EEG data is applied to discover directional flow between neural sources through effective connectivity techniques such as Granger-causal (GC) models. Because of the complicated relationship between brain fields and the exercises, it is essential to understand the causal connections between brain initiations and efficient networks of brain cells [39, 40, 41, 42, 43]. Granger causality is one of the models based on effective connectivity estimation strategies [44]. Directed Transfer function (DTF) and partial directed coherence (PDC) are some of the measures implemented from this model [45].

The critical problem observed during the study of connectivity between cerebral zones is that links between scalp EEG signals do not match connections between hidden neural sources. The reason is that EEG signals do not provide normal activity under the area of one electrode.

However, the superposition of all dynamic neural sources found anywhere in the cerebrum can be obtained by using volume conduction effects in the brain. The impact of superposition leads to errors in the synchronization between EEG signals, especially when sub-cortical generators included. In this thesis, we propose a framework that the connectivity studies are based on a two-step approach. The first step involves an estimation of the brain sources and its time course using an inverse method, then calculating the connectivity metrics using the estimated time courses of brain source.

The validation of brain connectivity analysis based on EEG is more complicated than the reconstruction of the source. Validating the connectivity in real data is difficult, as the source positions are not available, and connectivity between them is not straight forward. However, it is also hard to identify suitable performance measures even when the ground truth is possible, as localization errors can lead to inappropriate assessments of the source connectivity of exact source positions. It is a prevalent practice that authors perform brain connectivity evaluations on real data and report them only as limited empirical validation of the methodology is being used because of existing problems. Some studies have simply presented the measure of connectivity as the definition of communication. The connectivity is based on dipole interaction modeling with MVAR. The MVAR procedure shows how the sources of the brain are connected, especially when the impact of one variable is on another. This process used in any type of EEG data since the directional connection between the dipole sources detected without knowing the position of the EEG source. This thesis aims mainly to identify which area of the brain can manipulate statistical dependence between cerebral neurons.

1.5 Motivation

Detection and tracking of electrical neural activity can improve our understanding of how the human brain functions. Neural activity tracking techniques have helped to improve the understanding and treatment of severe neurological disorders such as epilepsy and Parkinson's disease. More specifically, these techniques used to distinguish between different kinds of seizures based on the location and orientation of the seizure foci, thus resulting in improving the outcomes of epilepsy surgery.

A comprehensive analysis has been done on the role of neural synchrony in brain functions with EEG [46]. Most of the studies carried out at the sensor-level EEG connectivity analyses. The analysis of the corresponding networks is not straightforward as the volume conductive effect significantly distorts signals due to the electrical conduction properties of the

head [47, 48] and the fact that many scalp electrodes receive information from the same brain sources to some extent. These factors cause real connectivity between brain areas to be incorrectly estimated. In recent years, the emphasis on determining the EEG connectivity at the level of cortical sources has increased considerably. The method proposed is known as EEG source connectivity. The inverse problem is the estimation of the localized current dipole model from EEG measurements. In this thesis, to solve the EEG inverse problem accurately advanced signal processing algorithms have been developed such as using the efficient implementations of PF that will enable real-time tracking of neural dipole sources. Assess the connectivity between the time courses of the neural sources for human brain mapping.

1.6 Problem statement

Developing a framework for estimating the unknown number of neural dipole sources and their time courses for real EEG data, with much fewer particles and also reduce the computational complexity using particle filters and estimating connectivity among neural sources.

1.7 Research objectives

In human brain mapping, connectivity is one of the main concerns. Connectivity enables connections through the nervous system across different brain regions. Based on an interactive time series, the causal connectivity between scalp sensors studied until now. The causal connectivity measurements acquired through the use of sensor time series does not permit an interpretation of interacting brain sources. It is because the locations of the channel cannot see as a physiological location of sources.

This thesis proposes an analysis methodology that partially overcomes this limitation.

Localization In which regions (brain octants) the sources are located?

The localization of the neural sources from the measured fields, based on the solution of an inverse problem, is complicated by several issues. The problem is ill-posed: there are infinitely many current distributions explaining a given measurement equally well.

The main focus of this study is on finding the source of the brain. Although specific methods demonstrate the flow of scalp sources, prior assumption in active brain regions

is still necessary. Here is a new approach to describe the brain sources in their respective position, amplitudes based on particle filters.

To alleviate particle degeneracy of the particle filter, some improvements have been suggested by developing resampling techniques for EEG applications. In this thesis, a new approach based on partial stratified resampling (PSR), branching, and MSV resampling methods in the particle filter for localization of the neural source of EEG data is proposed.

Connectivity Does the data contain interaction (between the two sources) at all? If so, which estimated source includes the sending and which one the receiving source?

The source connectivity methods used to assess statistically significant functional relationships between the temporal dynamics of sources.

EEG localization techniques and connectivity methods have been developed considerably over the past decades separately. The particle filter was applied to extract the sources and their amplitudes. Multivariate (MVAR) model is applied to the time courses of estimated sources, using the Granger causality techniques to obtain the connectivity measures of the given data.

1.8 Contributions of the thesis

Dynamic neural source localization using a particle filter demonstrated in this thesis for an unknown number of dipoles. The new approach proposed, which uses a particle filter (PF) that employs Partial Stratified Resampling, branching resampling, and MSV methodology to track the neural dipole sources of cerebral activity.

The time-efficient partial stratified resampling algorithm used for finding neural sources, and comparing them with traditional resampling algorithms, is described in the thesis.

The branching resampling is based on the weight of the particular particle and of the total weight of all particles that a decision to branch (or kill) a particle (that is, a decision to resample it more than or less than once), not on the weights of each other.

This thesis focuses on applying the minimum sampling variance resampling technique to locate the neural sources. Minimum sampling variance (MSV) is also called optimal proportional set resampling, and with this method, the sampling variance will be minimal. The variation in particle weight between before and after resampling is minimized with lower MSE,

high RA, and less computational time compared to other resampling processes when using the MSV resampling method.

In this thesis, proposed a novel approach for source connectivity based on particle filter to define the brain sources with their respective location, amplitudes, and the Granger causality measures used to estimate the directional causal flow across the sources.

Results indicate that the combination of particle filter and the Granger causality techniques used for focal epilepsy data and outcomes are significantly relative to the findings in this same task.

1.9 Outline of the thesis

The rest of the thesis organized as follows.

Chapter 2 reviews the most critical methods that have previously used to locate the neural sources and measure brain connectivity with EEG.

In chapter 3, the pre-processing of the EEG data is carried out, and also details about artifact removal of EEG data are supplied.

Chapter 4 contains an essential contribution of the thesis and describes all the steps of proposed methodology for source localization. It deals with the source localization of EEG data using particle filter with existing and proposed resampling methods.

In chapter 5, we use the approach presented in chapter 4 to determine the location of the neural sources and estimate the connectivity between sources using GC methods.

The concluding remarks and future research directions given in chapter 6. References given in the last section.

Chapter 2

Literature Review

2.1 Overview

The first recording of human electroencephalography (EEG) by Pravdich-Neminsky [49] began modern neuroscience. Some years later, Berger [50] began to research the signals of the EEG systematically and figured out the alpha human rhythm. Since then, in numerous psychophysiological experiments, a large number of neurophysiological processes were described and correlated with experimental parameters [51, 52].

EEG source connectivity approaches involve a few steps, each related to the significant Signal Processing (SP) topics such as raw EEG data preprocessing, i.e., artifact removal, denoising, inverse solutions, i.e., source localization and connectivity analysis among the sources, i.e., functional and effective connectivity measures.

2.2 Preprocessing

The EEG signals are a complex summation of electrical brain activity, which is recorded by distant electrodes with the laws of solid angle and volume conduction. The origin of each signal can be very complicated, so its exact significance is not clear. Electrophysiological results are often distorted through additive noise, including background brain activity, heart electrical activity, eye-blink, and other muscle movements, and line noise. These artifacts are a big challenge for the interpretation and analysis of EEG signals.

Multiple approaches used but with little effectiveness to alleviate artifacts. Digital filters may remove signals from a specified frequency or band. Their main disadvantage is that they do not differentiate between the artifact and brain waves so that all behavior at a selected frequency

is suppressed. Resulting, the actual anatomy of the brain activity may be distorted. The EEG and the electrooculogram channels may perform a regression in the time or frequency domain to remove the eye movement artifact. Still, it may not use to eliminate the muscle or line noise. Lins et al. have introduced the Principal Component Analysis (PCA) [53], in which eye objects may be extracted by PCA in a more efficient way than by regression or by the use of Spatio-temporal dipole models [54], by multichannel EEG. The PCA cannot be entirely distinguished from the brain signal by artifacts with the same amplitude [55, 56].

The techniques of blind signal separation (BSS) are the most effective way of separating the recordings into the components that "build" them. We consider the signals provided by independent sources are EOG, EMG, and other artifacts. BSS techniques must define and carry out the reconstruction of signal components without artifacts [57]. Independent component analysis (ICA) is a BSS method used extensively. In 1996, ICA applied for the first time in Makeig et al. [58] EEG experiments. Artifacts such as EOG [59] and EMG [60], forcefully removed from EEG signals. Recently, Independent component analysis used in EEG analysis with promising findings [61, 62].

2.3 Localization

Several studies concerning the source estimate have recently used physiological models of fMRI research. Physiological models are nonlinear, so methods that can handle these non-linearity are essential to determine the hidden physiological states and parameters of the underlying model. The physiological models have an input-state-output structure and are well adapted to a Bayesian analytical framework. In [63], the first Bayesian framework established to estimate the model. Prior parameter restrictions used in their approach.

Few methods have been applied to solve the EEG/MEG inverse problem, including PCA [53], ICA [58], multiple signal classification (RAP MUSIC) [22, 28], spatial filters or beam-formers [27], dynamical statistical parametric mapping (dSPM) [64], MNE [65], sLORETA [33] and Bayesian methods [23, 24, 26, 29, 30, 66, 67].

One of the most widely used methods for finding a linear transformation is the Principle Component Analysis (PCA), i.e.,approaches which find information only in a data covariance matrix during second-order moments. The underlying concept behind PCA is to represent the data based on their highest variance. Also, the mixing matrix containing forward models, while the correlation between sources is usually a questionable assumption, is not a correct assump-

tion in various parts of the brain. PCA is thus commonly not used as a source localization method but as an approach to reducing data dimensionality.

ICA is a solution to the problem of blind source separation. The objective of ICA is to achieve a linear representation of non-Gaussian data so that its components can be independent. The underlying assumption is that the sources are independent. In ICA, the number of components is equal to the number of channels, and need to identify which one is source manually. ICA is not an excellent source reconstruction method if you choose to study connectivity among sources.

The Multiple Signals Classification (MUSIC) is a technique that covers the dominant subspaces of the data vectors structure. The data vector space splits into the subspace of the signal and the noise space, which is orthogonal to the signal. It defines the source positions for which the principle angle between the noise subspace and the forward model of the source is maximum or minimal for the principle angle between the signal subspace and the forward model. MUSIC scans all sources, despite the probability that multi-sources are involved simultaneously, and decides whether a source complies precisely with the measured evidence in each location. The drawback of MUSIC is that as the number of sources increases, it becomes difficult to locate several maxima.

The beamforming method is used to estimate the time course of a dipole at a particular location in the brain. Sensor data are combined linearly to decrease the activity of other sources interfering with sources of interest. It should be taken into consideration that the estimated variance of the source is significantly less than the actual value in the case of the correlated sources. Besides, if the independent sources are present, the dependent sources would be misestimated consistently.

The MNE is based on a search for a solution with minimal power, which leads to Tikhonov regularization. This method is useful for distributed sources, in which these models are likely to cover some regions of the cortical surface with dipole activity. In comparison to deep sources, MNE has an unusual pattern in identifying surface sources. Deeper sources need to have more potential to make the same inputs to the data as sources nearer the surface. At the same time, however, the method minimizes power, which ends in the profound source suppression.

By incorporating a depth compensation matrix, LORETA addresses deep sources in the MNE method. For the localization of source, Standardized low-resolution brain electromagnetic tomography (sLORETA) focused on a standardization of the current density. The current

density estimation is then performed using the MNE method and is further standardized using the associated standard deviation. This approach has been widely used with various head modeling schemes for source localization. The drawback of sLORETA is its poor resolution due to the regularization of the stability solution.

As Bayesian methods have been extensively used for tracking multiple objects, they provide suitable candidates for online tracking of current dipole sources [34, 46] and investigated in this thesis. Among sequential Bayesian estimation techniques, Kalman filtering (KF) can provide optimal parameter estimates for linear systems under additive Gaussian noise [68]. Although KF was used to solve the EEG inverse problem in [23, 24], KF is not applicable for highly nonlinear and non-Gaussian systems.

In the Kalman filter technique, the analysis discussed in [69] used a local linearization filter (LLF) [70], allowing for physiological noise in addition to the measuring noise, which is an entirely stochastic model. As well as estimating the states and parameters of the model, they use a set of radial basis functions (RBFs) for parameterizing the system's input, i.e., the neural activity. To make the solution lie within a regularly distributed but sparse space, the number of RBFs was a priori calculated in the work of [69]. Recently, the LLF technique used [71] to define the states and parameters for a physiological model.

Only measurement noise in system modeling addressed in work outlined in [72] for model-based optimization of parameter estimation. To approximate the BOLD response states and parameters, nonlinear filtering methods have also used, aside from the state-linearized filter approaches. The particle filters (PF) is suggested in [73], while the technique for fMRI data processing in [74] applies an unscented Kalman filter (UKF).

Estimates in nonlinear systems are especially important since virtually all realistic systems require some sort of non-linearity. Kalman Filter [75] used the mean and covariance of the state. The EKF [32] linearized all nonlinear transformations and assisted the linear transformations of the KF equations by the Jacobian matrices because all transformations were quasi-linear. The UKF [76], which distributes statistical knowledge through a non-linear transformation, has been enhanced to increase the accuracy and ease of use. The alternative solution to these problematic non-linear or non-Gaussian problems is particle filtering, which does not rely on the local linearization technique. Particle filtering (PF) is the more precise sequential Bayesian technique for estimating nonlinear and non-Gaussian dynamic systems [31, 32, 77] parameters.

For nonlinear systems [32, 78], PF provides an alternative to approximate Kalman filtering [68]. To approximate the posterior density, the PF uses a collection of weighted random samples. To estimate the un-observed parameters, the PF method was [73] superior to LLF [69] and was both precise and robust. They use a PF for state estimation in their work and an offline maximum likelihood method for parameter estimation. The work in [79] discusses the problem of estimation but also considers the hemodynamic parameters as known with weight to advances in PF. For both State and parameter estimation, a regularized PF is used in this work [75]. They suggest that the filtering framework [57] is the foundation of their research. Given the highly nonlinear EEG measurement model, PF is more suited to solve the inverse EEG problem. PF was used for estimating the locations of neural dipole sources [24, 26, 29].

Particle generation and weight calculation are the primary operations of particle filter processing. Particle filter makes use of an arrangement of particles to sample the state space of the framework. The measurement process then weighs these particles to achieve the state posterior density. When new measured information is available, particle weights are updated recursively to anticipate the future condition in the framework. After a few iterations, in the steps of the particle filter, only a few particles will have a large weight, and most of the particles will have a small weight, leading to particle degeneracy.

Researchers have worked over the past few decades to increase the sensitivity of the particle filter estimates. One way is to investigate a more robust importance distribution of proposals. The particle filter builds an empirical approximation of the posterior probability distribution using a set of independent identical distribution (i.i.d) particles sampled from the proposal and then used to assess expectations. Consequently, the design of an appropriate particle filter plays a significant part in a successful proposal distribution. The measured particle decay will intensify by the inappropriate distribution of proposals. Some particles are in the area of high probability, while others are in the field of low probability. The particle weights distributed in the low probability range are insignificant after weight updates.

In the recent past, a few adaptions of particle filters have proposed to address the issue. Some of those adoptions include Rao Blackwellized particle filters [80], auxiliary particle filters [81], adaptive particle filters, unscented particle filters [82], regularized particle filters [83] and Gaussian particle filters [84].

J. Yun et al.[85] proposed the APF in which both observational information and the state equation data combined to propose distribution. The Nudged PF (NuPF) proposal introduced from J. Miguez [86] was to move a subset of sampled particles in the state space to highly

probable areas when the expected model dynamics are significantly different from the system currently provided by available observations. Haomiao Zhou et al. [87] proposed a new sampling method based on their Pearson Correlation Coefficient, which generates particles near the actual state. To use this observation in its entirety, a two-stage particle filter algorithm proposed by J. Wang et al. [88]. The UKF and the IEKF have incorporated into the particle filter frameworks for each particle updated sequentially. When observations were relatively accurate, the algorithm for particle filters with the latest consideration was more effective for optimization of the proposal distribution. However, these adjustments can only be used for offline prediction.

A technical enabler for exploiting the linear substructures that are in the state-space model is the marginalized particle filter (MPF), also referred to as the Rao-Blackwellized particle filter (RBPF). It allows for the use of high-dimensional state-space models as long as the (severe) nonlinearities only affect a small subset of the states. In this way, the structure of the model is utilized, so that the particle filter is used to solve the most difficult tasks, and the (extended) Kalman filter is used for the (almost) linear Gaussian states. In Rao-Blackwellization, the optimal solution is computed for the linear dipole moment parameters through a set of Kalman filters, while the non-linear source locations are sampled with a particle filter; this reduces the number of particles needed to obtain a given accuracy, however, a covariance matrix has to be computed by inversion at each time step for each particle. Although statistical efficiency increases, the cost of the matrix inversions is still higher than that of the particle filter we use in this study.

In most cases, the particle filters, despite various changes to the standard PF framework, are still subject to a severe setback, i.e., particle degeneracy, in which most particles will have negligible weights after a few iterations. An additional resampling [89] phase should be applied in the particle filters. This stage helps us to quickly change the numbers and weights of the new sampled particles. Deteriorations in measured particles such as degeneration are avoided. For particle filters, resampling is playing a crucial role.

Without considering the resampling in the particle filter, particles with large weights will end up commanding low weighing particles. This means that the assessments achieved might be incorrect and that there may be vast differences. These decays deformed by resampling; that's why resampling is necessary for particle filters. As a result, resampling thoroughly investigated and, consequently, a large number of traditional resampling methods suggested. Firstly, multinomial resampling proposed by Gordon et al. [77]. Residual resampling, proposed by Carpenter et al. [90], Liu and Chen [91] developed stratified resampling, and Doucet et al. developed systematic resampling[31]. The combination of residual resampling and systematic

resampling, i.e., residual systematic resampling (RSR), was developed by Bolic et al. [92]. A few years ago, Murray [93] proposed by accelerating the resampling stage in particle filters using a Metropolis step. Apart from the advancement of resampling techniques, there are additionally some studies looking at the comparison of various resampling methods [94, 95, 96]. From most related research, resampling is a vital issue for the performance of the particle filter. In [97, 98], the researchers compared a multinomial, stratified, systematic, and residual resampling for the remaining useful life of the battery model, among the four most commonly used methods of resampling. The reliability of the resampling was calculated by the mean square error (MSE), relative accuracy (RA), and the computational complexity based on the time required to perform. In [99], the authors suggested that selecting the correct proposal distribution will also solve the particle degeneration problem because resampling techniques can lead to particle impoverishment.

As shown in [100], the bottleneck in real-time PF implementation is the resampling operation. Although these algorithms are the most widely used and standard, more advanced algorithms are still required for specific applications. We mainly study the performance of time-efficient partial stratified resampling and branching resampling in the particle filter to estimate the location of neural sources from EEG data. This thesis focuses on applying the minimum sampling variance resampling technique [101] to locate neural sources. Minimum sampling variance (MSV) is also called optimal proportional set resampling, and with this method, the sampling variance will be minimal. Our goal is to verify whether and to what extent each method of resampling can use the synthetic and real data to locate dipole sources.

2.4 Connectivity

Mapping scalp potentials into brain space is just half the issue in EEG studies of brain connectivity. Another critical problem is how functional relationships among EEG sources in brain space can be identified and characterized. It is a particularly acute concern to study interactions between brain systems [102].

Models that describe the dynamics and interaction activity in the brain regions on a macroscopic scale are an intermediate step towards unified brain modeling techniques. It is the approach adopted by several researchers in the field of brain connectivity. There are several competing interpretations of "connectivity," and there are many more disputes about how connectivity should be calculated by the various meanings. There was a strong consensus regarding a distinction between structural, functional, and effective connectivity [103, 104]. Structural con-

nectivity refers to the standardized brain structure that can be achieved, for example, through a continuous scan using structural MRI [105] or a diffusion tensor imaging system [106]. The functional and effective connectivity of neuronal processes refers to the "coupled" behavior of two neuroanatomic people when performing tasks. The common difference that effective connectivity is directed, i.e., it determines the driver-receiver relationship, while functional connectivity is not. Initially, functional connectivity equated with instant correlation [103], but expanding this principle to arbitrary measurements of undirected functional interactions that are symmetrical in their arguments is helpful. Each asymmetric function can also quantify effective connectivity. The proposed measures for connectivity are numerous and come from various fields such as graph theory, signal processing, and Bayesian statistics. This thesis primarily concentrate on functional and effective connectivity measures.

In the 1960s, functional brain connectivity measured by cross-correlations between pairs of EEG signals [107]. Increased correlations indicate more reliable useful connections among similar brain areas. To calculate functional connectivity in the frequency domain, the use of Magnitude Squared Coherence (MSC) or coherence introduced. Coherence allows spatial correlations between signals in different bands to be measured [108]. Coherence is responsive both to changes in power and to changes in phase. In other words, if either power or phase changes in one signal, the coherence value is affected. When the original relation between the two signals does not change over time, then the amount of coherence remains unity. It means that coherence does not describe the direct interaction of two signals, but rather the reliability in power asymmetry and phases of interaction. The correlation, on the other hand, can be measured across a single time or several epochs and depends on both phase and polarity irrespective of the amplitude. Yet under normal physiological conditions, no abrupt and robust power asymmetries are needed. The effect of power on coherence should be marginal, and coherence measures should predict results similar to those provided by correlation.

Neural assemblies synchronize and actively communicate with the visual, motor, or cognitive functions in local or distant areas. These functions represent complex interaction that involves stimulus anticipation, stimulus attention, and planning. A bidirectional or unidirectional coupling may achieve such a cycle of interaction. The first scenario is analogous to the mutual synchronization, where the two processes adapt their rhythms, while the second represents a causal relationship between the driver and the recipient. The effective connectivity measures can be divided roughly into dynamic causal modeling and Granger-causal modeling approaches [109].

Dynamic causal modeling (DCM) [110] assumes that different mechanisms exist for generating observation sequences. Such simulations include conceptual source regions, the signal transfer from the source regions to measuring sensors, and a directed graph representing the causal relations between the source regions to be evaluated. No specific method is available to compare models; the field knowledges of the mental activity under review must be explicitly defined. The parameters of the different models are tailored in the DCM approach to matching the data as best as possible, satisfying certain previous assumptions, and also to be predetermined. DCM's main drawback is that prior knowledge of the connectivity framework is required. Incorrect model specifications can lead to estimated connectivity results that differ significantly from the real underlying structure. Due to the prior distributions, further wrong parameter estimates may result, so the prior distribution has to be carefully specified [111].

Under the term granger-causal modeling (GCM), a large class of effective connectivity measurements is widely incorporated to describe the existence of the following two properties. First, unlike DCM, it is generally not limited by a predetermined network topology to estimate effective connections between varying interest variables (i.e., sources). However, the existence of connections is measured in an entirely data-driven approach for all pairs of variables exhaustively. Therefore, driver - receiver connections are calculated on the basis that the cause (the driving variable is measured) briefly precedes the result (the receiving variable). So far as time series is concerned, this means that the transmitting variable time series provides information about the possible values of the receiving variable time series. One way to calculate this effect is through granger-causality. Granger interprets that the experience of the time series of the driver will later enhance the prediction of the receiver. GC methods have been used to calculate directed influence among EEG sources in the frequency domain using linear vector autoregressive (VAR) models [40, 102, 111, 112, 113, 114] More recently, some information theory-based GC indices were introduced that are immune to non-linear interactions as well [115].

The preliminary task of every GC-based study is to estimate MVAR model parameters. Following the adaptation of the MVAR model with the time cycles of the estimated sources, a range of time domain and frequency domain measurements can quantify directed interactions. The frequency-domain MVAR modeling has been applied to numerous applications, and this method will be further discussed in Chapter 5, which is focused on effective connectivity measures like Directed Transfer function (DTF) [40], Partial directed coherence (PDC) [102].

PDC based EEG connectivity estimation methods diagnose the longstanding vegetative patients [116]. The DTF used in fully automated preterm infant connectivity measurements [117]. Significant differences can be observed in the participant and control community [118]

of PDC-based neuro-dynamic traces of childhood absence epilepsy. Undirected and directed connectivity discussed in bivariate and multivariate models. The critical evaluation [119, 120] is conducted in both simulation and GC (granger causality) multi-channel EEG-based parameters for the identification of false connectivity. Various extensions used to remove incorrect connections to reach the exact neural network underlying the brain [121, 122].

Nevertheless, not every solution to the temporal preservation of effective connectivity comes under the Granger causality category [43]. The methods in [122] and [123] are counterexamples of fully model-free connectivity analysis approaches. They are focused on the study of the imaginary portion of the time series cross-spectrum, which detects non-zero phase delays.

There is a continuing discussion on whether DCM, GCM, or phase lag analysis would be used in brain-effective connectivity analysis [124]. The characteristics of the measuring method used to study connectivity are essential to take into account. Metabolic measures as fMRI and PET help to study inner brain dynamics at high spatial resolution. Their temporal resolution, however, lies within a second range, which is disadvantaged in terms of time precedence for the processes that define drivers and receivers. Granger-causal fMRI data analysis resulted in minimal amounts of meaningful connections [125], which indicated that fMRI resolution is overly low in time to capture transferring, at the relevant scales.

Electrophysiologic measures are more direct than fMRI and PET to reflect neuronal activity and with sampling rates of up to several kHz. Unlike with fMRI and PET, the internal brain activity measured outside the head cannot be precisely reconstructed from electrophysiology. Consequently, an effective connectivity analysis of the brain driven by electrophysiology requires either invasive measures or the solution to an ill-posed inverse problem. The invasive human recording is rarely used, which leaves us with electroencephalography (EEG) and the associated magnetoencephalography (MEG). These methods use extra-cranial sensors to collect signals from gross synchronized neuron populations related to electrical activity. For EEG, these are scalp electrical potential, while MEG measures the magnetic fields corresponding to them. In both cases, the signal is spatially diffused when traversing through a mechanism called volume conduction from the source regions to the sensors. This raises a significant problem concerning the accuracy of EEG / MEG in the underlying active source areas. In brain connectivity studies, where multiple sources are assumed, whose contributions are however mixed in with each sensor, the situation is most extreme. It has become increasingly necessary that volume conduction is accounted for in EEG- and MEG-based brain connectivity analysis

[122, 126, 127]. This thesis resulted in a proposal for real EEG and MEG source connectivity analysis, i.e., the brain connectivity analysis based on source estimates from EEG data.

Earlier work has undertaken in the fields of sensor space [40, 102] and intracranial records on effective connectivity analysis. However, the volume conduction effects, as the multiple sources mix at the sensor levels [128], seriously affect the sensor level connectivity analysis. This is why several studies show that in EEG-based brain connectivity studies, volume conduction must be considered [40, 102, and 126].

The authors apply PDC to neonatal sensor level recordings in [129]. They compare a short time sliding window approach and an adaptive Kalman filter method for estimating time-varying PDC and show that the short-term window method better captures transient parameter changes. In [130], the authors perform an effective connectivity analysis of the source space using Structural Equation Modeling (SEM) and DTF. The source reconstruction performed with a minimum norm approach and anatomically specified regions of interest activation time intervals used in connectivity research. In [131], the authors used adaptive MVAR models and extended the analysis so that time-varying efficient connectivity could be calculated. In [74] the authors use a Kalman smoother to estimate the flow of information to analyze the source space connectivity. They pursue an efficient two-step method for determining connectivity. Using the Brain Electrical Source Analysis (BESA) program, they recreate the dipole sources and obtain the source waveforms.

In the thesis, a two-stage connectivity analysis will perform similar to the approaches presented in [74, 130, 132], where the sources will first identify and connectivity analysis performed on the extracted source waveforms. It is not easy to evaluate the connected networks because the volume conductive effect significantly distorts signals because of the electrical conductiveness of the head and often scalp electrodes derive input from the same sources in the brain.

These factors help to estimate the real connectivity between brain regions inaccurately. The suggested approach is referred to as EEG source connectivity. The inverse problem is the estimation of the localized current dipole model from the EEG measurements. In order to solve the inverse EEG problem, advanced signal-processing algorithms such as the efficient implementation of PF have been built to facilitate direct exposure to neural dipole sources in real time and measure the connectivity of neural sources time courses using functional and effective connectivity measures. PF was used for estimating the locations of neural dipole sources. Resampling is an essential component for the PF because without it, the SIS will quickly produce a

degenerate set of particles as the weight discrepancy between particles increases with time. The motivation of resampling includes, but is not limited to, combating sample degeneracy (while avoiding impoverishment) and adjusting the number of particles online. We contend that until no new observation is used in the resampling process, the distribution of particles should be identical before and after the resampling, namely the identical distribution (ID). However the distributions before and after resampling are more or less different, except in very rare cases. Therefore, understanding how much difference the resampling process makes to the distribution, or rather how well the resampling is able to maintain the original distribution, is important both in theory and in practice. In order to determine the ID attribute of various resampling methods, minimum sampling variance method is introduced. Eight typical resampling methods are compared via simulations in terms of sample size variation, sampling variance, computing speed. Since resampling is a relatively independent procedure that is in general not correlated with the other operations required by the PF, we focus on the resampling operation only while omitting the other filtering operations for which there exist a variety of different versions. This allows a clear understanding of our contributions. Chapter 4 discusses the source reconstruction algorithms. Chapter 5 discusses connectivity measures. In this thesis, due to its well-known properties and proven robustness, the analysis of real EEG data will be carried out with GC indices such as Directed Transfer (DTF) and Partial Directed Coherence (PDC).

Chapter 3

Preprocessing of raw EEG data

3.1 Introduction

The preprocessing is the process of converting raw data into a format that is more convenient and user-interpretable for more analysis. Preprocessing, in the case of EEG data, typically refers to eliminating artifacts from the data to move back to the actual neural signal.

Scalp EEG has been utilized as a surgical method to identify and diagnose brain disorders and is employed in the qualitative study of human neurophysiology as a noninvasive technique. EEG signals are a detailed description of brain activity captured by the laws of solid angles and volume conduction by distant electrodes. The root of each signal may be quite complex, and the precise significance is also not visible.

EEG data is sometimes distorted by additive noise, which involves background brain function, electrical heart behavior, eye-blink, and other electrical muscle movements. These artifacts constitute a significant problem in the processing and assessment of EEG signals. Various approaches were used to mitigate them but were not sufficient. The signals of a specified frequency spectrum or band may be removed by digital filters. Their major drawback is that the artifacts and the brain waves do not differentiate and that all behaviors on the chosen frequency are excluded. As a result, the exact anatomy of the brain function can be skewed. In EEG systems, time and frequency domain regression may be used to remove eye activity artifacts, but it can't apply to remove muscle or line noise.

Simple frequency-dependent filtering is not enough because of its different spectral properties to eliminate these noise signals. In comparison, EEG spatial resolution is rather low. Due to this, advanced methods of spatial filtering such as CSP, PCA, and ICA in the preprocess-

ing are popular to reduce these noise signals and increase their spatial resolution. The usage of PCA cannot distinguish objects with identical amplitudes as the brain signal [55, 133].

Independent component analysis (ICA) [134] is a methodology that takes advantage of independence to derive a source approximation from signal mixtures to improve certain contrast functions. It was initially developed as a technique for distinguishing separate voices speaking concurrently ("cocktail party problem") [135, 136]. This was later applied to other forms of signals. If the data derives the individual time courses of various brain and artifact sources, corrected EEG signals may be obtained by removing the artifact source contributions.

This stage aims at cleaning up and de-noising the digital data captured to enhance the appropriate knowledge stored in the signals [137]. The following would identify as the numerous vital stages of the EEG preprocessing pipeline:

- Downsample the EEG data
- Filtering the data
- Removal of bad channels and interpolate all the removed channels
- Artifact identification and removal

3.2 Downsampling the EEG data

The sampling rate is the number of samples acquired in one second measured by Hertz (Hz). It is worth noting that every time-point in EEG data reflects a measurement of voltage, normally measured in microvolts (μV). Imagine we have a 29-channel EEG network and a sampling rate of 1000 samples per second (or 1000 Hz). If each sample is interpreted as a 32-bit float, that is $(29 * 1000 * 32)$ = 928,000 bits per second, or 116 kb / sec. Although it might not seem to be much, please note that all this information will probably be transmitted through the transmitter, processed, and stored repeatedly. If the number of samples was reduced, this will all be changed. The reduction in the number of channels, however, can be troublesome and poses the question of how to reduce the sampling rate.

It is essential to select a sampling rate because the recorded discrete samples can be used to represent continuous voltages. The standard sampling rates range between 250 Hz (i.e., one sample per 4 ms) and 2000 Hz (i.e., one sample every 0.5 ms). High sampling levels

significantly increase the temporal resolution of the signal. On the one hand, the storage of recorded data requires a considerable disk space; on the other, it can be tough to process.

To reduce the sampling rate, need to apply downsampling to the EEG data. This is a strategy for reducing the number of samples used while preserving (hopefully) the information required. Mainly when the sampling rate is too low relative to the highest frequencies the signal being measured, aliasing errors can be introduced (i.e., non-existent signals). In other words, the sampling rate in the signal must be at least twice the maximum measurable frequency.

It is important to choose the sampling frequency based on the requirement. For example, if you detect Alpha waves (up to 15Hz), you need at least a sample rate of 30Hz to detect a 15Hz signal. In the same way, a 200Hz sample rate is as low as possible when taking into account Gamma waves up to 100Hz. Moreover, an even higher frequency is preferred according to the techniques performed, and some studies which look at high frequencies (e.g., frequency after response) need to have high sampling rates. It is necessary to downsample as small as possible and be aware that the results can be marginally changed. A low-pass filter is typically needed before downsampling to prevent aliasing errors.

3.3 Filtering the data

Looking at the frequencies of a digital signal, whether it's audio, EEG, or otherwise, filtering those frequencies is a common thing to do, so that either some frequencies are eliminated, or some frequencies that remain. The implementation of digital filters is one of the most essential steps in the preprocessing of EEG data. Digital filters are typically employed to improve the signal-to-noise ratio by attenuating the disruptive frequencies.

Filters are defined based on their order, cutoff frequencies, passband, and stopband. Passband shows the portion of the frequency range where the filter doesn't attenuate. The remainder of the frequency spectrum where the filter attenuates is called the stop-band. High-pass and low-pass filters are the most widely used filters for EEG data that attenuate low and high frequencies.

While looking at alpha waves, it is only required the range of 7.5Hz-12.5Hz, so it is useful to use a bandpass filter between such values so that noise is eliminated outside the range. To exclude very low-frequency signals, high-pass filtering can be applied. They are too slow to come from the cortex, and typically in the recording context are a symptom of long-term

drift. Fluctuations of the AC power line, power supplies, and fluorescent lamps can produce substantial sinusoidal noise (50Hz and its multiples) in the electrophysiological data. A notch filter may be used to approximate and remove 50Hz and its multiples on the raw signal for eliminating this line noise.

3.4 Removal of bad channels and interpolate all the removed channels

The EEG data often contains bad channels that do not provide correct details. Early elimination of these bad channels is necessary as it can affect future research if the data is preserved. Bad channels may result from a cap change, which can lead to gel not forming a firm contact between scalp and electrode, moisture, a lousy cap fit, or lousy coagulation of the skin.

The easiest way of finding the wrong channels is to inspect the raw data after the data has been collected. Upon viewing the results, then search for channels that either don't have a signal or seem to be considerably noisier than others. Notice that merely removing wrong channels can result in substantial loss of information when data have several bad channels. In that case, the omitted channels may be configured or interpolated.

It is standard practice to interpolate data for bad channels after flagging bad channels, depending on the data from the proper channels. Interpolation is a method of filling out missed data based on the other available data. Interpolation of the channel primarily makes an intelligent understanding of the activity on the weak channel using the nearby channels. Interpolate a channel only after it has been interpreting very badly for a long period of time. The EEG study relies primarily on average, over epochs. It minimizes the influence of a couple of epochs with a noisy channel. But if a channel is continuously noisy or exhibits unusual behaviors for a long time, interpolation will be done.

3.5 Artifact identification and removal

Artifacts are signals that the EEG system receives but do not originate in the brain. There are several different sources of EEG data artifacts that are shown differently. EEG artifacts can be categorized as biological or natural.

External artifacts come from outside world interference, such as power lines, lose contact electrodes, or other human movements during the experiment. Power line interferences can be avoided by using a 50 Hz notch filter. The effect of environmental artifacts can be minimized somewhat by the use of active electrodes (electrodes with an additional low-noise amplifier). The most effective way to mitigate its effect is by changing the atmosphere, i.e., by shielding the room and by securing the electrodes correctly.

Biological artifacts come from the body's origins. Eye blinks, eye gestures, head movements, breathing, and muscle noise are some of the most common biological artifacts. Such artifacts may be identified by using accelerometers, Electroocculograms (EOGs), or eye-tracking data for artifacts of eye motions, and Electrocardiograms (ECGs).

A major issue for EEG analysis and interpretation is extreme interference of EEG activity from eye blinks, muscle, and heart and line noise. Many techniques for eliminating eye movement and other artifacts from EEG recordings were suggested. The rejection of contaminated EEG epochs simply results in a significant loss of information collected. For removing a wide range of artifacts in EEG measurements we propose using ICA [133, 138]. Our findings indicate that ICA can track, isolate, and eliminate activity from a variety of artifact sources on EEG data.

ICA is a linear decomposition method to produce the most temporarily independent signals on the channel data. The number of independent components (ICs) is the same as the number of channels when a data rank is maximum (i.e., no channel can be interpreted as a linear mixture from the other channels). ICA helps to establish time-independent signal sources. Therefore ICA may also describe by a scalp map, namely projection patterns of each independent activation for the source on the scalp surface.

The ICA ability enables the source separation in environments with the assumptions: 1) linear mixing media and limited propagation delays, 2) the source timescales are independent, and 3) the source number is equal to the number of sensors; that is to say, when N sensors exist, N sources are defined by the ICA algorithm [58]. For EEG signals, assume that the multichannel EEG recordings are mixed brain and artifact signals.

Numerically simulated simulations have shown that, while there are substantial numbers of time independent, low level sources [139], ICA algorithms must be confident in separating time activation and scalp topography from simulated scalp data, of relatively large and time-independent sources. The method uses spatial filters derived from ICA and does not require

an artifact source reference channel. By removing the contributions of artifact sources from independent time courses from various brain and artifact sources of data, artifact-corrected EEG signals can be extracted [140, 141, 142].

The fundamental matrix algebraic formulation of the linear signal decomposition used in ICA is schematically visualized in Figure 3.1.

We begin with the mixtures in the time-domain signal recorded on electrodes. The data can be seen as 2D matrix, in which rows represents the channels and columns represents time samples. The matrix values are the voltage amplitudes recorded for each channel at each time sample. Now produce an unmixing matrix W (ICA matrix) which transforms the mixed data X into IC activations U when multiplied by the data matrix X.

$$U = W * x \tag{3.1}$$

The activations matrix U contains components as rows and time samples as columns. The components in activation matrix U can be defined as a linear sum of weighted channel activations. While the effective number of statistically distinct components contributing to a scalp-EEG is unknown, it is apparent from the matrix representation that as many as electrodes are possible, since the combined N channels is decomposed into a linearly weighted sum of N components [58]. The W rows are now the vector from which the activity of an independent component can be measured. Each dipole has an activity (which projects to all electrodes linearly). Brain source activity (dipole) is unit less when it is projected onto the electrodes. So any dipole at each electrode site produces a contribution. The components of ICA are the same.

As shown in Figure 3.2, both a fixed scalp map and the time series of an independent component (process) of an EEG data set (or IC for short) provide the relative amplitude (or "activation") and polarity (both positive and negative) at any point in time. The scalp map [143] shows the relative weights or strengths of the projection (and polarities) from the component process to each position of the electrodes. The time-series for component activation gives the relative amplitude and polarity of the activity. Since EEG source are described as spatially stable, a scalp map of the component remains constant over time.

Each component process is projected back to each scalp channel by the component-time series with the weight of the scalp map for the channel. The IC back-projection on all the channels is the part or portion of the scalp data (on all channels). The channel signals are the quantities of all the individual component's back-projected activity. In other words, the

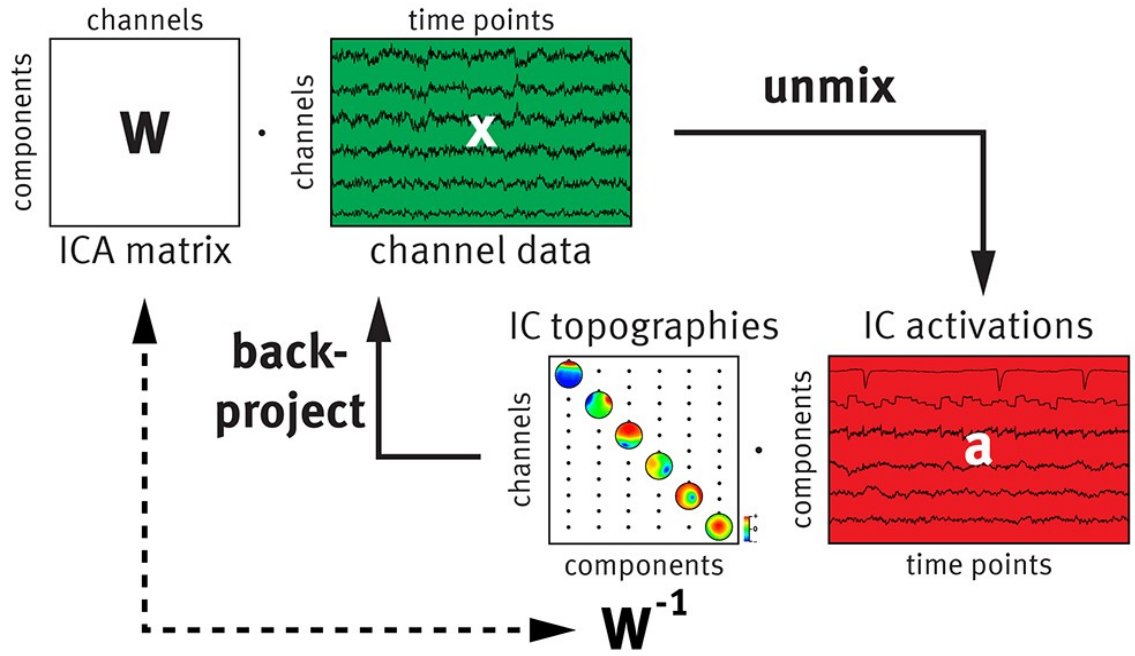

Figure 3.1: Data decomposition and back-projection schematic flowchart for Individual Component Analysis (ICA).

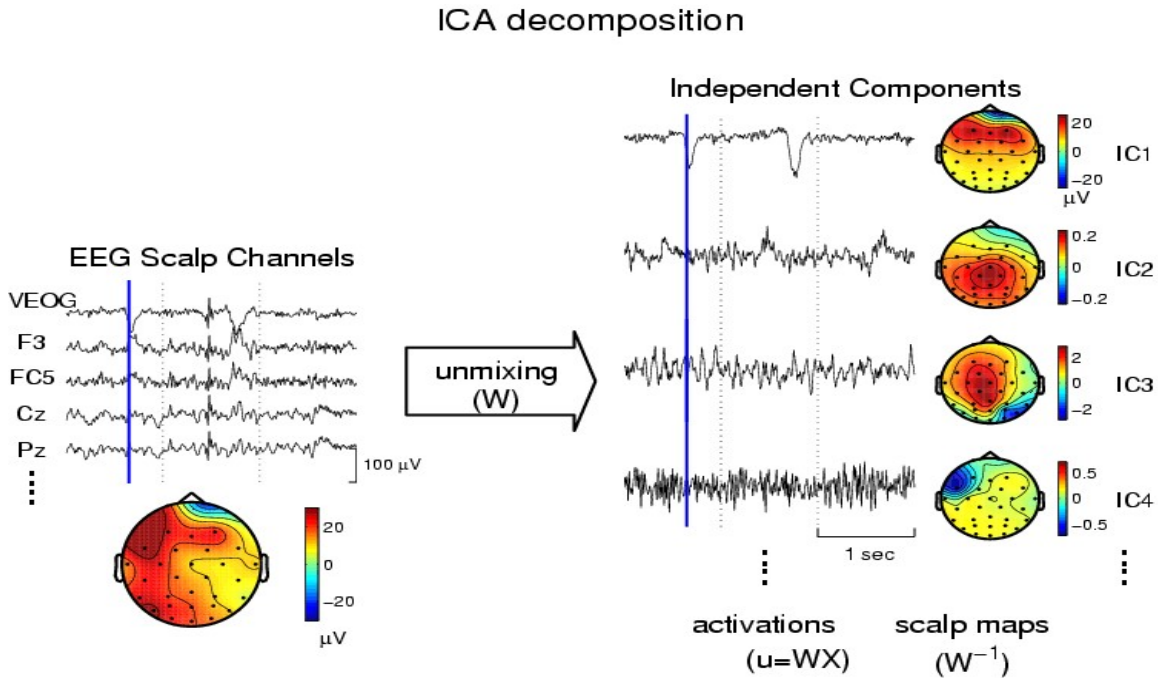

Figure 3.2: EEG decomposition

scalp data capture all the summed back projections of all the different components on the entire channel.

$$clean\_data = W^{-1} * U \tag{3.2}$$

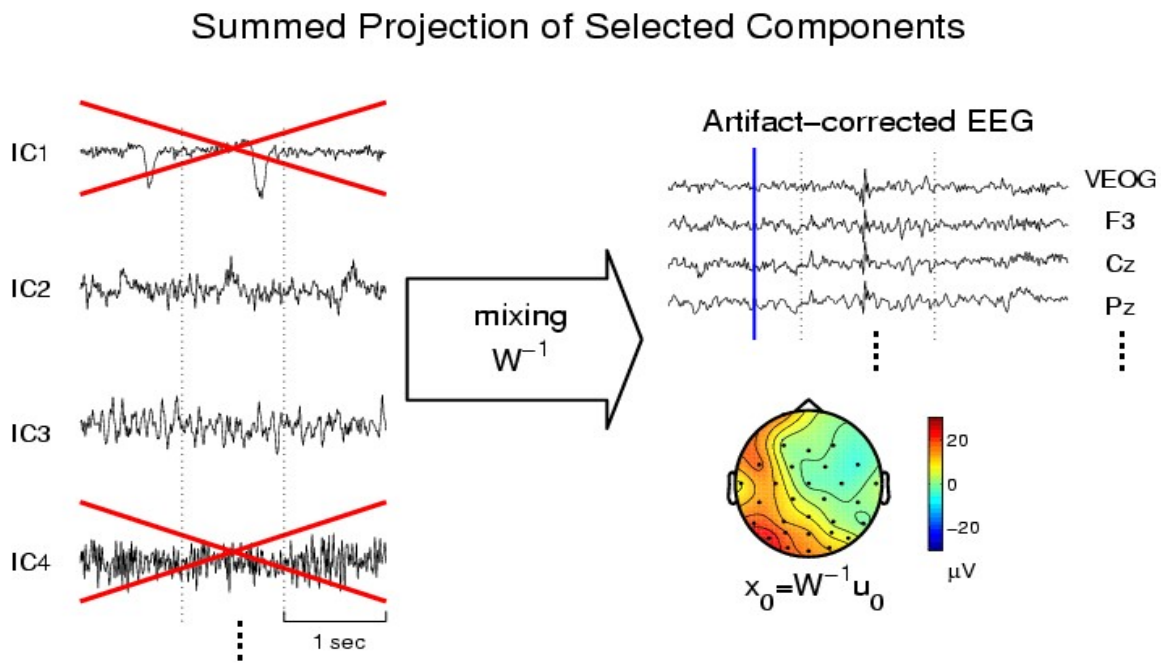

Figure 3.3: Projections of ICA to the scalp

Now we'll see how one component can be re-projected to electrode space. It means that by multiplying the IC activation matrix U by the inverse matrix W^{-1} the unmixing process can be reversed. The columns of the inverse matrix W^{-1} provide the corresponding weights and polarities of the back projections from each component onto each electrode that can be traced as a topographical map. As shown in Figure 3.3, the number of non-artifactual ICA components was projected back to the scalp to produce artifact-free brain signals.

3.5.1 Identification and elimination of artifactual independent components

After applying ICA to EEG data, first, identify the artifactual components and then either remove only those components that represent visible artifacts (e.g., ocular artifacts) or to keep only those components that arise from specific brain activity, removing all the remaining components.

Although removing any bad electrodes from EEG recordings is relatively simple and not too disastrous, detecting them by visual inspection of hundreds of simultaneously recorded EEG channels is not always trivial. It is not easy to automatically create algorithms for artifact identification on individual channels. The visual analysis of the potential maps is a significant contribution to removing artifacts from data [144].

Eye component

Eye components define eye movement. The electric field can be represented adequately as an "equivalent current dipole" (ECD) in each retina (a portion of the eye that detects incoming light). The eye movement divided into two elements: vertical movement and horizontal movement. The frequency spectrum for all eye parts is varied because of experiments and people; usually, the majority of the frequencies are below 5 Hz because people typically don't shift their eye faster than that.

The vertical movement has a topography of the scalp that can model on two ECDs that are upside down in each eye and that look positive or only negative since EEG recordings rarely record from the base of the head. The activity of the component should show relatively clear spikes due to blinks. There can even be drift when you look up or down.

Horizontal eye movement has a topography of the scalp, which is based on the ECD between the eyes and is left / right centered, with positive and negative values on the other side. Components of horizontal movement of the eye tend to be step functions.

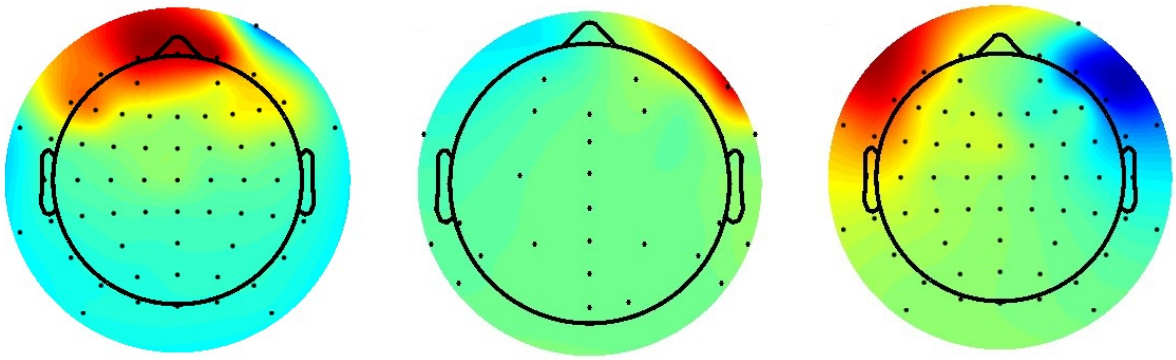

(a) (b) (c)

Figure 3.4: Eye Components (a) Eyeblink (b) Eye movement in right side and (c) Eye movements in both directions.

Figure3.4a shows the effects of the eye blinks reported in this component. The topography of the scalp shows that the component has an approximately equal effect on the electrodes around the eyes. Figure 3.4b shows the effects of the eye movement reported in this part. The topography of the scalp suggests that the source is in or close to the eyes. Figure 3.4c shows the results of horizontal eye movement recorded in these components.

Muscle component

Muscle components define the electrical field, called Electromyography (EMG), and produced by muscle activities. These are powerful in comparison with EEG, but the action poten-

tial of the motor units (the underlying EMG source) is not coordinated, allowing the maximum of EMG power to be distributed through higher frequencies. Such components can still look dipolar, however, but they seem very shallow because they are not located within the brain.

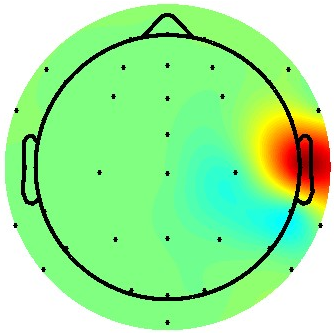

Figure 3.5: Muscle component

Figure 3.5 indicates a component of the muscle. The topography of the scalp suggests a shallow source.

Heart component

Heart components absorb the electric potentials generated by the heart known as electrocardiography (ECG). The cardiac pattern is prevalent and is known as a QRS complex. Those will take place at about 1 HZ. Due to the distance of the head, the scalp map looks like that of a very distant dipole, so it looks like a linear gradient almost.

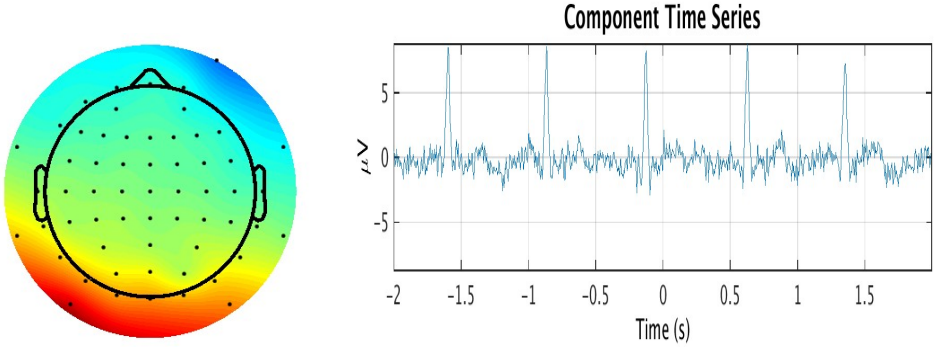

(a) (b)

Figure 3.6: (a) Heart component (b) Component time series.

Scalp topography, as typical of heart components, is a long, approximately linear gradient shown in Figure 3.6a. In the time series plot, a regular QRS complex is immediately visible as shown in Figure 3.6b.

Line noise

Line noise caused by the AC current used for controlling all lighting systems and electronics in the room. It can be 50 Hz in frequency. Although in the data cleaning steps, this noise is usually eliminated by using notch filters before ICA implemented, ICA can isolate line noise if there are enough channels and data to work with. The line noise components are most evident from their sharp peak power spectrum at 50 Hz.

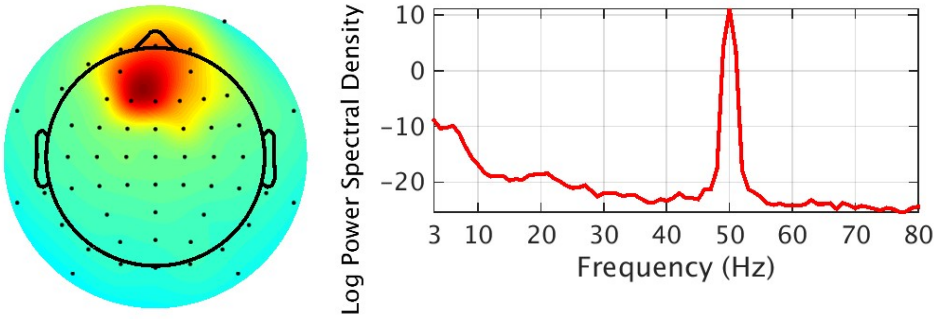

(a) (b)

Figure 3.7: (a) Line noise component (b) Power spectrum of line noise component activations.

The topography of the scalp shown in Figure 3.7a is not informative beyond probable permitting one to guess the direction of the source of line noise. The only accurate indicator is that the power spectrum peak at 50 Hz is enormous, as illustrated in Figure 3.7b.

Channel noise

If during a recording a channel is bumped or if it has poor contact, often significant artifacts will generate which don't affect any other channels. Often ICA separates these into its component, which is channel noise components. It may be challenging to identify these components as much as they can look very close to muscle components, as represented in Figure 3.8.

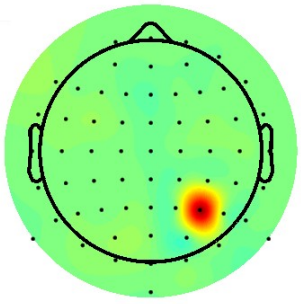

Figure 3.8: Channel noise component

3.6 Sample experimental results

For this study, on the applicability of ICA on electroencephalogram, the EEG consists of 29 signals, recorded by electrodes at a sampling rate of 256Hz. In Figure 3.9, the EEG data with 10s duration has been shown. After ICA applied to the data, the ICA component activation matrix is shown in Figure 3.10. The independent components projected on scalp topography are shown in Figure 3.11,

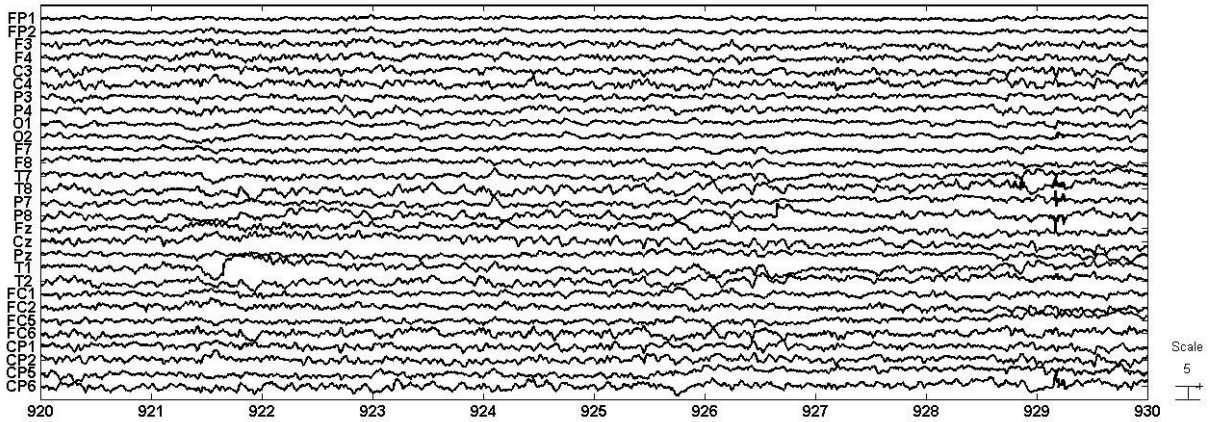

Figure 3.9: 10 seconds of EEG data before pre processing

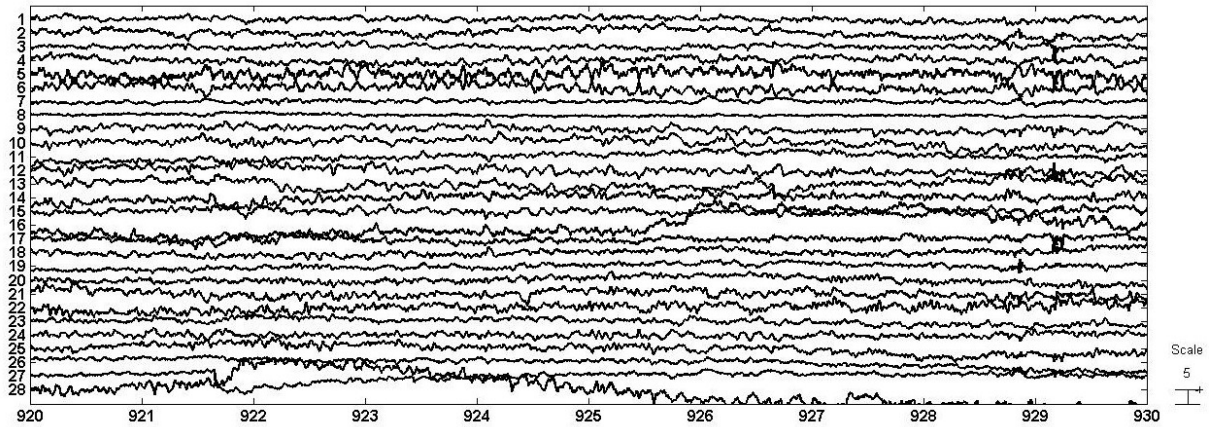

Figure 3.10: Independent Components activations of the corresponding EEG data

The components that are considered to be artifacts are chosen and remove the # IC 5 (shown in Figure 3.12a), # IC 6 (shown in Figure 3.12b), # IC 8 (shown in Figure 3.12c), # IC 11 (shown in Figure 3.12d), # IC 16 (shown in Figure 3.12e), and # IC28 (shown in Figure 3.12f) components from the total components. Then the cleaned EEG data from the remaining ICA components are reconstructed.

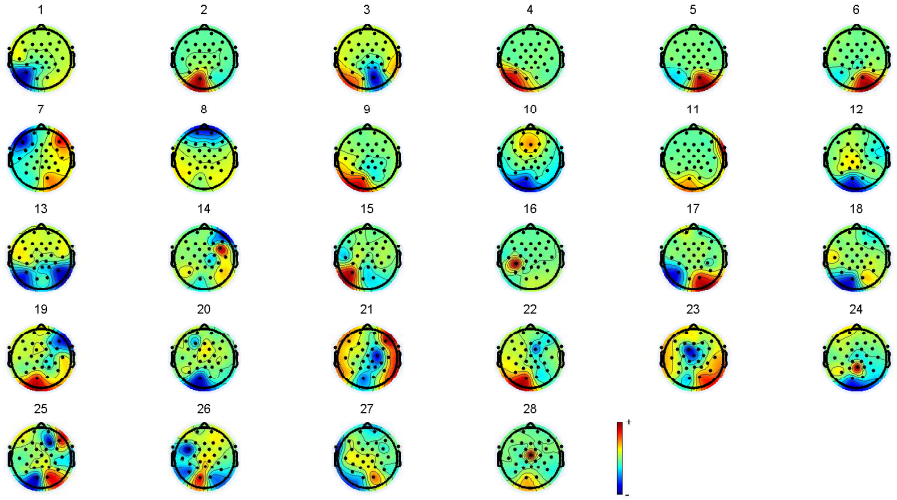

Figure 3.11: Scalp topography of total independent components of EEG data

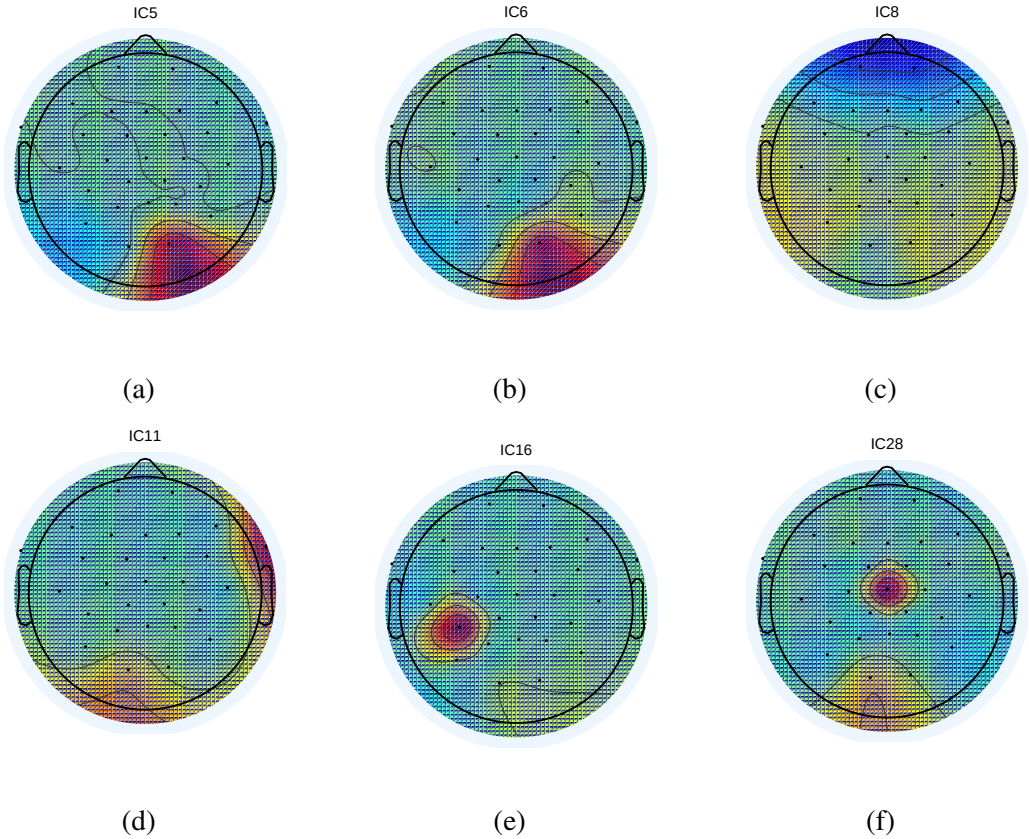

Figure 3.12: (a), (b) Right Occipital artifact (c) Eye movement-related artifacts (d) Muscle artifacts (e), (f) Channel noise related artifact.

The difference between the initial EEG results shown in Figure 3.9 and the results after preprocessing techniques, as seen in Figure 3.13. It can be observed that the artifacts have been deleted, and the data are now accessible for our next steps.

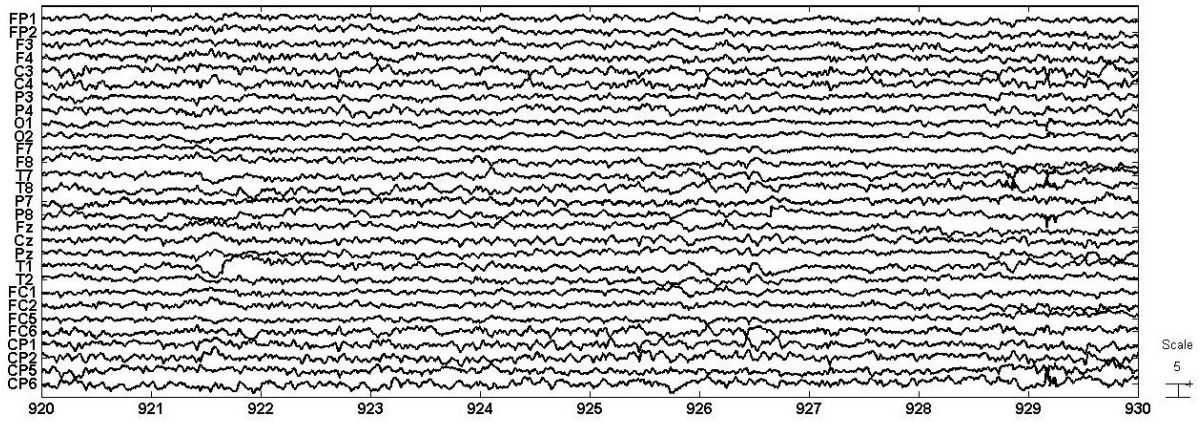

Figure 3.13: Corrected EEG data after removing artifactual components

After the elimination of the artifacts, one independent examiner (Dr. Aditya, Apollo Hospitals, Hyderabad) reviewed the initial samples and EEGs to visually detect the same morphology and the removal of the artifact. Artifact sources were easily identified; in several cases, the collection and removal process had to be repeated several times until each artifact was removed. The removal of the artifact component led to an apparent clearing of the signals in all samples. The examiners decided entirely on the identification and the existence of the artifact and before and after the removal of the artifact.

3.7 Summary

The biomedical signals are a rich source of physiological process information, but are frequently contaminated with artifacts or noise and usually mixes of unknown combinations of sources which sum up in each sensor differently. Therefore, even the existence of the sources is an open problem for specific data sets. EEG data are generally not clean, such that some preprocessing steps are needed. In most simple data analysis, the above-mentioned preprocessing steps are appropriate.

Sometimes, filters like high pass filters added to eliminate the DC components of the signals (with a cutoff frequency of 1 Hz). The high-frequency elements can also be removed with a low-pass filter. For EEG, frequencies above 90 Hz that are similar to the Gamma spectrum are rarely observed. A number of other pre-processing techniques, such as EOG, are needed to apply if the subject is kept open his eyes in the recording since blinks and eye motions produce strong electrical fields that disrupt our EEG records.

Here, we concentrated on ICA applications for the study of EEG signals. ICA is capable of separating individual components from recorded signals. Brain signals captured by EEG are signal mixtures and can thus evaluate with ICA. Specific analysis of components may be very helpful in finding different components that suit different brain generators. Our study findings indicate that ICA can be a valuable method in normal EEGs for detecting and removing typical EEG artifacts without modifying the behavior of data. Once our signals are clean, i.e., preprocessed, then proceed for source localization and connectivity between the sources.

Chapter 4

Localization

4.1 Introduction

Electroencephalography (EEG) is a non-invasive neurological investigative tool used to quantify electrical fields produced by neural development in the cerebrum. EEG-based estimates are used to locate neural action and prompt new medicines, treat stroke, epilepsy, and Parkinson diseases. Neural source localization has been used to distinguish sources of seizure activity in the brain since the position of a seizure between the basal cortex, temporal cortex, and lateral cortex can be separated by a neural dipole moment [145]. This must be accomplished if neural sources can be accurately classified from estimates. This issue referred to as the EEG inverse problem [30].

Moreover, since current dipole models have been used effectively to determine the electrical current appropriation of the cerebrum, the inverse problem can be used to approximate the factors from EEG observations of localized current dipole cerebral sources [146]. Even though EEG yields high temporal resolution when observing cerebral activity, high spatial resolution is also required for effective diagnostics. As a result, different sensors are placed over the whole scalp, and advanced filtering techniques are used to find an ideal solution to the inverse problem [34, 147].

To know how the cerebrum works, first see how the scalp produces EEG observations. The primary sources of EEG voltages measured at the scalp derive from the current movements of many of the adjacent neurons that coincide in the same direction. In an activated area of the cerebrum, the aggregate electrical current is displayed regularly as a numerical current dipole with a sufficient dipole moment in that area. Furthermore, many of these present dipoles speak to current streams of similar orientation and can be replaced by an equivalent current dipole [99].

Currently, two major research areas exist in modeling neural generators. The first modeling technique involves utilizing imaging models, which clarify the information using a thick arrangement of current dipoles circulated at settled areas. A second method is a parametric approach that takes advantage of the fact that these dense sets of current dipoles can be supplanted utilizing one equal current dipole [21]. Although the imaging-based techniques can create a precise map of the cerebrum's neuronal activity, the parametric methodology provides a direct mapping of the EEG measurements to a few parameters [22]. By using the parametric approach, the equivalent current models can provide more intuitive interpretations that explain the electrical activity in the cerebrum and can be fostered in emerging technologies, such as BCI systems.

An essential challenge of the parametric methodology is the estimation of the areas of the equivalent dipole sources in the 3D volume of the cerebrum utilizing EEG estimations recorded from the scalp. Most of the previous work [23, 24, 26, 27, 28, 29, 148] in EEG source localization is based on two assumptions (1) the quantity of dipoles is fixed (2) the locations of the sources are fixed in time.

In general, however, the quantity and positions of neural dipoles vary dynamically over time. In [30], the number of neural dipoles and their locations are dynamically evaluated and updated at every step described from the measured data. The unknown source positions and moments can be taken as the hidden state function, and EEG data is considered as the state-space model's measurement function. The optimal estimation of the hidden state in a Bayesian context depends on the state's posterior density function (pdf) given in the observations [149].

The Particle Filter (PF) is a sequential Monte Carlo procedure that uses Sequential Importance sampling to approximate the state's posterior distribution at each step [32]. Particle filter uses particle arrangement to sample the framework's state-space. These particles are then weighted utilizing the measurement model to give a measure of the state posterior density. These weights fit in with the improvement of the system activities concerning time. Particle weights are repetitively updated whenever new measured information is available to anticipate the framework's future condition. The particle filter is suffering from particle degeneration after a few iterations where many particles will have small weights. This implies that with a minimal number of iterations, most particles will have irrelevant loads and, thus, the arbitrary measure they determine is undependable. Several resampling algorithms are suggested in the particle filter system to overcome particle degeneration. Resampling considered to be a bottleneck in implementations due to the increasing complexity. Advanced resampling algorithms proposed to deal with such difficulties.

In this chapter, the different methods of resampling for identifying neural sources hd been examined. The primary focus on the performance of time-efficient partial stratified resampling, branching resampling and minimum sampling variance methods in the particle filter to estimate the location of neural sources from EEG data and conduct a comparative analysis of these methods with conventional resampling algorithms i.e., multinomial, systematic, residual and stratified resampling methods [89, 96]. Our goal is to verify whether and to what extent each method of resampling can use synthetic data to locate dipole sources. Our study aims to provide a comparative analysis of localizing neural sources with particle filter using different methods of resampling to analyze real EEG data.

4.2 EEG source localization model

The localization of neural sources from the measured EEG data, which is called the inverse problem, is one of the most critical issues for electrophysiology. An inverse problem solution can provide us with a model that maps generators to the recorded projections. The inverse problem is to determine the exact functional tomography by identifying the source with minimum error. Nonetheless, the main challenge for this issue is that there is not enough information on generators in the measurements to make the problem inconsistent and, therefore, does not provide a perfect tomography. This is because various configurations of internal sources produce the same external electromagnetic field, and only a relatively small number of locations calculate these fields [150].

The origin of the EEG signal is closely related to the fundamental mechanism of neuronal interaction, including a synapse. Intracellular space is electrically isolated from its surroundings by the insulating cell membrane. The intracellular environment compared to the extracellular is negatively polarized (the membrane potential in the resting state is usually around -70 mV) due to a disproportionate distribution of Na+, K+, and Cl- ions across the membrane at the resting state.

A synapse is a functional link between two neurons, which enables the transmission of signals between them. When the presynaptic axon terminal of an active neuron receives an action potential (AP), particular molecules called the 'neurotransmitters' is released through the synaptic gap between neurons. Such molecules bind to particular transmitter-gated proteins (receptors) on the other neuron postsynaptic terminal. The receptors are appropriate for the specific ion community as a result of such an interaction. The ion transfer around the cell membrane produces a possible postsynaptic potential. The influx of positive ions i.e., Na+,

K+ into the cell creates an EPSP, which results in depolarizing membrane potential and thus increasing the likelihood of AP generation. In contrast, negatively charged ions (Cl-) have an IPSP result in hyperpolarizing membrane potential and thus reducing the likelihood of AP generation. During EPSP, the incoming movement of ions produces a local "sink" (lack of positive ions near the apical dendrites). Simultaneously, the ions are redistributed in the neuron. This causes the membrane to depolarize near the cell body and, as a result, to flow outwards of positive ions (return current). It produces an extracellular 'source.' Therefore, the 'sink' (have negative polarity) and 'source' (have positive polarity) form the potential difference that allows an electrical current to pass through the volume conductor. Such extracellular fields around the neuron can be modeled as dipole and give rise to the potential measured with Scalp EEG [34, 151]. It should be noted that given the undoubtedly significant function of EPSP, IPSP currents can also generate extracellular potential [152, 153]. There is even less electrical potential in a single neuron to be observed on the scalp with EEG [37]. Electrical fields from individual neurons summed up during stimulation of the neuronal population, and the resulting domain can be calculated by electrodes [154].

To sum up, EEG detects the superposition of post-synaptic activity in cortical populations entering the scalp surface because of the volume conduction. When modeling electrical neuronal activity based on extra-cranial measurements, this physiological process forms the basis for various mathematical approaches.

The brain cortex, which is the outer surface of the brain, contains 10 billion neurons. The most observed scalp activity occurs within this 1.5 to 4.5 mm thick part of the brain. The synchronous, synaptic simulation of a large number of neurons [155] guides the dipole current source onto the cortical surface. The measured EEG is simply the distribution of this current on various electrodes. To model the EEG data using the forward problem [156], it is essential to quantify the relationship between the distribution of different primary dipoles and the data collected on electrodes. The brain sources need: i) EEG data, ii) scalp electrode 3D position data, iii) Head model information on the electrical and geometrical properties of the head and iv) Source Model information on the location/orientation of dipole sources. The accurate measurements of electric fields in the brain were provided with realistic head models using the spherical Head Model, Boundary Element Method (BEM), or Finite Element Methods (FEM) [157]. The efficiency of EEG improves with the inverse solution by increasing accuracy in the definition of the head structure with related conductivity.

The primary current distribution used to model the neural activity generating the electromagnetic field calculated by EEG that is approximated by the superposition of an unknown

number of the current dipole. We use the current dipole model in this work, where neural current is modelled as a small collection of point sources or current dipoles; each dipole reflects the behavior of a small patch of the cortex of the brain as a single-point localized electric current. A present dipole is a six-dimensional object: three coordinates describe the position of the dipole inside the brain, three more coordinates define the orientation of the dipole and strength (the dipole moment). In dipole theory, the pair $(r^{'}, q)$ indicates a single dipole, where $r^{'}$ is the integer variable that is the dipole position in a given discrete source space and q the dipole moment is the three-dimensional vector. A dipole moment is a measure of the two opposite electric charges separation. Moments of the dipole are a vector quantity. The magnitude is equal to the charge multiplied by the distance from the negative charge to the positive charge. This is illustrated in Figure 4.1.

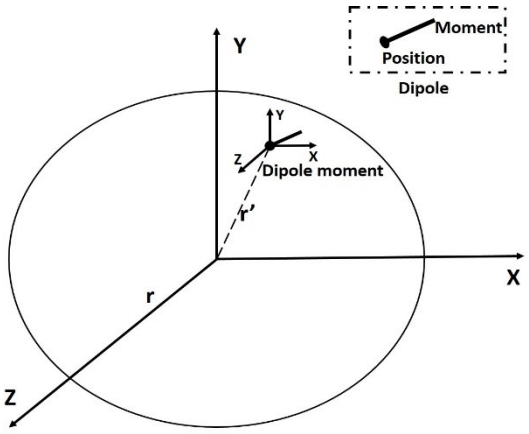

Figure 4.1: Dipolar position and moment coordinate system for the spherical head model. A dot shows a dipole position, and a tail represents a dipole moment with an orientation and strength.

In MEG and EEG, the useful frequency spectrum is usually less than 1 kHz for electrophysiological signals, and most of the literature covers frequencies between 0.1-100 Hz. Therefore, a quasi-static approximation in Maxwell's equations can be defined as mechanically in MEG and EEG. Maxwell's equations are complied with by electromagnetic fields in the cerebrum. The magnetic field calculated is a linear combination of the magnetic fields that each dipole induces. Let us consider the neural development arises at some point in the cortex positioned at $r^{'}$ and observing the measurement at the sensor location r on the skull. The static magnetic field equations are $\nabla \times b\left(r^{'}\right) = \mu_0 J\left(r^{'}\right)$ the curl of the magnetic field at the location $r^{'}$ is proportional to the current density, and $\nabla \cdot b\left(r^{'}\right) = 0$ the divergence of the magnetic field is zero. In a closed volume of finite conductivity's, we are looking for current density. The conductivity and current density outside this volume are zero. The current density $J\left(r^{'}\right)$ of a head volume at the location $r^{'}$ is related to magnetic field $B(r)$ at location r is given by the Biot-Savart equation [22, 147]:

$$B(r) = \frac{\mu_0}{4\pi} \int J\left(r^{'}\right) \times \frac{r - r^{'}}{|r - r^{'}|^3} dv' \tag{4.1}$$

Here, the magnetic permittivity of vacuum is denoted by μ_0, and it is steady inside the volume as well. In (1), the current density $J\left(r^{'}\right)$ consists of two parts: the 'primary' current $J^p\left(r^{'}\right)$is the source of neural activity, and the volume current is a result of the interaction of the primary current within a conductive medium $J^v\left(r^{'}\right) = \sigma\left(r^{'}\right)\ E\left(r^{'}\right)$. The $J^p\left(r^{'}\right)$, can be modeled as a point source given by an equivalent current dipole as $J^p\left(r^{'}\right) = s\delta\left(r - r^{'}\right)$ with moment $s = \int J^p\left(r^{'}\right)$. The total current density in the head volume is given as,

$$J\left(r^{'}\right) = J^p\left(r^{'}\right) + J^v\left(r^{'}\right) = J^p\left(r^{'}\right) + \sigma\left(r^{'}\right) E\left(r^{'}\right) = J^p\left(r^{'}\right) - \sigma\left(r^{'}\right)\ \triangledown V\left(r^{'}\right) \tag{4.2}$$

Where $\sigma\left(r^{'}\right)$ is the conductivity profile of the head tissues, the electric field $E\left(r^{'}\right)$ is the negative gradient of the electric potential $V\left(r^{'}\right)$.

Assume that the head consists of a set of concentric layers with isotropic conductivity of $\sigma_i, (i = 1, 2, 3)$, which is the brain, skull, and scalp. Now the Biot-Savart theorem can be rewritten as a sum of primary and volume currents [8]:

$$B(r) = B_0(r) + \frac{\mu_0}{4\pi} \sum_{ij} \sigma_i - \sigma_j \int_{S_{ij}} V\left(r^{'}\right) \frac{r - r^{'}}{|r - r^{'}|^3} \times dS'_{ij} \tag{4.3}$$

Here $B_0(r)$ is the magnetic field is only because of the primary current. The second term refers to the contribution to the magnetic field from volume current, which constitutes a surface integrals across the boundaries between brain-skull, skull-scalp, and scalp-air.

The general equation states that if we consider the primary current and the potential $V\left(r^{'}\right)$ on all surfaces, the magnetic field can be measured. The potential can be calculated similarly, although the derivation is somewhat difficult [147, 158] and is given as,

$$\left(\sigma_i + \sigma_j\right) V(r) = 2\sigma_0 V_0(r) - \frac{1}{2\pi} \sum_{ij} \sigma_i - \sigma_j \int_{S_{ij}} V\left(r^{'}\right) \frac{r - r^{'}}{|r - r^{'}|^3} \cdot dS'_{ij} \tag{4.4}$$

Where $V_0(r)$ is the electric potential at location r because of primary current distribution on the surface S_{ij}. Therefore, these two equations are essential solutions to the forward problem. The primary current distribution is defined as $J^p\left(r^{'}\right)$. A primary electric field and a primary magnetic field can be measured by using,

$$V_0(r) = \frac{1}{4\pi\sigma_0} \int J^p\left(r^{'}\right) \cdot \frac{r - r^{'}}{|r - r^{'}|^3} dr') \tag{4.5}$$

$$B_0(r) = \frac{\mu_0}{4\pi} \int J^p\left(r'\right) \times \frac{r - r'}{|r - r'|^3} dr' \tag{4.6}$$

The primary potential $V_0(r)$ for all surfaces is then applied to solve Eq.4.4 and addresses the forward EEG problem. So for external magnetic fields, these surface potentials $V(r)$ and the primary magnetic field $B_0(r)$ are used to solve Eq.4.3.

The closed-form solution for forward models of heads that have conductivity profiles, which can be modeled as nested concentric spheres. In reality the head models is not spherical. The spherical models work well for the MEG measurements rather than EEG because it affects the volume currents [159].

To solve equations 4.3 and 4.4, need to extract surface boundaries from MR or CT images for the brain, skull, and scalp. There are several automated and semi-automated methods for extracting surfaces from MR images [160]. The surfaces can then be used in the estimation of the forward fields using the boundary element method (BEM). Usually, BEM methods are very time consuming; if implemented as part of an iterative inverse solution, these approaches may seem impractical. Indeed, BEM can be made very realistic for MEG and EEG applications by the use of fast numerical methods, pre-calculation, and interpolation of pre-calculated fields [161].

One problem remains: these methods need to know the conductivity of the head. To develop a solution for the source localization model in EEG and to calculate the scalp potentials of the dipole, we use the Scalp–Skull–Brain head model, the concentric nested sphere head model of the three layers. The electrical conductivity of each layer is $\sigma_i, (i = 1, 2, 3)$, and differs among layers. The conductivities 0.3300, 0.0042 and 0.3300 s/m correspondingly [156]. The BEM just relies upon the head geometry and conductivities. This volume current can be approximated using forward calculation [157, 162, 163].

The present dipole is an augmentation of the model of the combined charges dipole in electrostatics. Note that cerebral action does not comprise discrete arrangements of physical current dipoles, but instead, the dipole is a helpful portrayal of the intelligible interaction of many cells. The present dipole model is the core of EEG behavior because an essential current source of an arbitrary amount can only separate into small regions, where every area is summarized by a proportionate current dipole [164].

Computation of the scalp potential requires a particular source to demonstrate that must be understood numerically. In case that the model relies upon realistic head shapes, the calculation might be a positive test. Such models are mechanically utilized as a part of most extreme clinical and study bundles aimed at EEG source localization.

The EEG inverse problem is to recover the primary current distribution $j^p(r)$ from noisy measurements of the field b, at any given sampled time point. The imposition of the inverse problem means that the neural currents cannot be precisely reconstructed from the measured information. More precisely, many (infinitely many) neural current configurations exist due to the non-uniqueness of the solution, generating exactly the same data. The goal of inverse problem algorithms is to choose the best solution from the infinite set of solutions. In fact, such a selection is partly performed a priori, by using specific models for the neural currents. Two alternative models were used in recent decades for solving the inverse problem: a distributed source source model, in which neural current apparently represents a continuous vector field, and a focal source model, which is believed to superpose neural current to a small number of focal sources, each of which is representative of the behavior of a single region of the brain. To solve inverse problem, which is described by computational approach

$$b = \wedge.j \tag{4.7}$$

where b is a data vector containing a field determined on all sensors at a given time point, $\wedge$ is a Biot-Savart operator's grid discretization (also called the lead field matrix) and a j is the discretization of the current field.

A single current element is used in the focal source model to reflect a whole active region; the current dipole, which has the form, is the most commonly used model given in equation 4.7. The current dipole is also the simplest current factor possible and can be considered as the first-order moment of any distribution of electrical current.

The neural current can be represented by a set of N dipoles under realistic conditions, with multiple brain regions activated is given as,

$$j^p(r) = \sum_{i=1}^{N} q^i \delta\left(r - r^i\right) \tag{4.8}$$

The parameters of the neural current to be calculated from the data in the parametric method are then the number of sources N, the source positions $r^i, i = 1, 2, \ldots, N$, and the dipole moments $q^i, i = 1, 2, \ldots, N$ are given at a given time point. As the number of dipoles N is unknown, the

state-space of the unknown primary current j is defined as $j = (r_1, q_1, \ldots, r_N, q_N)$. The i^{th} dipole moment is defined as $q_k^i = \left(o_k^i, s_k^i\right)$. Where o_k^i is the 3-dimensional orientation vector and s_k^i is the amplitude of the dipole.

Let z_k be the set of EEG measurements at time k, taken from the scalp with the number of sensors N_s. Each $z_k = \left(z_k^1, \ldots z_k^{N_s}\right)$, where i^{th} element is the measurement at time k by i^{th} electrode. The EEG data collected by N_s electrodes defined as

$$z_k = \sum_{i=1}^{N} L\left(x_k^i\right) s_k^i + v_k \tag{4.9}$$

here v_k is a white Gaussian noise with variance σ_v^2, $L(.)$ is a lead field matrix and x_k^i is a source parameters vector which consists of dipole location, the orientation of the i^{th} dipole at time k. $L(.)$ depends on i th dipole location r_k^i and i^{th} dipole orientation o_k^i at time k. While $L(.)$ gives an estimate of the source distribution in the cortical space that is reasonably precise, it is artificially discretized to a small number of fixed positions. The leadfield matrix (the source signal) for dipole i is denoted by $L\left(x_k^i\right) \in R^{n_s \times 3}$. A combination of Head geometry, electrode positions, and dipole localization gives the non-linear function $L\left(x_k^i\right)$. Sensors measure the electrical activity due to dipole source. And these dipole sources contain unity moments along x, y, and z directions. These have zero moments in other directions. Using [156], a lead field matrix $L(.)$ at time step k was developed byusing the following equation

$$\begin{aligned} L_{k,m,j} = \frac{1}{4\pi\sigma} cos(\theta_{k,j}) \times \left[\frac{2}{d_{k,m,j}^3} \left(|\Gamma_{k,j}| cos(\gamma_{k,m,j}) - r \right) + \left(d_{k,m,j} |\Gamma_{k,j}| \right)^{-1} - \left(r |\Gamma_{k,j}| \right)^{-1} \right] \\ + \frac{1}{4\pi\sigma} sin(\theta_{k,j}) sin(\beta_{k,j}) sin(\gamma_{k,j}) \times \left[\frac{2r}{d_{k,m,j}^3} + \frac{d_{k,m,j} + r}{r d_{k,m,j} \left(r - |\Gamma_{k,j}| + d_{k,m,j} \right)} \right] \end{aligned} \tag{4.10}$$

here r is the radius of the head model, $d_{k,m,j}$is the distance between the j^{th}dipole source and the m^{th}sensor, $\gamma_{k,m,j}$ is the angle between the vector pointing to the m^{th} sensor and the vector pointing to the j^{th} dipole location, $\theta_{k,j}$ is the angle between the j^{th} dipole orientation and the vector pointing to the j^{th} dipole location, $\beta_{k,j}$ is the angle between the plane formed by the j^{th} dipole and the origin, $|\Gamma_{k,j}| = \sqrt{\left(r_{k,j}^x\right)^2 + \left(r_{k,j}^y\right)^2 + \left(r_{k,j}^z\right)^2}$ and σ is the head tissue conductivity constant.

To compute the forward model 'z_k', a priori knowledge of head geometry, electrode position is necessary. It is possible to obtain the probability of every measurement from 4.9 using,

$$p(z_k | (x_k, s_k)) \propto exp\left\{ \frac{(z_k - L(x_k)\, s_k) R_{z_k}^{-1} (z_k - L(x_k)\, s_k)}{2} \right\} \tag{4.11}$$

where R_{z_k} is the covariance matrix of z_k, the objective is to estimate the location of the sources using given measurements z_k.

The x_k states to be calculated are the geometric locations and neural activity signals of N dipoles in the PF framework of the dipole localization problem. We don't have a dipole position or signal information a priori. In fact, such a model is accurate, notably for characterizing brain sources of atypical brain function, such as epilepsy seizures. Therefore in the source localization space, we consider the state transition to be a random walk model (first-order Markov chain). A random walk model does not presume any knowledge of the source positions and moments a priori.

$$x_k = x_{k-1} + u_k \tag{4.12}$$

where u_k is a zero-mean, Gaussian white noise with $\sigma_u^2 I$ covariance, where the I is identity matrix denoted. The u_k is considered to be independent of past and present states. The whole state-space model of the problem of dipole reconstruction is thus as follows:

$$\begin{cases} x_k = x_{k-1} + u_k & \text{state transition model} \\ z_k = L(x_k)\, s_k + v_k & \text{observation or measurement model} \end{cases} \tag{4.13}$$

From the above equations, the EEG can model as a state-space model. To evaluate the dynamic parameters (i.e., location in x, y, and z directions) in the cerebrum, the PF is used by considering the measured signal z_k at time point k.

4.3 Inverse model

To calculate the dipole parameters from the measured signal the inverse problem has to be solved; inverse problem is emerging from the forward model. There are several sources inside the skull that provide the same data that have been measured, and the problem is that there is not a unique solution. The objective is to find a meaningful solution among the many solutions which are mathematically correct. Over the last two decades, methods of determining the source from the EEG signal obtained have been used widely to derive a single source estimation. But it remains a challenge to determine the distribution of the source. The most popular methods i.e., MNE, sLORETA, etc. used to identify electrical sources in EEG presume there is no temporal component of electrical sources inside the brain. The source parameters are used to estimate at each point in time, but there is no connection with the previous time point. These methods are constrained to fixed dipole assumptions and cannot predict the source activity variability.

These approaches are constrained in their ability to integrate problem-specific anatomic or physiological information by considering a static placed dipole. It is very common to assume that the source varies rather than is constant in time. Using a time variable source model, we will investigate at each point in time the source distribution and provide variability estimates. In the context of this notion, a state-space model is used for the time evolution of the source. Our aim is to find the source parameters posterior distribution. A predictive dipole model is the consequence of our reformulation of the inverse problem. It brings out that our predictive model's posterior distribution of sources can be viewed as an analytical solution to the inverse EEG problem.

The Bayesian methods project the problem overall rather than look for the single optimal solution and estimate the entire posterior probability density function. Estimation of dipole parameters can be considered as the Bayesian problem, and for sampling, the posterior distribution Markov Chain Monte Carlo method has been used [166].

In the Bayesian filtering, The posterior density at time point k is calculated with the posterior-density at time $k-1$ which relates to the dynamic problem is computed in a two-step procedure: in the *evolution* step, the prior density at time point k is calculated from the posterior density at time $k-1$; in the *observation step*, the posterior density at time k is computed from the prior at time k . The Bayesian filtering algorithm leads to the popular Kalman filter, under linear Gaussian conditions. In [23], the authors consider the inverse problem as a complex one and apply Kalman filtering to a linear distributed source model. If Bayesian filtering is used to approximate the parameters of EEG data point sources, the non-linear dependence of sources prevents the use of Kalman filters. It involves an approximation technique to monitor the time-specific sequence of posterior densities. A particle filter [31, 32] is used to investigate the posterior densities due to the model's non-linearity.

4.3.1 Nonlinear Bayesian tracking

Two elements describe a Bayesian tracking problem [32, 149]:

1. The state model: defines the state's evolution with time $\{x_k\}$, initial distribution is defined as $p(x_0)$ and the transition equation is given as $p(x_k|x_{k-1})$.
2. The measurement model: describes the noisy measurements correlated with the state model. This can be written as $\{z_k\}$, it is meant to be based on $\{x_k\}$ and the measurement equation is given as $p(z_k|x_k)$.

These models can be used in a probabilistic context, in a filtering context, and in the following forms, models are given [89]:

$$x_k = f(x_{k-1}, u_k) \leftrightarrow p(x_k|x_{k-1}) \tag{4.14}$$

$$z_k = h(x_k, v_k) \leftrightarrow p(z_k|x_k) \tag{4.15}$$

where x_k consists of N number of unidentified parameters (locations of the sources in EEG model) at time k, z_k contains N_s number of observations (EEG measurements) at time k, $f(.)$ and $h(.)$ are considered to be nonlinear functions where $f(.)$ is related to state-transition and $h(.)$ relates to the state vector along with the observation vector, u_k is the state model error, and v_k is the observation noise.

The Bayesian method is based on all available information, such as the knowledge of the system or collections of observations, to construct a state's posterior probability density function. An optimal estimate of the state can be obtained in principle (with regard to any criterion) [32]. A filtering approach is used to estimate the state recursively. According to [32], it ensures that data collected should be sequentially processed rather than as a batch such that a full data set cannot be stored nor the data re-processed if new measurements are available.

In this model, to evaluate source parameters x, consider the posterior probability density of the x based on the EEG measurements can be written in terms of Bayes theorem as:

$$p(x|z) = \frac{p(z|x)\, p(x)}{p(z)} \tag{4.16}$$

where $p(x)$ is the probability distribution of source parameters x, the encoding of all unknown information available before measurement. $p(z|x)$ is the probability function, including the forward model information and the statistical noise characteristics.

4.3.2 Particle filter

Stastical model

The unknown and the observations are modeled as Random Variables in the Bayesian approach to inverse problems and the solution is the entire posterior probability density function of the unknown, obtained by the Bayes theorem. In the case of dynamically inverse problems, a two-step algorithm known as a Bayesian filtering is mediated by the sequential implementation

of the Bayes theorem, which involves a prior density in each step and the use of Chapman-Kolmogorov equation.

Let x_k and z_k be the realizations of X_k and Z_k, the primary current distribution and the measures data at k, in the EEG application. Assume that the X_k is the stochastic process of first order Markov process, Z_k is with respect to X_k. The conditional posterior probability distribution $p(x_k|z_k)$ can be estimated using recursive Bayesian filter using two steps, based on the complete probability formula:

1. Prediction: the state model is used for calculating the prior pdf of the current state at time k using the Chapman–Kolmogorov equation:

$$p(x_k|z_{1:k-1}) = \int p(x_k|x_{k-1})\, p(x_{k-1}|z_{k-1})\ dx_{k-1} \tag{4.17}$$

2. Update: the new measurement available at time k is used to update the prediction pdf using the Bayes law:

$$p(x_k|z_{1:k}) = \frac{p(z_k|x_k)\, p(x_k|z_{1:k-1})}{\int p(z_k|x_k)\, p(x_{k-1}|z_{1:k-1})\, dx_k} \tag{4.18}$$

where $p(x_k|x_{k-1})$ is the transition kernel of the stochastic process underlying the data. It is expressed in the dynamics of brain sources in general assumptions such as temporal continuity. $p(z_k|x_k)$ is the likelihood function defined by the forward model and the noise statistics. Equations 4.17 and 4.18 are used to construct a prediction-update process. This helps us to recursively obtain the state's posterior probability density function. From $p(x_k|z_k)$ the estimation of source parameters such as location and amplitude of the dipoles can be computed. The posterior probability density function is, however, typically hidden and cannot be obtained easily. The above equations preserve the parameters of a current dipole set independently of the source and forward models, used in particle filters.

In Bayesian filtering, when applied to EEG inverse problem, in the course of time, neural sources might emerge, become stronger, shift, weaker and vanish. The primary current at time k is usually a collection of N dipoles and it is given as, $X_k = \{R_k, Q_k\} = D_k$. Where the dipole locations $R_k = \left\{r_k^1, \ldots r_k^N\right\}$ and dipole moments $Q_k = \left\{q_k^1, \ldots q_k^N\right\}$ denoted respectively. For a single dipole, it is represented as $d_k^1 = (r_k^1, q_k^1)$.

We model the primary current as an RFS [167] of dipole in order to apply Bayesian filtering. RFSs, like RVs, have density functions for probability. Bayesian filtering equations 4.17

and 4.18 applies to RFSs, as long as the integrals concerned are known as specified integrals [Voet et al., 2005]. Here X_k is the realizations of RFS. The Bayesian filtering equations now interpret:

$$p\left(X_k|z_{1:k-1}\right) = \int p\left(X_k|X_{k-1}\right) p\left(X_{k-1}|z_{k-1}\right) dX_{k-1} \tag{4.19}$$

$$p\left(X_k|z_{1:k}\right) = \frac{p\left(z_k|X_k\right) p\left(X_k|z_{1:k-1}\right)}{\int p\left(z_k|X_k\right) p\left(X_{k-1}|z_{1:k-1}\right) dX_k} \tag{4.20}$$

The actual implementation of Bayesian filters includes the understanding of three functions of probability density: the very first prior density for initializing the algorithm, the likelihood function and transition kernel of the equations given above. Since we believe that only N_{max} dipole can be simultaneously involved, N_{max} probability measures are sufficient to describe the reliable estimation.

- Prior density: The first prior density must be specified however the last density is determined automatically using the algorithm at $k > 1$. Since we have no prior knowledge of the number of sources, the marginal likelihood $p(|X_1| = i) = (1/(N_{max} + 1)), i = 1, 2, \ldots N_{max}$, where $|X_1|$ is the number of sources in set X_1 and N_{max} is maximum the number of simultaneous sources allowable. As we presume simultaneous dipoles are independent, the prior density for a single dipole is sufficient to evaluate. In the brain volume, the prior for the dipole locations is uniform; we note that dipole locations are limited to a finite set of values for computational reasons. In the sphere, the prior for dipole orientation is uniform, and log uniform is the prior for dipole power. We use a uniform brain volume distribution for r_1 locations, and we use a zero-mean Gaussian distribution $N(0, \gamma_q)$ for dipole moments q_1, where the standard deviations γ_q is order of magnitude of the expected sources.

- Likelihood function: The data sequence can be modeled with Random Vectors Z_k since the dimension of the measurement vector is fixed. The forward operator, denoted as $L(.)$, relies on the volume conductor properties. The model contains Additive Noise V_k:

$$Z_k = L\left(X_k\right) S_k + V_k \tag{4.21}$$

the probability or likelihood function function is $p(z_k|X_k) = N(z_k - L(X_k), \sigma_{noise})$where the standard noise deviation σ_{noise} is determined by the pre-stimulus period.

- Transition kernel: A transition kernel based on a random walk codes our lack of information about true dynamics of the neural origins. Furthermore the probability of transitions between sets of different dipole numbers are consistent. In our model, a new dipole can emerge at any point of time and previous dipoles can disappear; in addition, dipole positions, orientations and strengths can change. The transition density thus accounts for the probability of dipole birth, dipole death and dipole parameter evolution. The evolution of a dipole set with N dipole in time k is governed by: a new dipolar source can emerge each time with probability p_{new} and density π_{new}, with probability p_{dis} an existing dipole can vanish, or with probability $1 - p_{dis}$ an existing dipole can persist and evolve according to a single-dipole model $\pi(d_{k+1}|d_k)$ evolution. It is assumed that all these events are independent. The model equation in terms of RFSs

$$X_{k+1} = S(X_k) \cup X_{k+1}^{new} \tag{4.22}$$

  $S(X_k)$ is the RFS of survived and evolved dipoles, where X_{k+1}^{new} is the RFS for the new sources, containing at most one new dipole. Assuming dipole evolution is independent, the probabilities p_{new} and p_{dis} along with the single dipole development model $\pi(d_{k+1}|d_k)$ and density $\pi_{new}(d_{k+1})$ can be demonstrated to completely evaluate the beliefs measure and hence the transition kernel in equation 4.19.

  - the probability that N dipoles are included in the dipole set at time $k + 1$ is 1/3; the probability that $N + 1$ dipoles are contained is 1/3; the probability that $N - 1$ dipoles are contained is 1/3
  - If there are $N - 1$ dipoles in the dipole range at time $k + 1$, the dipole to be excluded is randomly chosen from the set
  - If there are $N + 1$ dipoles in the dipole set at time $k + 1$, the current dipole is taken from the same distribution as the prior initialization
  - The model of single-dipole evolution, which is a random walk inside the volume of the brain. The Gaussian densities $\pi(r_{k+1}|r_k) = N((r_{k+1} - r_k), \gamma_r)$ and $\pi(q_{k+1}|q_k) = N((q_{k+1} - q_k), \gamma_q)$, which have standard deviations of $\gamma_r = 0.5cm$ and $\gamma_q = 2nAm$, is charecterized by the transition kernel $\pi(d_{k+1}|d_k)$ for single dipole.

Computational algorithm

As the EEG forward problem is non-linear with respect to the dipole position, only numerically equations 4.19 and 4.20 can be solved. Here we have applied a sequential Monte Carlo technique called particle filter in order to obtain each step by discretizing equations 4.19

and 4.20 of a sample set ('particles'), distributed according to posterior density and adding a sampling stage, reducing the amount of unlikely sample points. The following is the general scheme of the particle filter we apply.

Draw N_p random samples (particles) $x_k^{(i)}$ with respective weights $w_k^{(i)}, i = 1, 2, \ldots N_p$, as an alternative to a posterior PDF. When the number of samples (particles) increases, the predictions get close to the PDF's functional description. Thus we approximately get the sample-based posterior PDF:

$$p\left(X_k|z_{1:k}\right) \approx \sum_{i=1}^{N_p} w_k^{(i)} \delta\left(X_k - x_k^{(i)}\right) \tag{4.23}$$

$\delta(.)$ is the Dirac delta function, with the sum of all weights should be equal to 1 i.e., $\sum_{i=1}^{N_p} w_k^{(i)} = 1$. The weights are selected according to the importance sampling principle [32]. The importance sampling assumption gives that it is possible to obtain samples from the posterior by sampling from a suitable proposal distribution and applying importance sampling corrections. Drawing samples from $p(X)$ are challenging, but from $q(X)$, which is proportional to $p(X)$, can be determined. Also, let $x^{(i)} \approx q(X), i = 1, 2 \ldots N_p$ samples generated from the importance density $q(.)$. Choose an importance density to make it close to the posterior density such that $q\left(X_k|z_{1:k}\right) = q\left(X_k|X_{1:k}, z_{1:k}\right) q\left(X_{k-1}|z_{1:k-1}\right)$ having the weights as $w_k^{(i)} \propto p\left(x_t^{(i)}, z_{1:k}\right)/q\left(x_k^{(i)}, z_{1:k}\right)$.

In order to make a particle filter work in practice, a good importance distribution is important. Instead of drawing randomly from the brain when birth is indicated, the new dipole position is sampled according to a heuristic distribution dependent on the data. Although the closeness of this distribution to the optimum importance distribution can affect the variance of the estimator, the sampling correction of importance guarantees that under very mild conditions we achieve consistent estimate (in the number of particles). A death is suggested with nearly the greatest probability, unless a birth is proposed. We suggest using the following importance distribution:

$$\begin{aligned} q(x_k|x_{k-1}, z_k) = p_{new} \times q(r_k^{N_k}, q_k^{N_k}|z_k, x_{k-1}) \times \prod_{n=1}^{N_{k-1}} \delta_{r_k^n, r_{k-1}^n} N(q_k^n, q_{k-1}^n) \\ + p_{dis}(x_{k-1}, z_k) \times \sum_{n=1}^{N_{k-1}} \pi(d_k^n|d_{k-1}, x_k) \times \prod_{n=1}^{N_{k-1}} \delta_{r_k^n, r_{k-1}^n} N(q_k^n, q_{k-1}^n) \\ + (1 - p_{new} - p_{dis}(x_{k-1}, z_k)) \times \prod_{n=1}^{N_{k-1}} \delta_{r_k^n, r_{k-1}^n} N(q_k^n, q_{k-1}^n) \end{aligned} \tag{4.24}$$

we propose birth at a fixed rate, in our algorithm we use $p_{new} = 1/3$. If there is no (close-to-optimal) proposal, new dipole detection is one of the algorithm's most challenging tasks. It is

therefore appropriate to allocate a significant proportion of the computing resources to this task. We assume that $\pi_{new} > 1/100$. The new dipole position is indicated when birth is suggested from a distribution of the heuristic proposal $q(r_k^{N_k}, q_k^{N_k}|z_k, x_{k-1})$ computed from the data and obtained by considering the equation 4.21.

By considering equation 4.17, the posterior density is written as,

$$p\left(X_k|z_{1:k}\right) = \frac{p\left(z_k|X_k\right) p\left(X_k|X_{k-1}\right)}{p\left(z_k|z_{1:k-1}\right)} p\left(X_{k-1}|z_{1:k-1}\right) \tag{4.25}$$

weights are updated for the next time point as,

$$w_k \propto \frac{p\left(z_k|X_k\right) p\left(X_k|x_{k-1}\right)}{q\left(X_k|X_{1:k}, z_{1:k}\right)} \frac{p\left(X_{k-1}|z_{1:k-1}\right)}{q\left(Xk-1|z_{1:k-1}\right)} = \frac{p\left(z_k|X_k\right) p\left(X_k|X_{k-1}\right)}{q\left(X_k|X_{1:k}, z_{1:k}\right)} w_{k-1} \tag{4.26}$$

finally, the state estimation will become $\widehat{X_k} \approx \sum_{i=1}^{N_p} w_k^{(i)} x_t^{(i)}$. The sampling importance sam-

Algorithm 1 Sequential Importance sampling Particle Filter

- **Initialization of the particles:** draw the particles from the initial distribution $x_k^{(i)}$ from $p\left(x_0^{(i)}\right)$
- **Particle propagation:** Particles are taken from $q\left(x_k|x_{k-1}^{(i)}, z_{1:k}\right)$ which is an importance density function, where $z_{1:k} = \{z_1, \ldots z_k\}$.
- **Weight update:** Particle weight can be calculated as $w_k^{(i)} \propto w_{k-1}^{(i)} \frac{p\left(z_k|x_k^{(i)}\right) p\left(x_k^{(i)}|x_{k-1}^{(i)}\right)}{q\left(x_k^{(i)}|x_{k-1}^{(i)}\right)}$
- **Weight normalization:** the sum of all weights should be equal to 1, i.e., $\sum_{i=1}^{N} w_k^{(i)} = 1$.

pling (SIS) particle filter procedure is given in algorithm 1. The SIS alone method has been demonstrated to lead to the problem of particle degeneracy. After a few iterations, most particle weights decrease by nearly zero, only one weight increases by almost one. This causes the algorithm to become inaccurate and the computational resources to be wasted. PF requires a new stage, called a resampling, to prevent this degeneration. Resampling is a stochastic procedure which tries, by replicating particles with high weights and eliminating those of low weights, to address an inevitable increase in the variance in the sampling estimator of importance density. Precisely the product of N_p and its weight prior to resampling is the number of offspring expected for each particle.

4.3.3 Resampling

Resampling is the process of the particles with lower weights are displaced by those with higher weights. This substitution would re-weight the deposed particles with the objective that change among the weights would be diminished [94, 168]. The resampling should be applied only when it is necessary, and it is also essential when resampling is done. The threshold criterion for the resampling is the effective sample size of ESS. It is given as

$$N_{eff} = \frac{1}{\sum \left(w_k^{(i)}\right)^2} \tag{4.27}$$

The posterior distribution shall be resampled during each time step: N_p particles from estimated posterior density are chosen. This procedure ensures that particles of small or negligible weight are removed, while particles of more weight increase.

Resampling methods are divided into two types: deterministic and adaptive. In the deterministic type, the resampling has to be done at all time steps. In adaptive resampling, whenever the weight of a particle is below the threshold criteria, then resampling is triggered. This gives better performance by the PF than deterministic resampling gives. The model for actualizing resampling is generally used because of the variance of the weights, which replicates the level of weight degeneracy.

4.3.4 Resampling methods

Depending on duplication or removal of high or low-weight particles, updated particle distribution is resampled separately. Resampling steps are followed continuously and weights tend to be focused on fewer particles after several cycles in particle propagation. The larger part of the particles has insignificant weights which cause degeneration. Ideally, the propagation of the particles should be extended to manage degeneration, involving the use of different methods of resampling [169].

Multinomial resampling:

Multinomial resampling is also called as random resampling [77, 148, 170]. There is a very large population and it is difficult to identify every member of the population. The entire process of sampling is done in a single step with each subject selected independently of the

other members of the population. The term random has a very precise meaning and you can't just collect responses on the street and have a random sample. The main idea behind resampling is to produce $w_k^{(n)}$ which is N_p number of random measures from the distribution $(0, 1]$ and these numbers are used to pick the particles from x_k. For the particle $x_k^{(m)}$, the n$^{\text{th}}$ random number can be taken that satisfy the following condition,

$$Q_k^{(m-1)} < w_k^{(n)} \leq Q_k^{(m)} \tag{4.28}$$

where $Q_k^{(m-1)} = \sum_{i=1}^{m} w_k^{(i)}$. In the 'wheel' analogy [171] shown in Figure 4.2, this method of resampling estimates by picking N_p independent random directions from the center of the wheel and taking the pointing particle.

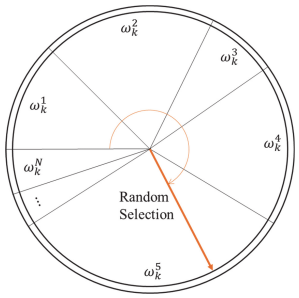

Figure 4.2: Wheel analogy of Multinomial resampling [171].

In this technique, each member of the population has an equal chance of being selected as subject. When there are very large populations, it is often difficult to identify every member of the population and the pool of subjects becomes biased.

Stratified resampling:

A stratified sample, in essence, tries to recreate the statistical features of the population on a smaller scale. Before sampling, the population is divided into sub interval called 'strata'. Then the population is randomly sampled within each category or stratum. In stratified resampling, where the total weights are added and divided into equal N_p pieces, i.e., pre-partitioning the $(0, 1]$ period into N_p sub-intervals $U\left(0, \frac{1}{N_p}\right] \ldots U\left(1 - \frac{1}{N_p}, 1\right]$, these subparts are called strata, as shown in Figure 4.3 [171]. Then $w_k^{(n)}$ it draws in each strata independently, which means that the particles of small weight are sampled at most once, and at least once the particles of considerable weight are sampled [172, 173].

$$w_k^{(n)} \sim U\left(\frac{n-1}{N_p}, \frac{n}{N_p}\right), n = 1, 2, \ldots N_p \tag{4.29}$$

This method attempts to overcome the shortcomings of random sampling by splitting the popu-

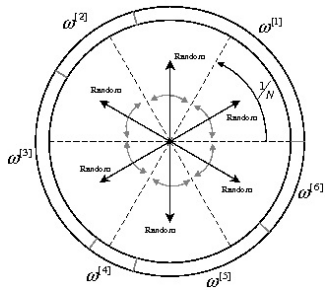

Figure 4.3: Wheel analogy of the Stratified resampling [171].

lation into various distinct segments and selecting entities from each of them. This ensures that every category of the population is represented in the sample. Stratified sampling is often used when one or more of the sections in the population have a low incidence relative to the other sections. Stratified sampling is the most complex method of sampling.

Systematic resampling:

In a systematic resampling, after you decide the sample size, arrange the elements of the population in some order and select terms at regular intervals from the list. Systematic resampling is also called as universal sampling; In this common technology, draw only one random number, that is, one direction in the 'wheel' for first particle and other particle with $N_p - 1$ directions, fixed at increments of $1/N_p$ of that randomly picked a direction [171], as shown on Figure 4.4. Presently, $w_k^{(1)}$ is drained from the regular distribution on $\left(0, \frac{1}{N_p}\right]$, and whatever is left over the ' u_k' information is acquired conclusively, i.e., $w_k^{(n)} \sim U\left(0, \frac{1}{N_p}\right)$,

$$w_k^{(n)} = w_k^{(1)} + \frac{n-1}{N_p}, \quad n = 2, 3 \ldots N_p \tag{4.30}$$

The main advantage of using systematic resampling over simple random resampling is its

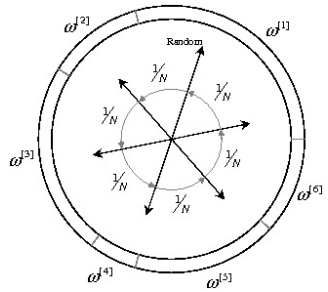

Figure 4.4: Wheel analogy of the Systematic resampling [171].

simplicity. Another advantage of systematic resampling over simple random resampling is the assurance that the population will be evenly sampled. There exists a chance in simple random resampling that allows a clustered selection of subjects. This can be avoided through systematic

resampling. The possible weakness of the method that may compromise the randomness of the sample is an inherent periodicity of the list.

Residual resampling:

Residual resampling is also called a reminder resampling. It consists of two stages. The first stage is to replicate the particle with weights more than $1/N_p$. The second stage is to resample the remaining weights. Here, the i^{th} particle is resampled by $F_k^{(i)} + S_k^{(i)}$, where $F_k^{(i)}$ and $S_k^{(i)}$ are the quantities of replicas from the first and the second stages. $F_k^{(i)} = |N_p w_k^{(i)}|$. The number of replicated particles from the first stage and second stage are $F_k = \sum_{i=1}^{N_p} F_k^i$, $S_k = N_p - F_k$.

The residual weights are acquired from

$$\widetilde{w}_k^{(i)} = w_k^{(i)} - F_k^{(i)}/N_p \tag{4.31}$$

In the second stage, particles are taken as per remaining weights by utilizing the multinomial resampling, where the selection of $x_k^{(i)}$ is compared to the remaining weight of that particle. The first stage addresses a deterministic reproduction; consequently, the assortment of the number of times a particle is resampled is just credited to the second stage. Residual resampling only needs to sample i times, which means that the amount of computation is also reduced.

Metropolis resampling:

Metropolis resampling requires only ratios between weights. In general, the posterior density of the particle filter is denoted by particles with their weights. But in this resampling, first draw a sample from desired importance density [93, 174]. Then, whether the new sample is accepted or rejected based on the acceptance ratio, which is given Eq. 4.32

$$r\left(x^n, x^{'}\right) = min\left\{1, \frac{p\left(x^{'}\right) g\left(x^n/x^{'}\right)}{p\left(x^n\right) g\left(x^{'}/x^n\right)}\right\} \tag{4.32}$$

where $x^{'} \sim g\left(./x^n\right)$ and $g\left(.\right)$ is the desired importance density. Generate a uniform random variable $u \sim U\left(0,1\right)$. Now compare the uniform random variable u and acceptance ratio $r\left(x^n, x^{'}\right)$. If $u > r\left(x^n, x^{'}\right)$ then set $x^{n+1} = x^n$. Else set $x^{n+1} = x^{'}$.

Branching resampling:

In this case, the particles are independently branched rather than collectively resampled, and branching happens only where there is a need. Branching resampling is one of the traditional variation resampling methods and based on residual resampling methods. These methods, the replicated particles, will be based on the integer parts of each weight in the same way, but residuals vary differently with the resampling method. The decision to branch or kill the particle is based the weight of the particular particle and the weight of all its particles (that is, the decision to sample more than once or not at all) and not on the individual values of others.

In the branch-kill method, if the weight of the particle is $w_k^{(i)} > U\left(0, \frac{1}{N_p}\right)$ then replicate the particle again, else kill the particle. In this approach, the number of replicated particles of $x_k^{(i)}$ is equal to $N_k^{(i)} = floor\left(N_p \cdot w_k^{(i)}\right)$ or $N_k^{(i)} = floor\left(N_p \cdot w_k^{(i)}\right) + 1$ with the probabilities $1 - p$ and p respectively. Where $p = N_p \cdot w_k^{(i)} - floor\left(N_p \cdot w_k^{(i)}\right)$.

Partial stratified resampling:

To reduce the computational complexity, resampling has to be done on only a few particles. The main idea behind partial stratified resampling is to complete the resampling only on few particles by joining the particles with higher weights and lower weights based on the upper threshold and lower threshold [177] The smaller weight particles which are below, the lower threshold (T_l) and the higher weight particles above the higher threshold (T_h) will be combined and resampled where low weight particles will be replaced with high weight particles. The particles which are in between low and high thresholds will not be resampled and will be considered for the next time step. The advantage of using PSR is, it will perform resampling in less execution time as only some of the particles will undergo resampling.

PSR algorithm can be executed in two steps; the first step is to classify (negligible, moderate, and dominant) the particles based on their weight, the second step is to perform stratified resampling on the particles, which are the combination of negligible and dominant weights. The threshold values have taken in between (0, 1], both low threshold, high threshold values started at 0.5. T_l Starts decreasing by 0.05 and T_h starts increasing by 0.05. Total of nine threshold values have been defined.

Minimum sampling variance:

Consider the concerns about streamlining the resampling calculation under certain sensible limitations. In the first place, to limit the variance of the weights (which to the highest degree

Table 4.1: threshold values for PSR

Threshold	Low threshold value $<T_l$	High threshold value $>T_h$	Moderate ($T_h - T_l$)
T1	0.1	0.9	0.8
T2	0.15	0.85	0.7
T3	0.2	0.8	0.6
T4	0.25	0.75	0.5
T5	0.3	0.7	0.4
T6	0.35	0.65	0.3
T7	0.4	0.6	0.2
T8	0.45	0.55	0.1
T9	0.5	0.5	0

diminishes the degeneration), the weights of the resampled particles might be set equivalent, as is usually done (i.e., $w_k^m = 1/N_p$). This is called as ideal weight condition, which completely expels the degeneracy.

Resampling is a critical procedure that is of both theoretical and practical significance for efficient implementation of the particle filter. First, identical distribution (ID) is established as a general principle for the resampling design, which requires the distribution of particles before and after resampling to be statistically identical. The sampling variance are introduced for assessment of the ID attribute of resampling, and a corresponding, qualitative ID analysis of representative resampling methods is given.

The new approach for the resampling technique is called minimum sampling variance (MSV) [178] resampling, which comprises two principle steps:

- Step 1: Each particle is first resampled $floor\left(N_p \cdot w_k^{(i)}\right)$ times, leaving a weighted residual $w_k^{(i)} = w_k^{(i)} - floor\left(N_p \cdot w_k^{(i)}\right)/N_p$. This step will yield, in total, L particles, where $L = \sum_{i=1}^{N_p} floor\left(N_p \cdot w_k^{(i)}\right)$.
- Step 2: The particle with relatively larger weight residual, $top\left(N_p - L\right)$, will be further sampled one more time each.

The MSV resampling ensures accomplishing the lowest sampling variance for a discretionary sample set while fulfilling the ideal weight condition and including precisely the predefined number of particles. The ideal identical distribution quality got by MSV resampling demonstrates a capacity to maximally protect the posterior distribution or, to state an ability to maximally diminish data loss during the resampling, which is profoundly the best approach, in principle.

Algorithm 2 Pseudo code for Sequential Importance Resampling

for $i = 1, 2, \ldots N_p$ **do**
    draw $x_0^{(i)}$ from $p(x_0)$
end for
for $k = 1, 2 \ldots t$ **do**
    for $i = 1, 2, \ldots N_p$ **do**
        draw $x_k^{(i)}$ from $q(x_k | x_{k-1}^i, z_k)$,
        $x_{0:k}^{(i)} = x_{0:k-1}^{(i)}, x_k^{(i)}$
        compute the weights
    end for
    for $i = 1, 2, \ldots N_p$ **do**
        normalize the weights
    end for
    for $i = 1, 2, \ldots N_p$ **do** perform resampling
        From the set $x_k^i = 1, 2, \ldots N_p$, pick N_p particles at random in such a way that the probability of extracting x_k^i are the same as w_k^i.
        A new estimate of the posterior density at time k is the set of uniformly weighted particles $\hat{x}_k^i$, and the particles that have greater weights appear more often in this set.
    end for
    for $i = 1, 2, \ldots N_p$ **do** Evolution of dipoles
        Let each $\hat{x}_k^i$ particle evolve by drawing a new x_{k+1}^i particle in accordance to the transition kernel $\pi(x_{k+1} | \hat{x}_k^i)$.
        In conjunction with the single-dipole transition kernel , each surviving dipole of each particle evolves.
        There could be new dipoles emerging. The uniformly weighted x_{k+1}^i particles are an estimate of the prior density at $k + 1$
        The number of dipoles in each particle can range from zero to maximum according to the RFS framework; dipole configurations may experience loss or birth of dipoles during temporal evolution.
    end for
end for

4.3.5 Estimate the number of sources

All the information available on the source constellation is stored in the posterior density of the current dipole set, so it is difficult to visualize as a whole; alternatively, separate calculations can be computed to obtain the necessary information. Random Finite Sets provide the mean to estimate the from posterior density of random variable N_k

$$p(|x_k| = i) = \int_{D(i)} \pi(x_k | z_{1:k}) \, \delta x_k \tag{4.33}$$

where $D(i)$ is the set of subsets of i dipoles, provides a time-varying estimate of the number of active sources by maximizing the posterior density function

$$\hat{N}_k = argmax\ (p|x_k| = i) \tag{4.34}$$

we used the RFS equivalent of the first moment of an random variable to measure the source parameters. It is a function in single-dipole space D, it is an integral function of probability hypothesis density (PHD) for region R, it calculates the number of dipoles in the region R and the peaks of this function can be used to measure the active dipole.

$$PHD(d_k) = \sum_{i=1}^{N_p} w_k^i \sum_{d \in x_k^i} \delta(d - d_k) \tag{4.35}$$

thus the problem of calculating the source parameters is turned into the problem of finding the integral function's local maximum that can be done using the above PHD equation 4.34.

4.3.6 Clustering

In the EEG data, the number of sources determined by the particle filter is not constant, so it can be difficult to trace the identity of the sources. Take for example, number of source at k is less than the source at $k-1$ there must have then been at least one source that was involved at $k-1$; but there is no convenient way to figure out which of these sources was actually dead." In the other hand it is exceedingly necessary for the EEG application to preserve the source identification, where the temporal waveforms of individual sources are among the principal subjects of neuro-scientific applications. In [[30]] the authors suggested by applying clustering approach to find the source positions.

To obtain a meaningful set of neural sources, we successfully applied an iterative algorithm based on the basic k-means clustering [179]. Clustering is carried out into a state-space: the position is three dimensions, the orientation is three, the time k where the source dipole was present. This temporal parameter ensures continuity of the source waveforms. The iterations are required since the number of clusters is unknown, while the k-means algorithm needs to be set in advance. First we need to assume the number of sources, then cluster the dipoles to the number of clusters assumed. Now apply Wilcoxon test [180] for statistical difference, and check whether all clusters are significantly diverse; if not decrease the number of clusters by 1 and again perform the clustering procedure until all the clusters diverse. The estimated dipole moment would be the average dipole moment for each estimated dipole location.

4.4 Simulation results

4.4.1 Workflow

To model the neural activity of the brain, the number of dipole sources are unknown and are time-variant. Therefore, the problem is to find N the number of dipole sources at each time point t. Here, there is no prior information about the number of dipoles. The particle filter is used to deal with the unknown and time-varying dipoles.

As mentioned above, the particle filter contains three phases. After performing the particle filter, at each time point of an EEG data to create time-varying evaluations of the dipole parameters are done. These dynamical assessments, in any case, don't distinguish individual neural sources in time, because there is no direct connection between dipoles evaluated and different time steps. The neural sources have different dipoles where they appear at different time points. Nevertheless, they represent the same neural source. So it is better to cluster them by locating their 3-d location. The k-means clustering gives diverse dipole source collection into different neural sources. To find out the 3-d location of the same source, it is better to take the average location of dipoles belonging to that group.

The process of estimation is as follows:

1. At time $t = 0$, define N_p number of particles as $x_0^{(i)}; i = 1, 2, \ldots N_p$
2. Assign weights to particles as $w_0^{(i)}; i = 1, 2, \ldots N_p$. Initially, the weights of the particles will be $1/N_p$
3. At time $t = 1$, the particle filter is initialized to estimate $x_1^{(i)}$
4. Sample $x_t^{(i)}$ from the importance density $q\left(x_t^{(i)}|x_{t-1}^{(i)}\right)$
5. Estimate the weights by using $w_t^{(i)} \propto w_{t-1}^{(i)} \frac{p\left(z_t|x_t^{(i)}\right)p\left(x_t^{(i)}|x_{t-1}^{(i)}\right)}{q\left(x_t^{(i)}|x_{t-1}^{(i)}\right)}$
6. Normalize the weights.
7. The particles are drawn at $t = 0$ in the sequential importance sampling particle filter; then the algorithm sequentially updates the particle set with step 4, updates the weights of the particle in step 5. The problem with this particle filter is the degeneracy of particle

Table 4.2: The positions of dipoles located in synthetic data

Dipole	Position (3-dimension) in cm		
	X axis	Y axis	Z axis
1	-1.37	-5.43	7.34
2	3.74	4.54	5.66
3	-2.04	3.73	9.56
4	2.96	2.11	9.42

weights. Here most of the particles with high weights will dominate the low weight particles. The dominance of these particle degeneracies leads to the poor posterior likelihood density function. Use **resampling** methods to discard the small weight particles.

8. Go to step 3

9. Prepare dipole configuration for the next time step.

10. After calculating the dipole positions and moments, these parameters don't recognize the actual sources in the brain. Now, apply the clustering to the dipoles based on the position. When dipoles have been consigned to various clusters according to various neural sources, calculate the average position of the dipoles in each cluster. This average position can be considered as a position of the neural source.

A schematic plot of the particle filter for source localization is given in Figure 4.5.

The mean square error and relative accuracy are utilized as measurements for the performance assessment to look at the outcomes from using the resampling methods of the particle filter for the localization of neural sources [97]. As the neural source localization is nonlinear and is an inverse problem, for real data, there is no accurate position of the source dipoles, and thus cannot say which resampling method is better. For this reason, synthetic data is used in which the positions of dipoles are known so that one can go for the analysis of the resampling methods. Then it becomes easy to analyze the algorithms using real EEG data.

4.4.2 Synthetic data

The algorithm is applied to the synthetic data [181] in which four dipoles are located to validate the location of the neural sources through the use of particle filter. The volume of the brain is 10 cm in radius. The dipole positions are shown in Table 4.2.

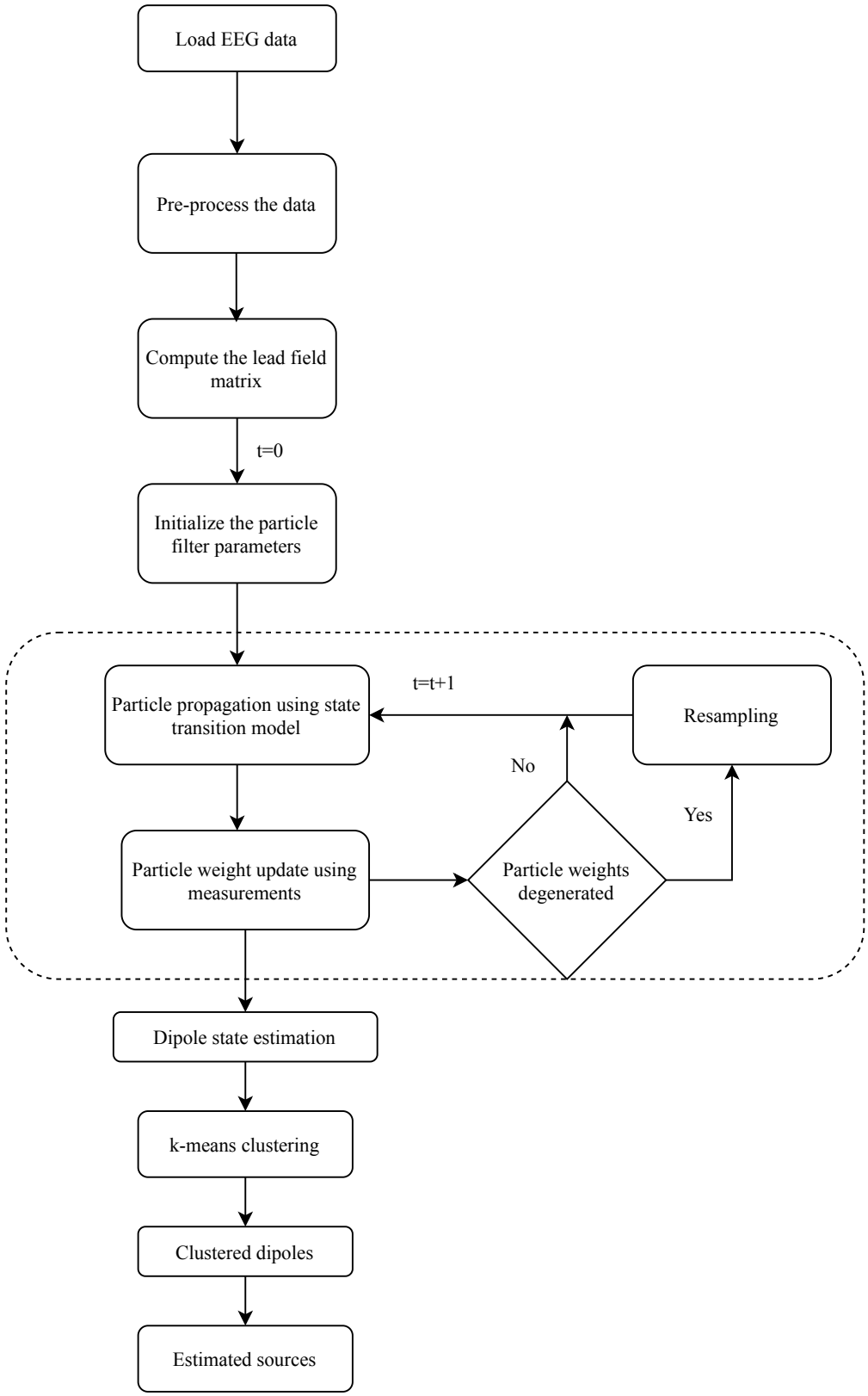

Figure 4.5: Flowchart of the particle filter for source localization

The number of particles for each resampling method are 10000, 20000, 50000, 100000 particles considered. The higher the number of particles, the better the approximation of proper

localization. The comparison of resampling methods has been made concerning mean square error between actual and estimated positions, relative accuracy, and computational time. The synthetic data has a total of 400ms in that analysis has been done from 100 to 150ms. In the data 0 to 100ms interval is the pre-stimulus interval. The sampling frequency of the data is 1000Hz [182, 183].

Computational measures

1. Mean Square Error (MSE): Mean square error between the position of the true dipoles and estimated dipoles can be calculated. It could be written as,

   $MSE = \frac{(x_{true}-x_{estimated})^2+(y_{true}-y_{estimated})^2+(z_{true}-z_{estimated})^2}{3}$

   In the above equation $(x_{true}, y_{true}, z_{true})$, $(x_{estimated}, y_{estimated}, z_{estimated})$ represent the 3D positions of the true and estimated dipoles.

2. Relative Accuracy (RA): The calculation of normalized error values between true positions and estimated dipole positions is relative accuracy.

   It is mentioned as, $RA = 1 - \frac{|TruePosition-Estimatedposition|}{\text{True Position}}$

3. Computational time: Measuring the computational time to implement the resampling methods for the particle filter will also explore the quality of the resampling methods.

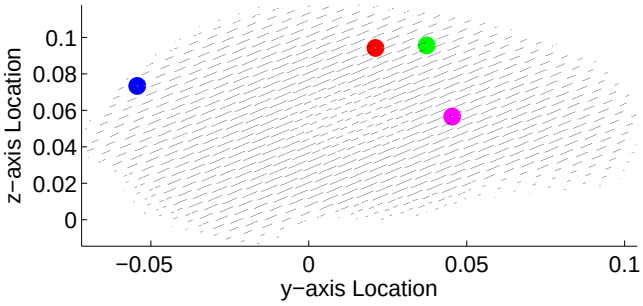

Figure 4.6: True source locations

The images shown here are the estimated dipolar sources for the synthetic data. In Figure 4.6 the true source locations of the synthetic data are shown. After performing the multinomial resampling,the four estimated sources are found which are displayed in Figure 4.7a and source amplitudes across the time interval are shown in Figure 4.7b. It can be observed that the amplitudes vary according to the source activation at the respective time point. In Figure 4.8. The estimated sources and their amplitudes of the synthetic data after performing the systematic

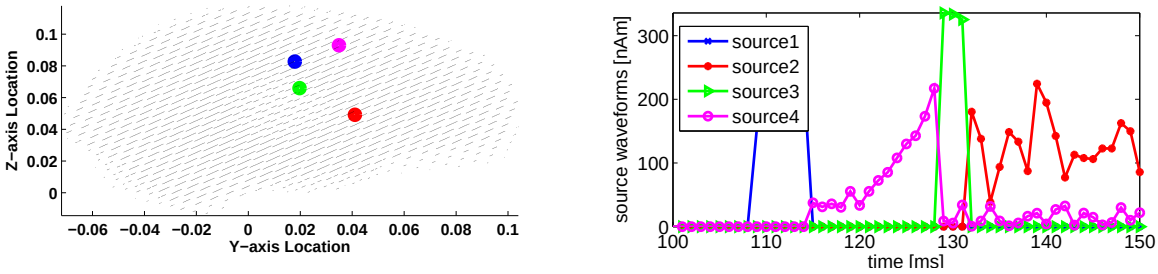

(a) (b)

Figure 4.7: (a) Estimated source locations using Multinomial resampling (b) shows the amplitude of each dipole across time.

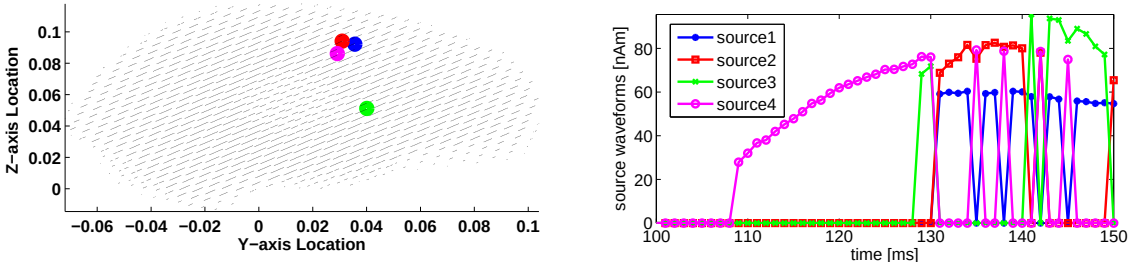

(a) (b)

Figure 4.8: (a) Estimated source locations using Systematic resampling (b) shows the amplitude of each dipole across time.

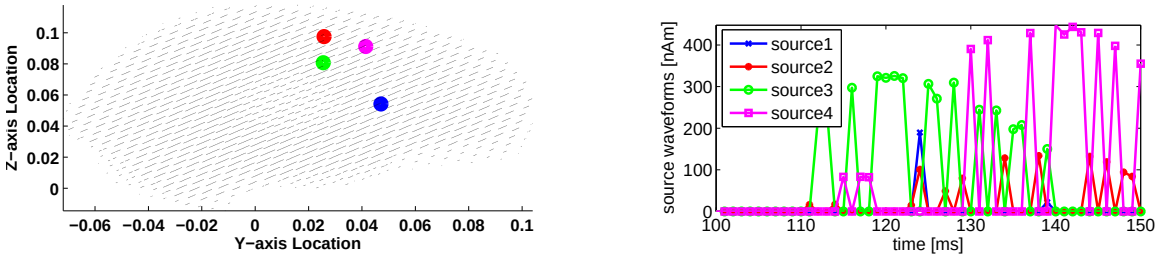

(a) (b)

Figure 4.9: (a) Estimated source locations using Residual resampling (b) shows the amplitude of each dipole across time.

resampling were given. Figure 4.9 represents the sources and their amplitudes of the residual resampling. Figure 4.10 represents the estimated sources and their amplitudes of the stratified resampling. Figure 4.11 shows the estimated sources and their amplitudes of the metropolis resampling. In Figure 4.12, the estimated source locations and their aplitudes using the PSR resampling for the threshold T7 were shown. Figure 4.13 presents the branching resampling based estimated source locations and their amplitudes for the synthetic data. Figure 4.14 shows the estimated source locations and amplitudes for the synthetic data using MSV resampling.

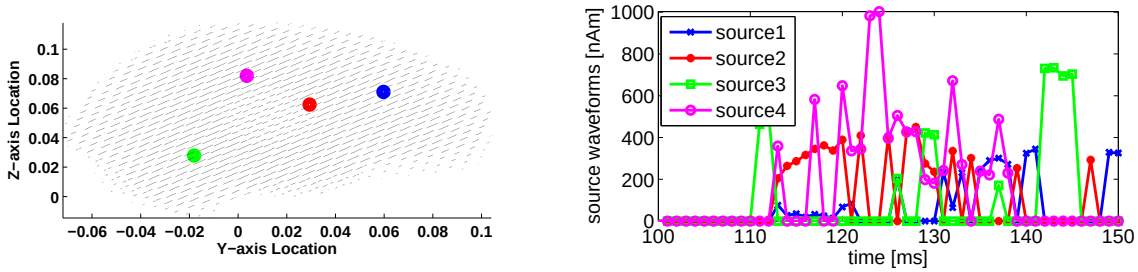

(a) (b)

Figure 4.10: (a) Estimated source locations using stratified resampling (b) shows the amplitude of each dipole across time.

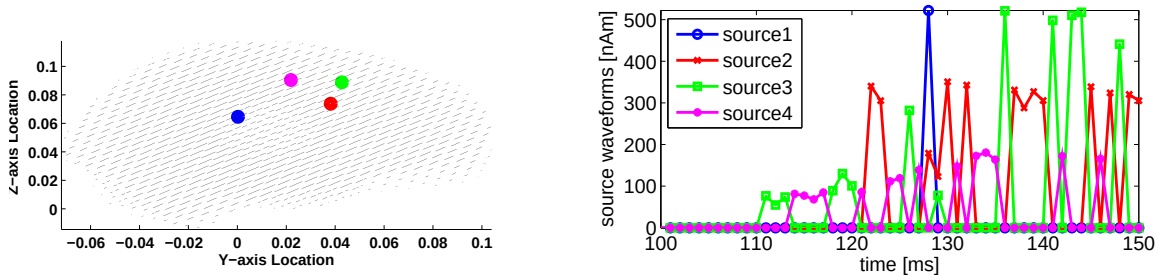

(a) (b)

Figure 4.11: (a) Estimated source locations using Metropolis resampling (b) shows the amplitude of each dipole across time.

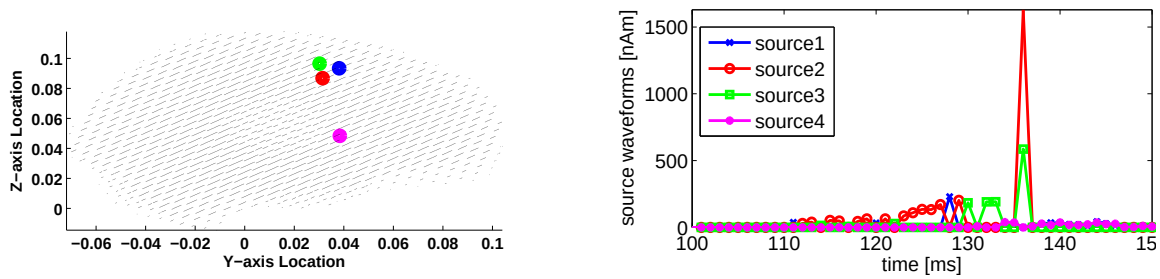

(a) (b)

Figure 4.12: (a) Estimated source locations using PSR resampling (b) shows the amplitude of each dipole across time.

The EEG source reconstruction analysis is an emerging field of evident relevance for fundamental neurosciences and clinical studies. However, the validation is still inadequate, and the reliability of available methods is confused. Researchers using Source Reconstruction analysis are interested in addressing research questions by rigorously validated under as realistic circumstances as possible in all aspects of the Analysis, including head modeling, source reconstruction. It is not easy to evaluate the quality of inverse solutions, because ground truth is not usually available. Simulations using synthetic data are an appropriate way of implementing such a source reconstruction in the lack of ground truth for real EEG data.

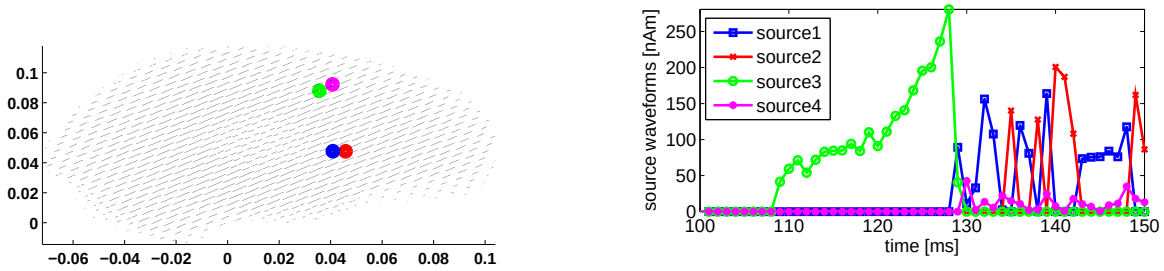

(a) (b)

Figure 4.13: (a) Estimated source locations using Branching resampling (b) shows the amplitude of each dipole across time.

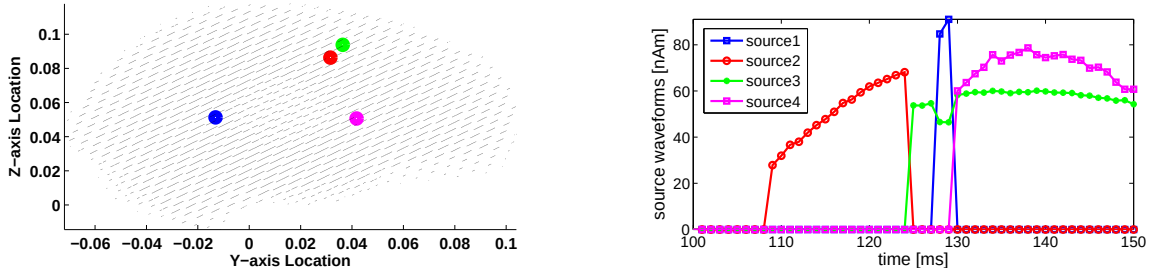

(a) (b)

Figure 4.14: (a) Estimated source locations using MSV resampling (b) shows the amplitude of each dipole across time.

Table 4.3: Average MSE of the 3D position (in cm) for the resampling methods for different number of particles

No of Particles	Average MSE							
	Multinomial	Systematic	Residual	Stratified	Metropolis	PSR	Branching	MSV
10000	0.019	0.016	0.023	0.025	0.019	0.015	0.016	0.015
20000	0.015	0.020	0.017	0.018	0.017	0.015	0.015	0.006
50000	0.021	0.023	0.009	0.032	0.015	0.020	0.021	0.010
100000	0.015	0.019	0.020	0.018	0.009	0.013	0.015	0.010

Table 4.4: Average Relative Accuracy of the 3D position for the resampling methods for different number of particles

No of Particles	Average RA							
	Multinomial	Systematic	Residual	Stratified	Metropolis	PSR	Branching	MSV
10000	60.11	71.10	58.10	50.48	68.03	70.08	59.47	77.5
20000	68.49	64.41	61.96	62.86	65.30	74.25	71.89	80.1
50000	65.65	51.36	80.49	49.02	68.34	61.56	68.27	75.33
100000	66.15	52.73	65.40	68.66	78.99	76.22	72.34	85.59

An MSE and RA for four different particle numbers for each method to determine the accuracy of synthetic data are calculated. A high MSE value means the estimated data is too far from the true data, whereas a low MSE indicates good accuracy in the estimate. A high RA value close to 1 corresponds to a small error between the estimated and true positions, making the

Table 4.5: Computational time for synthetic data between resampling methods for different number of particles

No of Particles	Computational time in sec							
	Multinomial	Systematic	Residual	Stratified	Metropolis	PSR	Branching	MSV
10000	60.58	34.32	35.87	39.43	64.83	32.32	34.5	31.2
20000	185.13	69.57	97.28	111.58	180.82	60.87	70.17	56.5
50000	871.62	191.43	217.39	188.59	374.30	186.05	195.78	175
100000	8019.25	348.34	516.01	469.51	602.55	283.57	312.05	190.68

estimate very accurate. The comparison analysis between resampling algorithms was evaluated in this article by taking into account both low MSE and high RA values. From Table 4.3 and Table 4.4, it can be observed that the MSE and RA of the proposed PSR, Branching, and MSV resampling methods are impressive for a different number of particles than other conventional methods of resampling. Concerning computational time, multinomial resampling takes more time to estimate the dipoles compared to other methods of resampling; the proposed methods show that it determines the source positions with very less time of execution given in Table 4.5. The average MSE is low with a different number of particles for PSR, Branching, and MSV resampling methods, and also, the RA is high compared to other methods of resampling. The computational time for PSR, Branching, and MSV resampling methods is very low. The branching method can improve the accuracy of the source estimate for a certain number of particles.

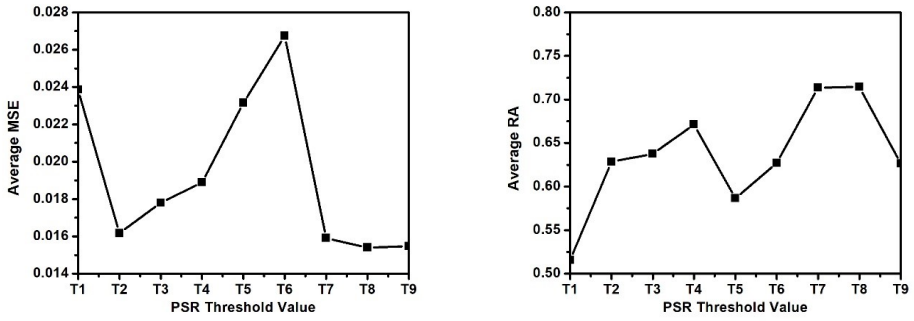

(a) (b)

Figure 4.15: Comparison of (a) average MSE (b) average RA for source localization with 20,000 number of particles using PSR threshold values.

In Figure 4.15a, the PSR method compares the average MSE by changing the threshold values. Observe that MSE is very low in the threshold values T_7 and T_8 . The comparison of average RA for the PSR threshold values was given in Figure 4.15b, and it is shown that high RA is observed for T_7 and T_8 threshold values. For T_1 , only the particles are resampled with very high weight and very low weight, and most particles are considered to be moderate weight

particles and are not sampled again. The majority of the useful data contained in moderate particles are therefore lost, leading to very bad predictability.

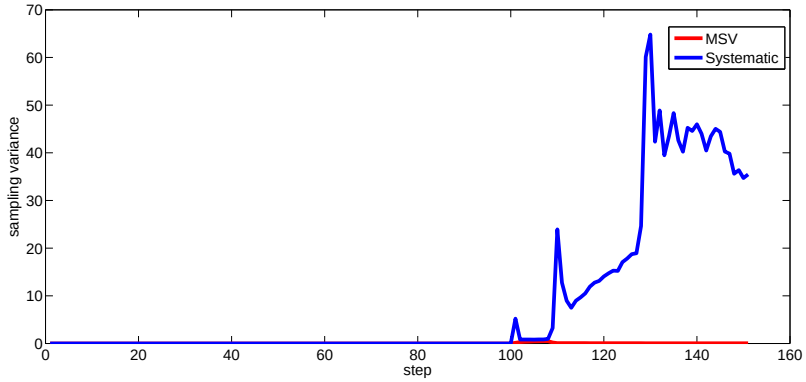

Figure 4.16: Sampling variance of systematic and MSV resampling methods for the synthetic data

Systematic resampling is the method having the lowest resampling variance when compared to other methods [95, 169]. Because of low sampling variance in systematic resampling, for this work, systematic resampling is chosen to compare with minimum sampling variance (MSV) resampling for the localization of brain sources. In Figure 4.16, the sampling variances of the particles before and after resampling for the MSV and the systematic resampling is demonstrated. This clearly shows that the variance in systematic resampling is very high.

Table 4.6: Comparison of RMSE of source position for synthetic data with other PF methods

Approach	Number of particles	Number of dipoles	Knowledge of dipole number	RMSE of position
PF [26]	100,000	4	Known	5.4mm
RBPF [162]	50,000	2	Known	6.3mm
DPF [30]	100,000	3	Unknown	6.2mm
PF-PHDF [99]	16,000	3	Unknown	6.9mm
Proposed PSR-PF [177]	20,000	4	Unknown	4.4mm
Proposed MSV-PF [178]	20,000	4	Unknown	7.59mm

The efciency of the proposed algorithm was compared with that of [26, 30, 99, 162] as illustrated in Table 4.6. In [162], the authors used RBPF, the RMSE of the RBPF is less than with the proposed approach. In Rao-Blackwellization, the optimal solution is computed for the linear dipole moment parameters through a set of Kalman filters, while the non-linear source locations are sampled with a particle filter; this reduces the number of particles needed to obtain a given accuracy, however, a covariance matrix has to be computed by inversion at each time step for each particle, which also means more computational complexity. Moreover, the number of dipoles need to be known priori. In [30], the authors used multi dipole particle filter method to estimate the dipole sources. Here the number of dipoles to be estimated is higher, but it took more particles, and it also resulted in higher RMSE compared to the proposed approach. In

[26], the authors used simple particle filter and they were able to recover only two simultaneous dipoles with help of R^{12} approach, with that implementation if the number of dipoles increases means the number of particles will also increases resulting in the more computational complexity. In [99], the authors used probability hypothesis density particle filter to estimate the unknown number of sources with very less number of particles. This is because the EEG/MEG signals require pre-processing to be divided into individual components such that each component is composed of a single dipole. All particles were then only for a single dipole source and the number of particles decreased to several thousand. The issue with this method is the number of sources will be equal to the number of channels i.e. the user has to choose the channels. Selecting which channals to choos will become very difficult.

The proposed PSR-based system has a 4.4 mm tracking error compared to [26], which has the best tracking efciency. The PSR only utilizes 20,000 particles and also has no knowledge of dipole numbers. In summary, the proposed system achieves comparable results for estimation of the unknown number of dipoles with considerably less computational complexity.The system with proposed MSV resampling method obtains comparable estimated results with substantially reduced computational complexity when tracking an unknown number of dipoles.

4.4.3 Real data

In this section, the estimation accuracy of the proposed algorithm using real EEG data has been shown. The data were taken from the Brainstorm EEG/Epilepsy dataset [184]. This dataset was collected from a patient who has suffered from focal epilepsy since the age of 8 years. He is not facing any dangerous risks from his epilepsy. Focal epilepsy is defined by seizures originating from a particular portion of the brain. From the surgical perspective, the epileptogenic area is better defined by individual MRI, in addition to reducing additional postoperative risks. The value of source localization of EEG data in epilepsy patients has already been proven. This method can locate brain resources from extratemporal to deep temporal locations, as demonstrated in earlier research [185, 186, 187, 188, 189]. Knowing the exact location of focal epilepsy revolutionizes epileptic treatments both internally and surgically. The proposed methodology can be viewed as a supplement to this diagnostic procedure. The localization of EEG sources indicates focal epilepsy in the brain around the temporal lobe.

The data were recorded at a frequency of 256 Hz using 29 channels. EEG signals were recorded from 29 terminals (FP1, FP2, F3, F4, C3, C4, P3, P4, O1, O2, F7, F8, T7, T8, P7, P8, Fz, Cz, Pz, T1, T2, FC1, FC2, FC5, FC6, CP1, CP2, CP5, CP6) as per the 10/20 International

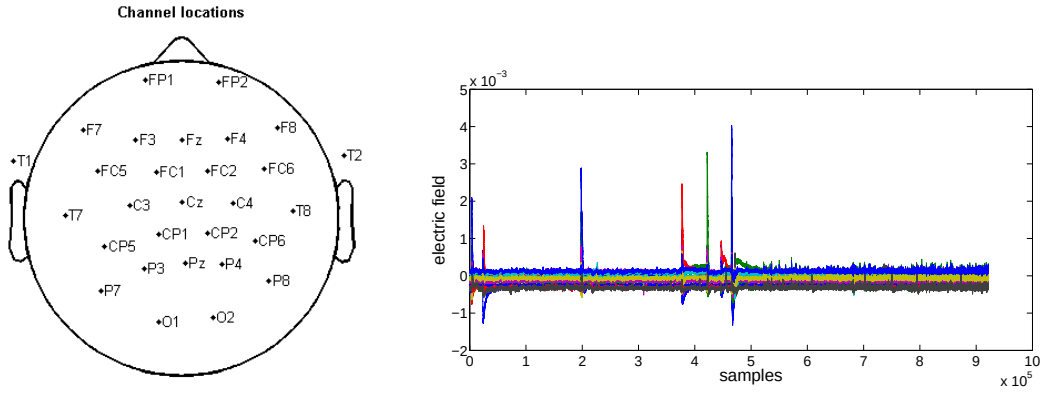

(a) (b)

Figure 4.17: (a) Channel locations (b) Real EEG data

framework. The channel locations were displayed in Figure 4.17a. The source of the reference coordinate system is situated at the focal point of the spheres with the x-axis indicating right-to-left, the y-axis pointing back to front, and the z-axis from the base upward [190]. The arrangement of the EEG source confinement problem requires a critical number of forward model assessments. The proposed calculation requires for its evaluation a large number and variety of source areas. Furthermore, 15,000× 3 grid points on the head model has been set roughly. The EEG data includes 921,600 samples. Between 137,000 and 200,000 samples, 10,000 ms of data is used. The real EEG data is shown in Figure 4.17b. There is no exact position of the source dipoles for real EEG data.

Focal seizures are characterized by focal epilepsy in a given part of the brain. In patients with epilepsy, the value of localization of EEG data sources has been proven. The technique can locate brain resources, from extra-temporal to low-temporal locations, as demonstrated in previous studies [186, 187, 188] For both internal and surgical therapies, the exact location of focal epilepsy is essential. The suggested technique can be considered in addition to the diagnostic protocol. The location of EEG sources indicated by focal brain epilepsy around the temporal lobe. Results of source location can confirm the EEG measurements that enhance the correlation between epileptic position and brain anatomy.

The dipole positions and source amplitudes of the real EEG data with multinomial, systematic, residual, stratified, metropolis, PSR, branching, and MSV resampling methods in particle filters were shown in Figures 4.18. For real EEG data, the results have shown for 20000 particles only. As can be observed from the picture, the dipoles are positioned across the brain. The source amplitudes are represented from the time 10000ms to 20000ms, where the activations of various dipoles are also given.

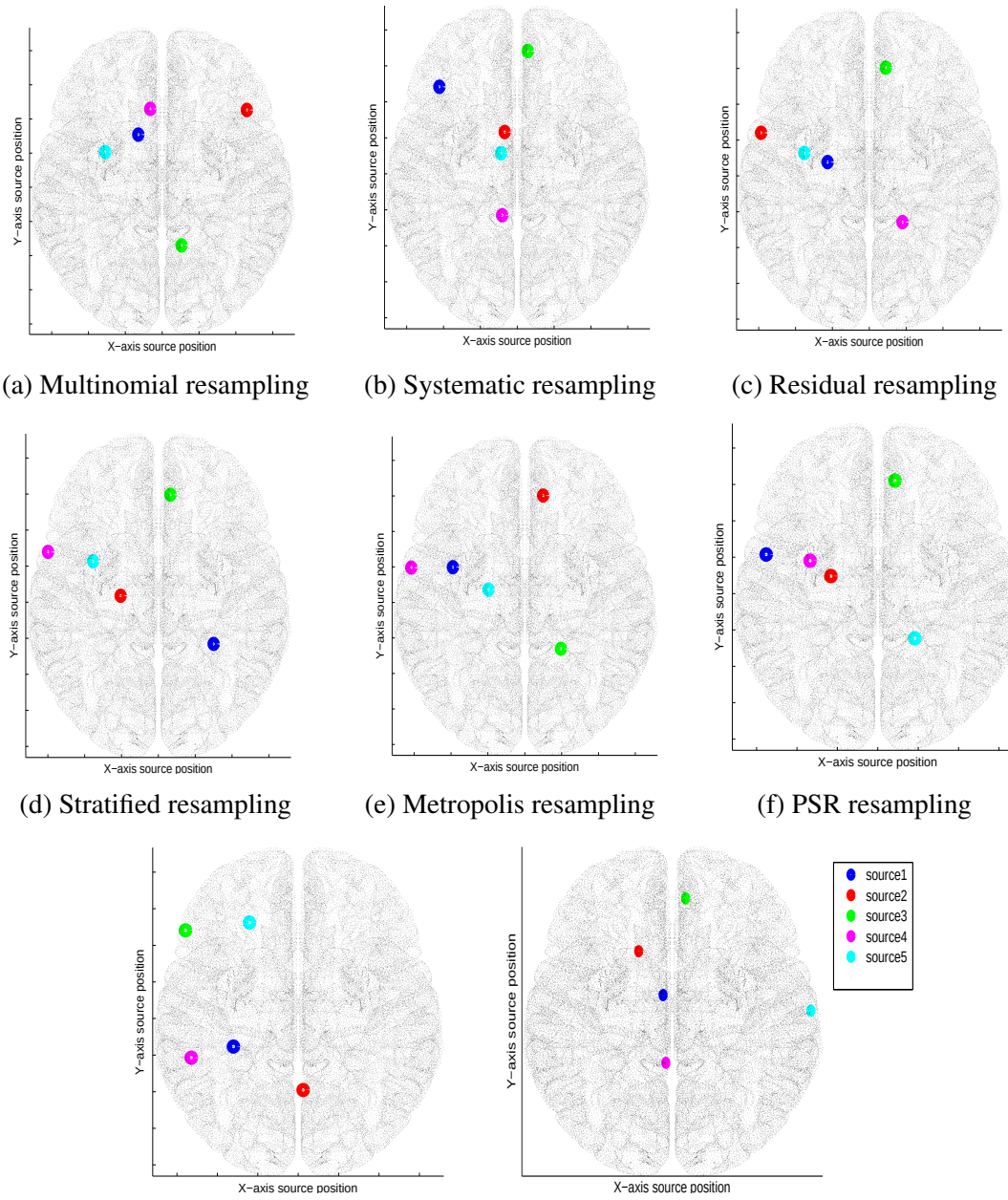

(a) Multinomial resampling (b) Systematic resampling (c) Residual resampling

(d) Stratified resampling (e) Metropolis resampling (f) PSR resampling

(g) Branching resampling (h) MSV Resampling

Figure 4.18: Source estimates using particle filter with different resampling methods.

From Figure 4.19, It is observed that the sampling variance of the particles before and after resampling is much less for the proposed approach in the PF to localize the neural sources. The computational time for the processing of real data for both methods is presented in Table 4.7. This clearly shows that the proposed methods are performing better in terms of sampling variance, as well as computational time.

The same dataset used in [184], is taken here to report the estimated sources of three widely used inverse methods, the standard dipole fitting method [191], sLoreta (Standardized

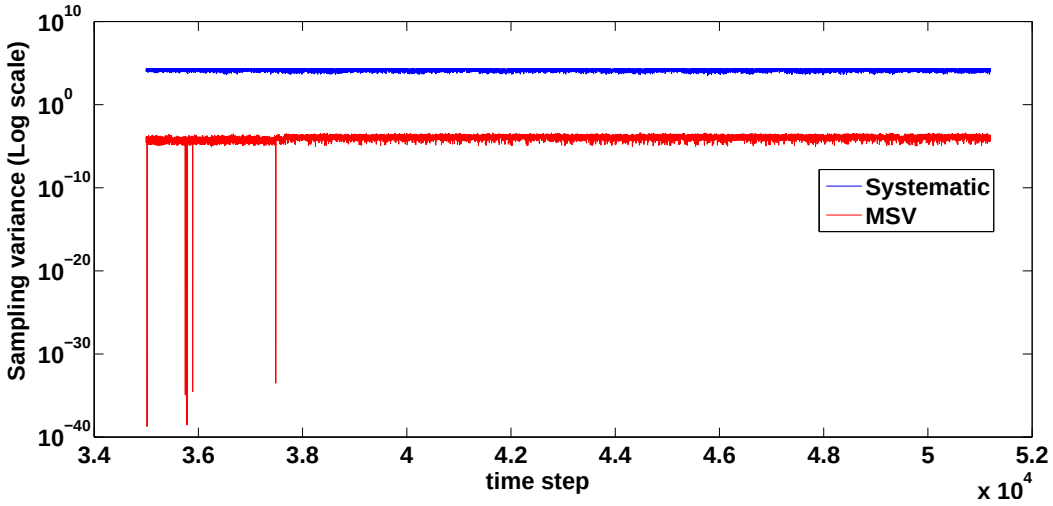

Figure 4.19: Sampling variance of systematic and MSV resampling methods for the real data in Log scale

Table 4.7: Computational time between Multinomial, Stratified, Systematic and PSR resampling methods for different number of particles for real EEG data.

No of Particles	Multinomial	Residual	Stratified	Systematic	Metropolis	PSR	Branching	MSV
10000	2025s	1508	1865s	1598s	2155	1313s	1250	1382
20000	9398s	2120	2596s	2820s	7270	2477s	2020	2114
50000	58840s	6284	6571s	7054s	25695	5662s	5780	5467
100000	97787s	17993	16487s	18133s	53174	11761s	15400	12270

low-resolution electromagnetic tomography) [33] and the MNE (Minimal Norm Estimation method) [65], for further validation.

We attempted to compare results with the standard dipole fitting procedure specified in [191]. First, independent component analysis is used to discover the independent channel in the dipole fitting process. The dipole fitting was then applied to the independent components. With this method, however, the number of dipoles is equal to the number of channels (29 channels for our real data), meaning that there are 29 dipoles. The components are rejected using maps, because the true positions and number of sources are unknown, and have taken five dipoles present in the EEG. This is to say, the number of sources are assumed to be fixed. The results of the dipole fitting are shown in Figure 4.20a. Selecting which components to accept or dismiss when viewing the map was very difficult. The problem of dipole fitting is that choices by the user generally take a long time. The PF technique generates position estimates with time tracking for the entire time series. This is the anticipated conduct for explaining the neurological phenomenon in the brain region.

Importantly, instead of a time series, these sLoreta and MNE methods take input as a single time point. The estimates obtained by a proposed particle filter using a time window are compared to those obtained from the same signal pick in that same window. Also, the two methods are based on a model of a distributed source instead of a model of a dipolar source. The sLoreta and MNE tend to provide large maps of relatively strong sources and less disseminated maps of relatively weak sources since a strong source's posterior probability is very high and vice versa. In Figures 4.20b and 4.20c, the estimates of sLoreta and MNE are correspondingly presented. The scaled plot of sLoreta and MNE is the colored area of the brain cortex, the colored bars on the right represent the strength of the inverse solution of sLoreta and MNE.

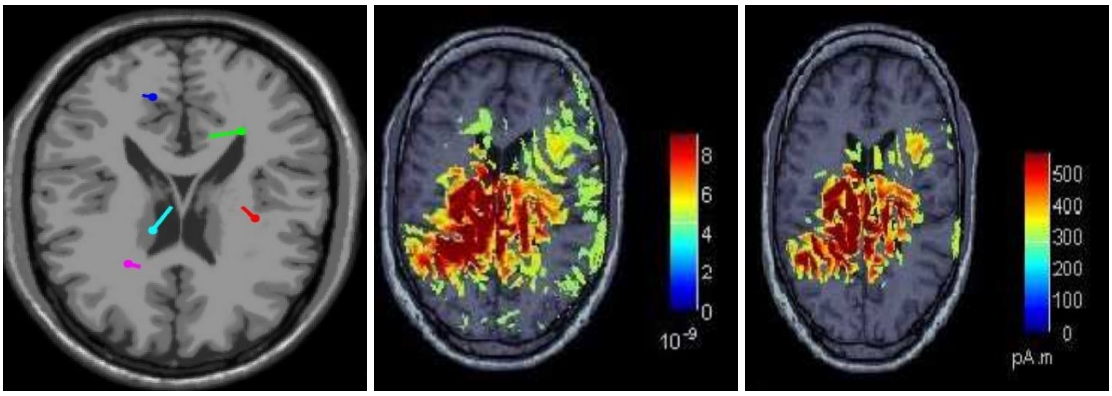

(a) Dipole fitting (b) sLoreta (c) MNE

Figure 4.20: Source estimates with other methods.

The sLoreta, MNE, and PF methods have considerably distinct interpretations. While the pictures created by sLoreta, MNE represent the estimated power of the neural current, the pictures generated by the PF algorithm depict the subsequent likelihood of a neural source being present at any given place. Despite these distinctions, it appears that the sLoreta, MNE, and the PF techniques are agreeable regarding a presumed position in the brain. PF results are comparable to those obtained by both dipole modeling, sLoreta, and MNE; however, the algorithm of the PF operates automatically, while the other methods require subjective decisions regarding what is to be seen as a true source.

To achieve qualitatively similar outcomes, traditional dipole modeling and minimum norm methods involve significant post-processing. The PF that described, immediately estimates the number of sources and the dipole parameters. The location of the source-reported focal epileptic activity in the cortex indicated the primary epileptic zone. The 3D location of the focal epileptic activity and the EEG data are available for identifying the location of the central epileptic region in the brain cortex, or the structure of the deeper temporal lobe. The results of the localization of a source can confirm that EEG measurements improve the correlation between epileptic

localization and brain anatomy. Our findings indicate that the location of the expected seizure is near the temporal lobe, which is consistent with prior research.

4.5 Summary

As an imaging tool, EEG provides a good time resolution to illustrate neuronal activity. Still, it leads to a poor spatial resolution, resulting in undesirable characteristics when used for locating the sources. Therefore, different methods were developed and explained by researchers for the solution of the EEG Inverse problem. Moreover, the effects of comparisons in computational time, localization error, and the mathematical relationships governing the methods are essential parameters, as described above.

Sequential Monte Carlo Particle filters implementations of Bayesian filtering, in which a weighted set of particles is used to trace the posterior probability density of an evolving process in time. The theoretical value of using particle filters requires limited assumptions of the spatial and temporal features of the neural sources underlying them. In this chapter, the dynamic neural source confinement by using the particle filter for the unknown number of dipoles are shown. Resampling is an essential practice for particle filtering, which is of both hypothetical and useful significance.

In this chapter, the partial stratified resampling, branching resampling and minimum sampling variance resampling methods of the particle filter for neural source localization has been discovered, and presented the comprehensive performance analysis for the multinomial, residual, systematic, stratified, PSR, branching and MSV resampling methods in the particle filters. Performance metrics such as source location mean square error, relative accuracy, and computation time are evaluated for resampling techniques. Among synthetic and real EEG data, computational results are demonstrated. Comparing with other traditional resampling approaches, the performance metrics show more consistent and accurate for proposed resampling methods. The results clearly show that the computational time of the proposed methods is lower than traditional resampling techniques.

Our results display that proposed resampling methods gives better performance in terms of MSE, RA and computational time, with these methods, results provide better location accuracy of sources when compared with other existing resampling methods for the synthetic data. Based on the results of synthetic data, conclude that these proposed resampling methods achieve excellent performance over other resampling methods for the real EEG data.

The results which determine the positions of brain activity due to focal epileptic information is consistent with current knowledge about neuropsychology. The location of the source-reported focal epileptic activity in the cortex indicated the primary epileptic zone. The 3D location of the focal epileptic activity and the EEG data is available for identifying the location of the central epileptic region in the brain cortex, or the structure of the deeper temporal lobe. The results of the localization of a source can confirm that EEG measurements improve the correlation between epileptic localization and brain anatomy. Our findings indicate that the location of the expected seizure is near the temporal lobe, which is consistent with prior research.

Chapter 5

Connectivity

5.1 Introduction

The neuroimaging techniques can be used to identify the brain network that is involved in healthy brain functions (learning, memory, mental or emotional stimulation) as well as neurological disorders such as epilepsy, autism, or schizophrenia [46, 192, 193]. Over the last two decades, the functional MRI has significantly expanded and is now commonly used for brain connectivity characterization [194]. Meanwhile, numerous studies show that EEGs may also provide useful information on regular cognitive activity [195], or tumor-related movement [196], along with appropriate signal processing techniques.

Neural connectivity analysis plays a crucial role in understanding the brain's overall functioning. Due to enormous advances in the areas of neuroimaging and mathematical modeling, such analysis has become feasible over the past two centuries. Because of its high temporal resolution, electroencephalography (EEG), is commonly used for brain connectivity. EEG based connectivity analysis is the estimation of interaction between neural sources based on the EEG recordings. Meanwhile, both functional and effective connectivity methods have established [197, 198] for EEG signals.

In practical terms, the transition from the electrode to the source space requires resolving an ill-posed inverse problem, which is based on the biophysical theory of the dipole. Some use the physiologically relevant knowledge both of the location of and the orientation of dipole sources at the origin of signals collected from the scalp among the numerous inverse methods proposed until now. Combining such details with an accurate representation of the volume generator, likely subject-specific or patient-specific (Realistic MRI [197]), such practices increase the accuracy of localized sources considerably, along with the estimation of time series that are equivalent to the local field potential. Such time series then becomes the input information of

what is known as "connective methods," which attempt to estimate the brain networks at the source field directly.

The analysis of sensors level recording connectivity measurements is not precise, given that these recordings suffer from low spatial resolution and are severely affected by field spread effects [198]. To overcome these problems, a series of attempts have been made [113, 195, 199, 200, 201], to apply connectivity methods on the temporal dynamics of reconstructed scalp EEG sources. This approach is conceptually very attractive because networks are located directly in the source space, typically in the neocortex. However, a number of methodological issues are raised. First, it requires the inverse EEG problem to be solved. Second, among the many available ones, a connectivity method has to be chosen.

Connectivity estimations are based on a two-step approach, which involves an estimate of the brain source firstly, and it's time course using an inverse method, then calculating the connectivity metrics using the estimated time courses of brain source.

Our approach to estimate the connectivity includes two significant aspects:

1. The inverse algorithm used to estimate and reconstruct the cortical sources of the EEG measurements at a given instant of time.

   The current source position estimation of EEG signals is an ill-posed inverse problem. An inverse problem is the estimation of the activation time courses and locations for neural sources contributing to an electroencephalographic (EEG) record. A wide range of inverse solutions exists to date, taking account of the fact that different experimental environments may require different source characterizations [34]. Distributed solutions estimate the whole brain's activity at once. Early approaches used restrictions on spatial smoothness to achieve a unique solution [202, 203]. Other scientists have introduced spatial focal sources of sparsity penalties [204, 205]. Simultaneous localization of the whole series of space and time dynamics, which have been modeled using different combinations of penalty terms, was also made possible by the development of robust computing solutions [206]. Other kinds of inverse processes are based on temporary assumptions only, whereas for each location of the brain, the source activity is estimated separately [28, 207].

   Generally, the number of dipoles and their location varies dynamically by the time. At every stage of the measurements described, the neural dipole numbers and its position are dynamically evaluated and updated with random finite sets to handle the unknown

dipoles number. In this thesis, used particle filter (PF) to find the location and amplitude for equivalent current dipoles of EEG signals, as described in the previous chapter (Localization).

2. The connectivity approach used to determine functional relationships between temporal source dynamics.

   The EEG based brain connectivity analysis, which is related to estimating the interaction of the sources based on the reconstructed time cycles. There is a wide range of methods exist which are based on various brain interaction models. Approaches defining interaction based on cross-spectrum are among the most popular methods [208, 209, 210], Granger causality [40, 43, 45, 211], dynamic causal modeling [111], and other nonlinear relationships such as correlations of the phases or amplitudes of brain rhythms [201, 212]. There are numerous literature on basic and clinical neuroscience research methods [113, 213, 214, 215]

The intriguing ability of neuronal populations to create large scale oscillatory couplings has been theoretically considered to be one of the fundamental brain mechanisms [46]. A dynamic pattern of brain connectivity causes these behaviors on a large scale. Anatomical connectivity refers to the particular arrangement of macroscopic fibers that link various brain regions within this macro-scope context. Functional Connectivity is a fundamental statistical concept which refers to the existence of synchronized patterns between the temporal activations of neural networks, which are often distinct. This definition may measure functional connectivity, e.g., by cross-relation, cross-spectrum [216], and mutual information [217].

It is not only essential to identify anatomical and functional links in highly interconnected brain systems, but it is also necessary to measure the extent to which the individual brain networks are contributing to the production of information and its exchange of information. Such directional interactions form effective brain connectivity that provides essential knowledge about mechanisms to incorporate functional integration in the brain.

However, brain connectivity evaluation is based on the correct localization and time series reconstruction. Consequently, it is more challenging than inverse source reconstruction alone and requires careful validation. The validation of brain connectivity analysis based on EEG is more complicated than the restoration of the source. Validating the connectivity in real data is difficult, as the source positions are not available, and connectivity between them is not straight forward. However, it is also hard to identify suitable performance measures even when the ground truth is possible, as localization errors can lead to inappropriate assessments of the

source connectivity of exact source positions. It is probably a prevalent practice that authors perform brain connectivity evaluations on the real data and report them only limited empirical validation of the methodology being used as a result of these problems. Some studies have simply presented the measure of connectivity as the definition of communication.

A significant challenge is the accurate identification of brain networks associated with specific cognitive functions from non-invasive data. EEG source space connectivity can be used to identify the connectivity among brain sources. EEG localization techniques and connectivity methods have been developed considerably over the past decades separately. Proposed that the inverse problem addressed based on particle filter and connectivity methods should be used jointly, which has never before been done. The particle filter was applied to extract the sources and their amplitudes and applied the multivariate model on estimated sources, using the Granger causality techniques to obtain the effective connectivity measures of the given data. This chapter aims mainly to identify which area of the brain can manipulate statistical dependence between cerebral neurons.

5.2 Connectivity measures

The purpose of any connectivity study in the brain is to understand the nature of the brain circuits and how they evolve over time [218]. To understand brain connections and associations between various parts of the brain, three forms of brain connectivity can be defined: anatomic, functional, and effective connectivity [219]. Techniques for anatomical connectivity depend on physical and structural neuronal unit connections. It is based on the identification of fiber pathways that link the brain regions physically. These are the anatomical network maps that show possible routes for signals to move in the brain [220, 221].

The goal of functional connectivity analysis is to explore statistically temporal or spatial co-variations in neuronal unit behavior, typically identifying cross-correlation or coherency steps, but the extent and orientation of the information flow and interactions between specific neuronal units are not taken into account in these kinds of studies [222]. Effective Connectivity takes the experience of functional connectivity and goes a step further and determines the direct or indirect influence of the neuronal network, including the direction of the dynamic information flow in the brain. Effective connectivity may be used to understand causal relationships between entities of the brain network and predict the activity of a brain structure by integrating information from past activities of other brain structures [223, 224].

5.2.1 Functional connectivity

The most widely used methods for functional connectivity in the EEG context are those focused on linear/nonlinear correlation, coherence, phase synchronization, mutual information. The efficiency of each approach, which typically has its advantages and limitations in every sense (cognitive study or clinical application), is a crucial issue and that there is no consensus about one standard method that outperforms the other. In this chapter, correlation, coherence, and the imaginary part of coherence are described as they are the most widely used methods of EEG connectivity.

Correlation:

One of the oldest and probably most classic measures of interdependence between two series of times is the cross-connection coefficient (r_{xy}^2). The linear correlation between two signals x and y , possibly delayed by τ :

$$r_{xy}(\tau)^2 = \frac{\left(cov\left(x(t), y(t+\tau)\right)^2\right)}{\left(std\left(x(t), std(t+\tau)\right)^2\right)} \tag{5.1}$$

$$r_{xy}^2 = \max\left[r_{xy}(\tau)^2\right], -\tau_{\max} < \tau < \tau_{\max} \tag{5.2}$$

Where cov , std denotes the covariance and standard deviation correspondingly, $\tau_{\max}$ is the maximum time shift between the two signals.

Coherence measures:

Coherence is a mathematical method quantifying the frequency and amplitude of oscillating brain activity connectedness in neuronal patterns. This technique quantitatively measures the neuronal patterns of scalp electrodes (EEG) synchronicity [225]. The consistency of the relative amplitude and phase between signals is calculated in the set frequency band. When the signal is in phase in the sensor space, its magnitudes are added and signals can be removed, and the value of coherence is decreased when they are out phase. The amplitude of the underlying source can be used in the source space to determine the connectivity strength.

The quantification method first applies a decomposition of the time-frequency, such as the Fast Fourier transform (FFT), to the time series. This produces an amplitude/phase sequence of components for each small-frequency bin (i.e., 2–4 Hz) in the FFT, which extends over the frequency (i.e., 1–100 Hz) of the data content. After a transformation into time-frequency

representation, the significance of network interactions can be calculated by measuring coherence that measures synchrony between signals in each FFT frequency bin. Coherence is a linear approach for neuronal connectivity measurements in the frequency field. The result is a symmetrical matrix with no directionality information. Coherence is the most common tool used to evaluate whether various areas of the brain are producing signals that are substantially correlated (coherent) or not (not coherent). Concerning coherence, measurements are used to evaluate the interaction between two data sets. This is used to determine whether two inputs have the same or different content of the signal. If two signals are similar, they have a coherence value of 1; depending on the variations between the measures, the coherent value approaches 0.

The coherence divided into two types: coherence, and imaginary coherence (ImCoh). These coherent measures between the different brain areas can be used to analyze seizures across brain regions.

Coherence: The coherence coefficient is a widely used metric, which is the computation of phase synchrony between two measured signals. The coherence mathematically corresponds to the frequency domain of the cross-correlation function. The squared value of coherence defines the amount of variance in one of the signals that can be explained by the other signal as a function of frequency, or vice-versa as analogous to the squared correlation coefficient in the time domain and this value is a complex quantity. The coefficient of coherence is a normalized value limited between 0 and 1, and is mathematically computed as

$$C_{12}\ (f) = \frac{S_{12}(f)}{\sqrt{S_{11}(f)\,S_{22}(f)}} \tag{5.3}$$

Where the spectral density between the 1 and 2 signals is $S_{12}(f)$. The coherence coefficient is $C_{12}(f)$ and ranges from 0 to 1. When the value is zero, the signals are not correlated, and when they are one, there is a high correlation between the signals. In equation (1), the coherency is normalized because need to focus on the phase difference between the signals. $C_{12}(f)$ is the coherency, and its absolute value is coherence.

Imaginary Coherence: Coherence is a measure commonly used to predict synchronicity across different sensor-level areas. The drawback in coherence is that volume conductivity is heavily influenced. New approaches have recently been suggested to eradicate this problem. The imaginary part of coherence is obtained when the complex-valued coherence is mapped onto the imaginary (y-axis) axis. Over the past few years, this measure has gained momentum,

particularly in EEG connectivity studies [226, 227]. The imaginary part of coherence (ImCoh) is a measure that represents the phase activity of two or more EEG signals at the same time. This approach has a 100% optimistic predictive quality, which means that any concerted action takes place as it generates significant values. It is given by

$$iCoh_{12}(f) = Im(C_{12}(f)) \tag{5.4}$$

If there is no constant phase difference between the two EEG signals, the exponent or imaginary part becomes zero, then $C_{12}(f)$ coherency is real-valued. But because of their exclusive reliance on the ImCoh, in some cases, even in the case of a substantial true interaction, functional connectivity calculations dependent on ImCoh are neglected, e.g. the phase difference between two signals is almost zero, or 2π. ImCoh can consider as robust to volume conduction artifacts. Here this robustness represents that the ImCoh disappears for independent sources, even if diverse into sensors or projected sources. If the ImCoh or other measures vigorous to volume conduction show a unique variation from 0, this shows a mark of true connectivity, which cannot be explained by a mixing artifact.

However, the interpretation of the cross-correlation function becomes complicated when it is estimated from neuronal signals with bidirectional interactions, which is the dominant interaction scenario in the majority of cortical connections. The cross-correlation functions of these interactions typically lack a clear peak. They have significant values at both positive and negative lags, indicating complex, bi-directional interactions that occur at multiple delays. The directionality of the communication between networks alone cannot be determined by coherence.

Specific techniques can be used to overcome this constraint, to determine how often past values of one time series will predict future values of other time series, and vice versa. This concept is formally applied to Granger's causality metric. This metric can be computed using a linear autoregressive model that fits the data and through the non-parametric computation of spectral matrices, which allows an estimation of directional interactions. In particular, the interaction from signal x to signal y and from signal y to signal x can be estimated separately.

5.2.2 Effective connectivity

Functional connectivity is a measurable phenomenon that can be quantified by statistical dependence measures such as correlations, coherence, or entropy transfer. Instead, effective

connectivity corresponds to a model parameter that tries to describe obvious connections (functional connectivity). The effective connectivity in this sense corresponds to the intuitive concept of coupling or directed causal influence.

From parametric spectral estimators, frequency-resolved estimates of directed brain interactions can be derived with multivariate autoregressive models (MVAR-models) [228]. The direct relationship can be measured with the direct Transfer function (DTF) [229] or with the partial directed coherence [40, 102] after fitting the MVAR model with the time courses of the estimated sources. These connectivity measures are designed as the frequency domain of the Granger causality (GC) [112].

Due to its simplicity, the effective connectivity analysis based on GC methods in recent years has received considerable attention. This is based on Granger's interpretation that knowing the time series of the carrier will, at a later time, enhance the estimation of the time series of the receiver [112, 128]. Many frequency domain connectivity estimators were carried out through MVAR EEG time series modeling [228].

To maximize model effects, the model order based on the Akaike information criterion (AIC) [230] and the Bayesian information criterion (BIC) [231]. Moreover, the critical issue for GC is the ratio between the number of independent observations (i.e., samples) and the complexity of the model (i.e., model order or parameters). If the number of observations is essential in comparison to the number of parameters, it is most likely the model order selection criteria are valid. If there are a limited number of findings, other parameters such as correct AIC for model order selection should be used.

The preliminary task of any GC based study is to estimate the MVAR model parameter. After an MVAR model has been applied to the time course of estimated sources, a combination of time domain and frequency domain measurements can calculate directed interactions. In many other applications, the frequency domain MVAR modeling was implemented based on effective connectivity measures, such as Directed Transfer Function (DTF) [40] and Partial Directed Coherence [102].

Granger causality modeling:

Based on Granger's theory, MVAR modeling is used to formulate the GC-based effective connectivity analysis. The MVAR model of K signal sources may be specified as

$$s(t) = \sum_{k=1}^{p} r(k)\, s(t-k) + a(t) \tag{5.5}$$

Here $s(t)$ represents the $M \times 1$ neural sources time series, M is the number of sources. $r(k)$ is the $M \times M$ coefficients matrix, which can be attained from the AR model, and Akaike and the Bayesian Information Criterion can calculate the model order p of the AR process. $a(t)$ is the vector of white noise input with covariance Σ_a . Rearrange the Equation 5.5

$$a(t) = \sum_{k=0}^{p} \hat{r}(k)\, s(t-k) \tag{5.6}$$

where $\hat{r}(k) = -r(k)$ and $\hat{r}(0) = I$. Convert the equation 5.6 to the frequency domain by applying FFT

$$A(f) = R(f)\, S(f) \tag{5.7}$$

Multiply both sides with $R^{-1}(f)$ to obtain

$$R^{-1}(f) * A(f) = R^{-1}(f) * R(f)\, S(f) \tag{5.8}$$

$$S(f) = Q(f)\, A(f) \tag{5.9}$$

where $Q(f) = R^{-1}(f)$ .The $A(f)$ system input (white noise), $S(f)$ system output, and $Q(f)$ the system transfer function can be seen in a linear filter above the frequency domain representation. This transfer function should give information about the structure of modeled system. Therefore, the system cross spectra can be extracted using the transfer function values.
The power spectral density can be given as

$$PSD = S(f)\, S(f)^* = Q(f)\, \Sigma_a Q(f)^* \tag{5.10}$$

The cross spectral density is given as

$$CSD = C_{ij} = S_i(f)\, S_j(f)^* = Q_i(f)\, \Sigma_a Q_j(f)^* \tag{5.11}$$

$*$ denotes complex conjugation and matrix transpose. C_{ij} represents the cross-spectral density of elements (i, j) . If the residuals are uncorrelated, the covariance matrix will be a diagonal matrix given as $\Sigma_a = diag\left(\sigma_i^2\right)$.

Based on the MVAR model, several time-domain and domain frequency measures are developed for the estimation of effective connectivity. Some of these measures and their mathematical formulation are subsequently presented.

Granger causality Index (GCI): It is a bivariate time domain measure based on prediction error. Let us consider the time series $s_i(t)$, $s_j(t)$.

$$s_i(t) = \sum_{k=1}^{p} r'_{11}(k)\, s_i(t-k) + a(t) \tag{5.12}$$

$$s_i(t) = \sum_{k=1}^{p} r_{11}(k)\, s_i(t-k) + \sum_{k=1}^{p} r_{12}(k)\, s_j(t-k) + a_1(t) \tag{5.13}$$

$$s_j(t) = \sum_{k=1}^{p} r_{21}(k)\, s_i(t-k) + \sum_{k=1}^{p} r_{22}(k)\, s_j(t-k) + a_2(t) \tag{5.14}$$

If $\Sigma_1 < \Sigma$, by including the terms of s_j, then it is said that s_j is Granger causes s_i. The directed influence between the two sources is given by the logarithmic ratio of residual variances as

$$GC_{ij} = \ln\left(\frac{\Sigma}{\Sigma_1}\right) \tag{5.15}$$

This definition can be extended to the multichannel system by considering how the inclusion of the given channel changes the residual variance ratios. To quantify directed influence from a channel s_i to s_j for n channel autoregressive process in the time domain, consider n and $n-1$ dimensional MVAR models. First, the model is fitted to the whole n -channel system, leading to the residual variance $var_{i,n}(t) = Variance(A_{i,n}(t))$ for signal s_i. Next, a $n-1$ dimensional MVAR model is fitted for $n-1$ channels, excluding channel j, which leads to the residual variance $var_{i,n-1}(t) = Variance(A_{i,n-1}(t))$.

Then Granger causality is defined as,

$$GC_{ij}(t) = \ln\left(\frac{var_{i,n}(t)}{var_{i,n-1}(t)}\right) \tag{5.16}$$

Directed Transfer Function (DTF): The DTF from the j^{th} source to the i^{th} source at certain frequency f is denoted by $DTF_{ij}(f)$ and is defined as the ratio of influence of $s_j(t)$ on $s_i(t)$, concerning the combined influence of $s_1(t), s_2(t), \ldots s_p(t)$ on $s_i(t)$. The DTF can be compactly expressed in terms of transfer matrix elements such as:

$$DTF_{ij}(f) = \frac{Q_{ij}(f)}{\sqrt{\sum_{l=1}^{p} |Q_{il}(f)|^2}} \tag{5.17}$$

Here $Q_{ij}(f)$ is an element of a transfer matrix of the MVAR model. The above equation defines a normalized version of DTF, which takes values from 0 to 1, producing a ratio between the inflows from channel j to channel i to all the inflows to channel i. 0 means no connectivity; 1 means full connectivity.

Partial Directed Coherence (PDC): PDC is given as

$$PDC_{ij}(f) = \frac{R_{ij}(f)}{\sqrt{\sum_{l=1}^{p} |R_{\ln}(f)|^2}} \tag{5.18}$$

In the above equation $R_{ij}(f)$ is an element of $R(f)$ —a Fourier transform of MVAR model coefficients $r(t)$. Since it is a function that operates in the frequency domain, $R(f)$ dependency on the frequency but does not have a direct correlation with the power spectrum. It follows from the normalization condition that PDC takes values from the interval [0, 1]. PDC only shows the direct flow between sources. Unlike DTF, PDC is normalized to show a ratio between the outflows from channel j to channel i to all the outflows from the source channel j, so it emphasizes instead the sinks, not the sources.

5.2.3 Implementation of proposed approach:

The process of measuring the connectivity is as follows:

1. Calculate the leadfield matrix and source space.
2. The number of dipole sources are unknown and are time-variant. For this situation, we model these multiple dipole sources as a random finite set.
3. Start analyzing the data at time t=1
   (a) Based on the probabilistic criteria, initialize the particle.
   (b) Assign the weights to each particle
   (c) Normalize the weights
   (d) Most of the particles with high weights will dominate the low weight particles. The dominance of this particle degeneracy leads to the poor posterior likelihood density function. Use resampling methods to discard the small weight particles.
   (e) Prepare dipole configuration for the next time step.

4. Extraction of dipoles and their time series using particle filter for EEG data.

5. The MVAR procedure portrays the connection between the sources inside the brain, particularly as far as the effect of one variable on another. MVAR allows us to derive time and frequency domain pictures of causality through the model order coefficients and their spectral representation.

6. The connectivity is calculated from the dipole communication modeling and estimation of the model order.

7. Connectivity measures able to compute causality in the time and frequency domain are correlation, coherence, the imaginary part of coherence, GC and PDC, DTF, respectively. Apply these measures and compute the directional connectivity between the sources.

5.3 Results

For the simulation of the proposed method, the data is obtained from Brainstorm EEG/Epilepsy dataset. The data were recorded at a frequency of 256 Hz using 29 channels (FP1, FP2, F3, F4, C3, C4, P3, P4, O1, O2, F7, F8, T7, T8, P7, P8, Fz, Cz, Pz, T1, T2, FC1, FC2, FC5, FC6, CP1, CP2, CP5, CP6) as per the 10/20 International framework. The simulation was performed for the EEG data from 137000 to 2000000 samples over 921600 samples.

The connectivity procedure contains two phases, i.e., source localization and connectivity estimation. In source localization, firstly, the leadfield matrix is computed using fieldtrip toolbox [232]. The leadfield matrix and the EEG data were applied to the particle filter to estimate the source position and source amplitude with respect to time. The estimated sources and their time series have shown in Figure 5.1a and 5.1b, respectively.

After the source localization, the source time series had been applied to the MVAR model to find the interactions over time. Source connectivity measures obtained by using functional connectivity methods have shown in Figure 5.2. In Figure 5.2a, 5.2b, and 5.2c, the connectivity measures obtained from correlation, coherence, and imaginary part of coherence methods were illustrated correspondingly.

Connectivity measures by using GCI of effective connectivity methods were obtained, as shown in Figure 5.3. The establishment of the relation between source1 to source4, source5 to source4, and source2 to source3 is demonstrated. The time-frequency maps between sources

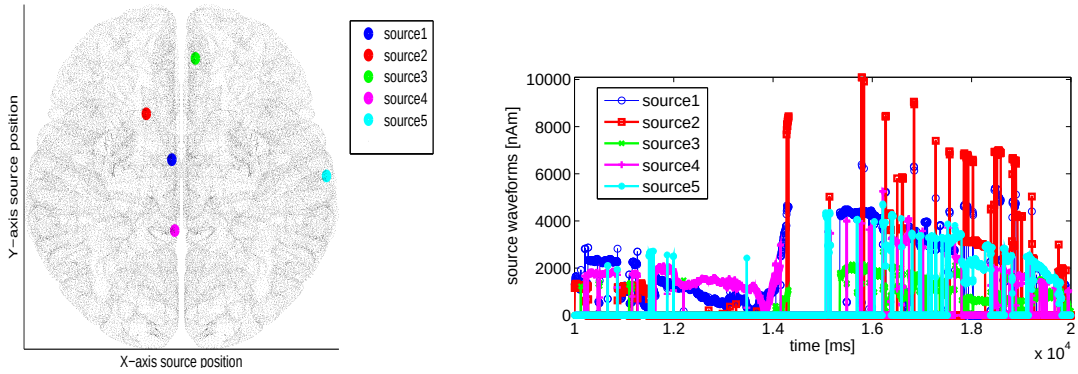

(a) (b)

Figure 5.1: a) Source Locations of the real data after the Localization b) estimated source time series after localization

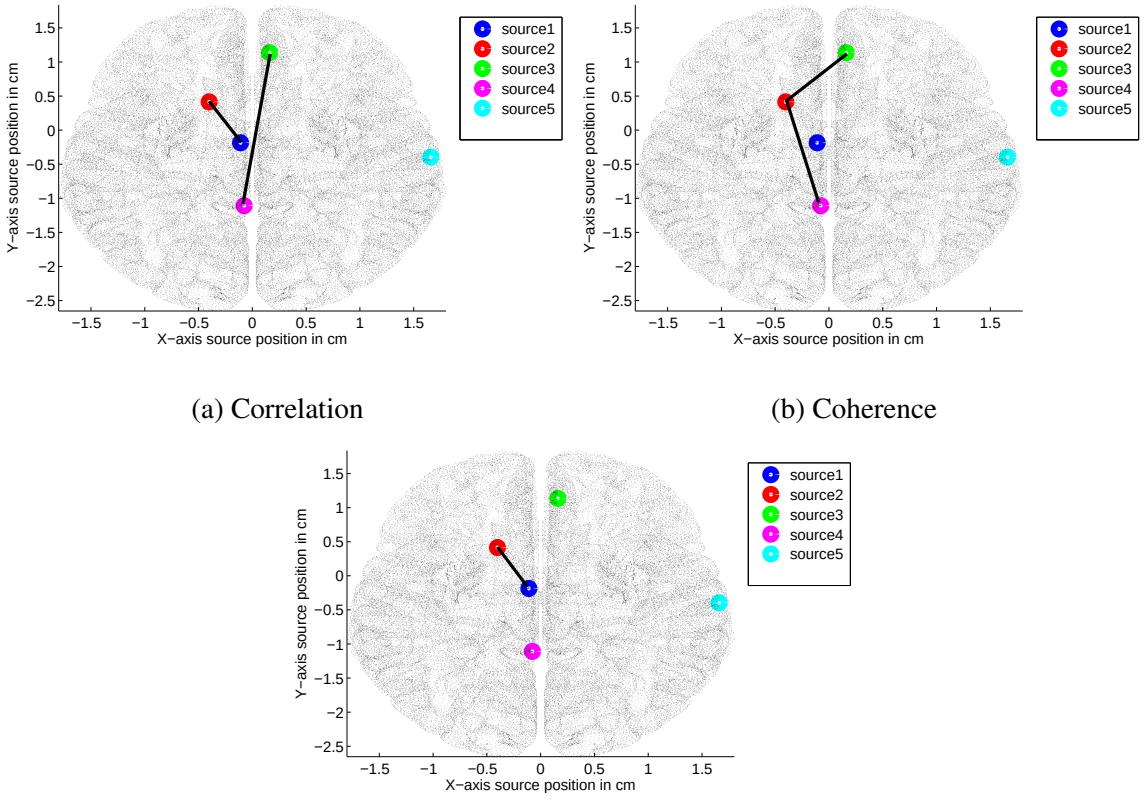

(a) Correlation (b) Coherence

(c) Imaginary Coherence

Figure 5.2: Source connectivity measure by Functional connectivity methods

1 and 4, 2, and 3, 4, and 5 for the GCI method is observed in Figure 5.4a, 5.4b and 5.4c correspondingly.

In Figure 5.5, Directed transfer function connectivity estimation is illustrated. In Figure 5.5a, the connectivity is shown from source1 to source2, source1 to source3, source1 to source4,

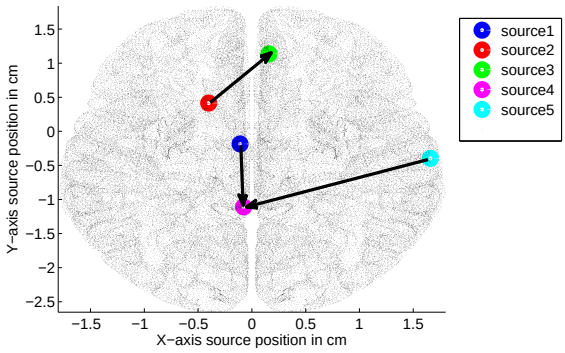

Figure 5.3: Source connectivity measure by GCI

source1 to source5 up to 4Hz. Figure 5.5b), the connectivity between source1 to source4 and source3 to source2 from 4Hz to 8Hz. In Figure 5.5c), the connectivity between source1 to source4 from 8Hz to 16Hz. After 16Hz, DTF does not show any connectivity between the sources. The time-frequency diagrams between the sources 1 and 3, 2, and 4 for the DTF method obtained using the DIPFIT toolbox were shown in Figure 5.6a) and 5.6b) respectively.

Figure 5.7 demonstrates the estimation of PDC with respect to frequency. In Figure 5.7a, the connectivity is shown from source1 to source4 and source3 to source2 up to 4Hz. Figure 5.7b, shows the connectivity between source1 to source4 from 4Hz to 16Hz. After 16Hz, PDC is not showing any connectivity between the sources. The time-frequency maps among the sources 1 and 4, 2, and 3 were shown in Figure 5.8a and 5.8b, respectively.

From the effective connectivity estimations, it can be observed that GC, PDC, and DTF demonstrate the directional connectivity between source1 to source4.

5.3.1 Discussion

The study of brain efficient connectivity based on EEG data is a challenging task because the volume conduction adversely affects the interpretability of sensor-space connectivity estimates and may also yield inaccurate results. The confounding effects of volume conduction complicate the interpretation of the connectivity measures at the source level. Where a 'traditional' inverse method is used before the connectivity measurement is computed, this applies irrespective of the connectivity measure used. Applying (any) inverse source reconstruction is often assumed to eliminate the effects of volume conductivity in the data so that connectivity measures designed to function well on unmixed data can be applied without hesitation to recon-

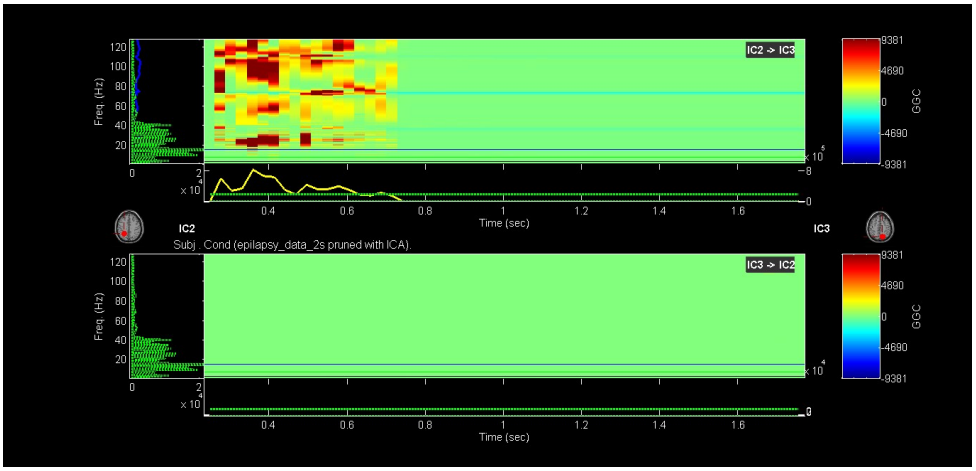

(a)

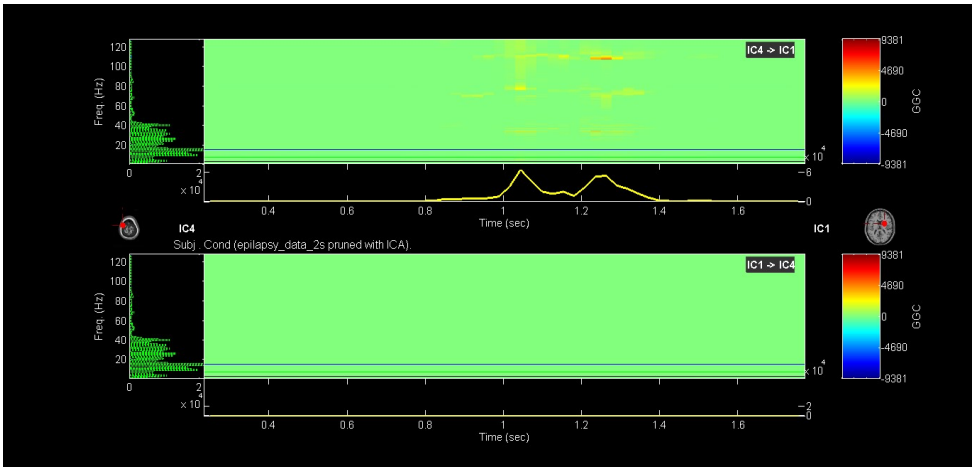

(b)

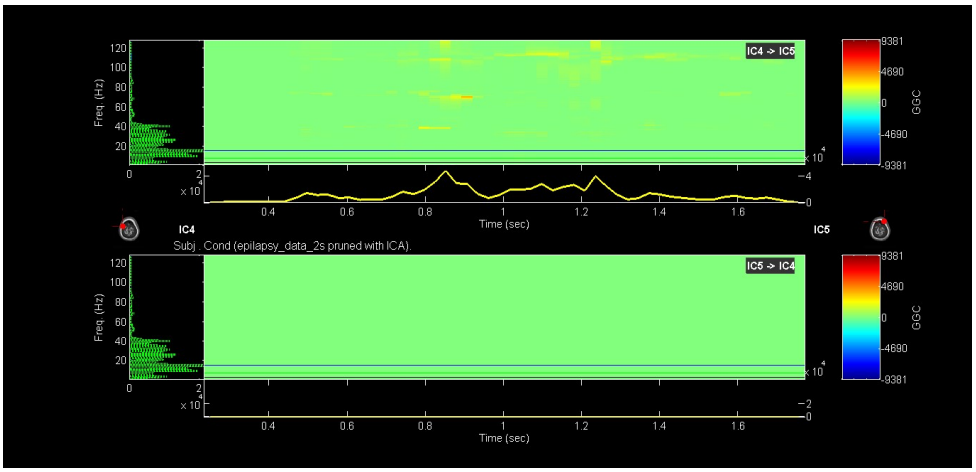

(c)

Figure 5.4: time frequency maps using DIPFIT Method- GCI- a) IC2 to IC3 b) IC4 to IC1 c) IC4 to IC5

structed sources. In this chapter, new methods are developed for reconstruction of interacting sources which are elegant in overcoming these issues.

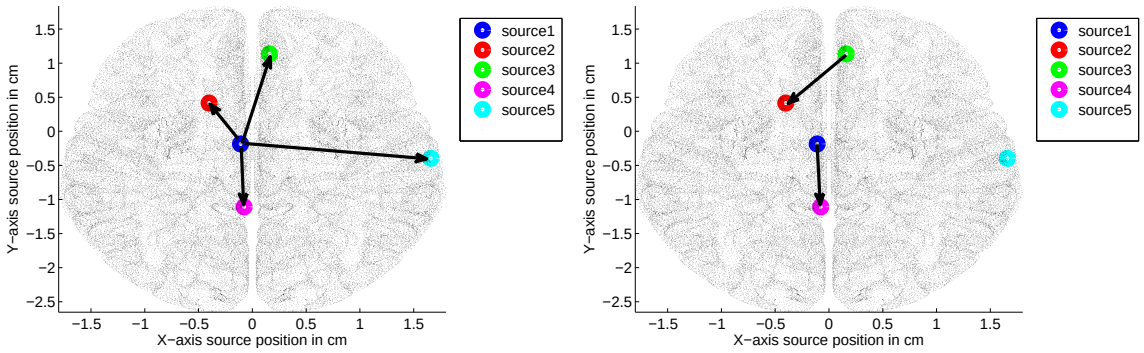

(a) Up to 4Hz

(b) From 4Hz to 8Hz

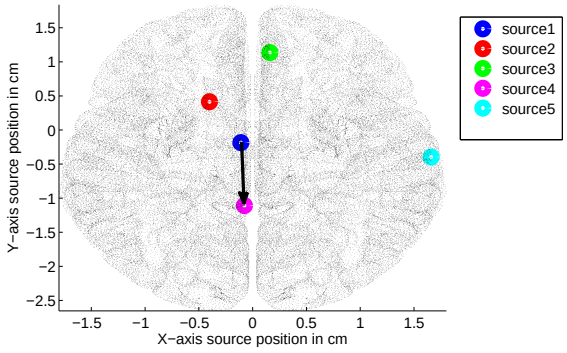

(c) From 8Hz to 16Hz

Figure 5.5: Source Connectivity measure by DTF

Two general directions are followed in this thesis: source reconstruction and connectivity between sources. The effect of volume conduction on sensor data and dependency between the underlying brain sources is taken explicitly into account in our procedures. As a result, they are outstanding in terms of the reconstruction of interacting brain sources. Our efforts in this area can be seen as an essential step in the analysis of EEG source connectivity. Our approaches model the estimated sources time course as a combination of correlated sources, whose connectivity is represented by a source model MVAR.

The current simulation study demonstrates that from the EEG measurements proposed method estimates brain source interaction. The functional and effective connectivity measures on real EEG data are tested. While effective connectivity measures are applied directly to the source time series, they estimate the correct direction of the information flow.

Inter-dependency analysis from bi-variate to multivariate signals has become increasingly attractive. This is important since pairwise analysis in cases where one driver drives two responses is likely to find spurious correlations. In this situation, all responses may have a shared driver, even though the reactions tend to be completely independent. Various techniques, such

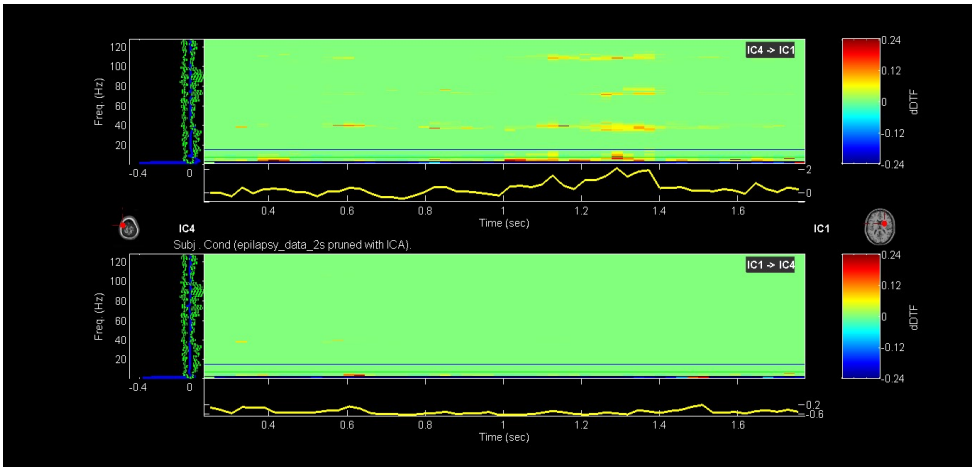

(a)

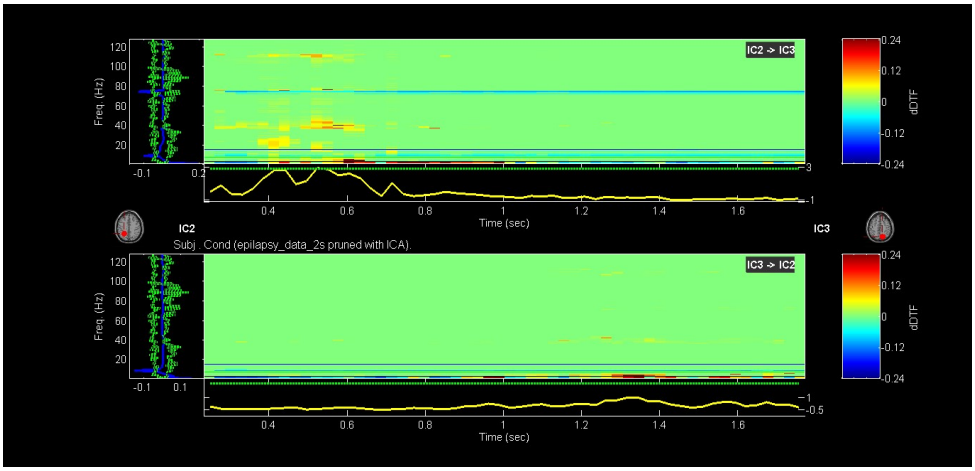

(b)

Figure 5.6: time-frequency maps using DIPFIT Method- DTF- a) IC4 to IC1 b) IC2 to IC3

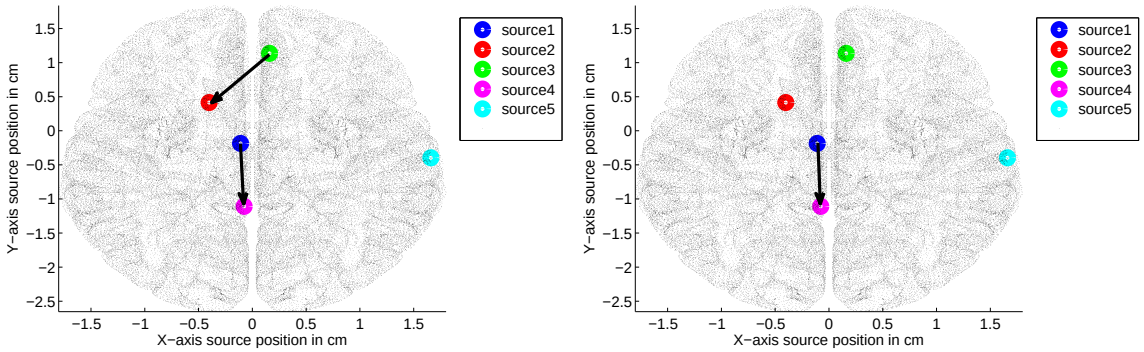

(a) Up to 4Hz (b) From 4Hz to 16Hz

Figure 5.7: Source Connectivity measure by PDC

as GC, DTF, PDC measures, are multivariate. These all methods depend however on the reliability of the fitted MVAR model and in particular on the order of the model. When the order is too low, the model misses the signal's dynamic nature, whereas when over-fitting is too high,

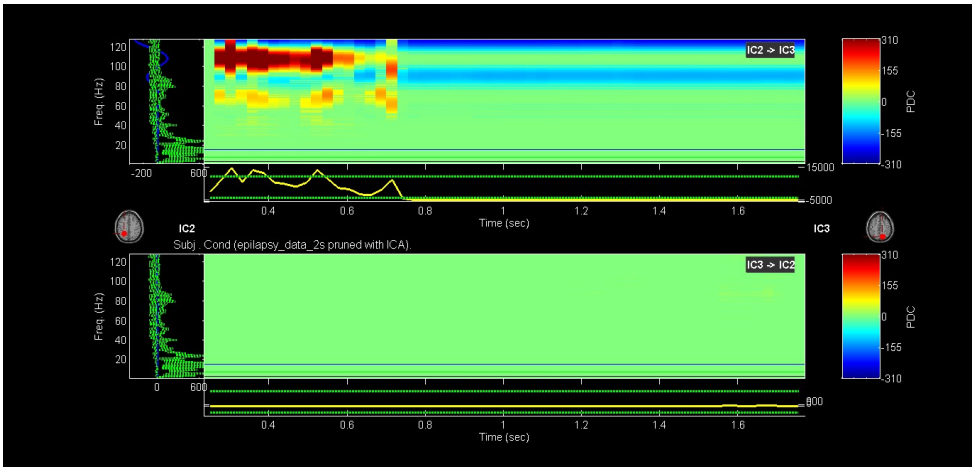

(a)

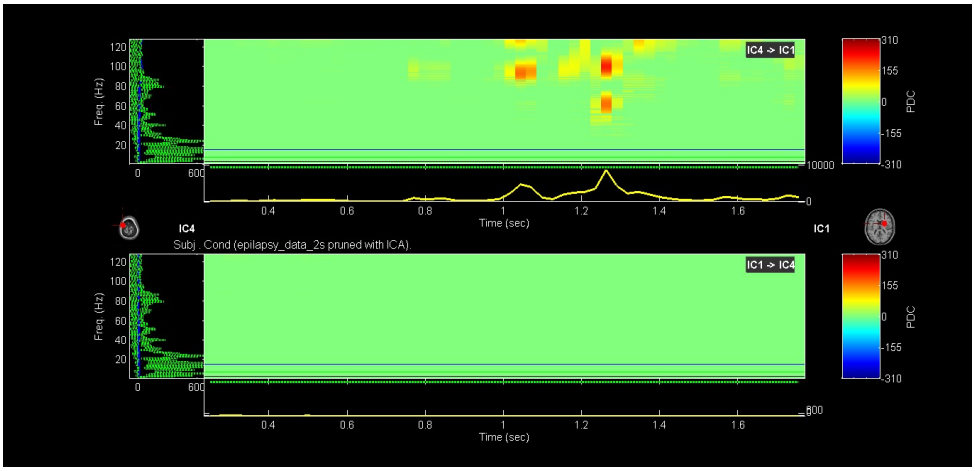

(b)

Figure 5.8: time-frequency maps using DIPFIT Method- PDC- a) IC2 to IC3 b) IC4 to IC1

noise is emphasized in particular. Several methods may be employed to evaluate optimal model order, such as the AIC or BIC. Granger causality, DTF and PDC, in particular, tend to estimate the flow of information between sources.

Continuous development of EEG neuroscience approaches has been effective in identifying the root causes of various neurological conditions and neurodegenerative diseases [233]. This section presents studies that implement different methods of connectivity. Efficiency depends significantly on how each connectivity method is applied and the underlying assumptions. Epilepsy is a common, extensively studied neurological disorder using EEG as well as MEG. Localization of epileptogenic brain-behavior to help identify a surgical lesion is one scientifically valuable application [234]. Visual examination of EEG tracings or conventional spectral analysis of focal epilepsy cannot reveal any variations in patients with a history of seizures and healthy controls. More sensitive connectivity techniques, however, are useful to assess neuro-

physiological activity and guide clinical management, which can identify subtle abnormalities [235].

A critical parameter is also the frequency bands used to calculate the effective connectivity. Granger Causality, DTF, and PDC are useful tools to investigate influences between neural groups. It can be applied to multivariate time series of different neural signal types. When applied to focal epilepsy data, it can be useful to non-invasively study inter-regional interactions with high spatial, temporal, and frequency precision in humans under normal physiological conditions. The results also demonstrate an illustration of the sources reconstructed for ROI (temporal lobe). Our results show that the location of the anticipated seizure is close to the temporal lobe. A critical parameter is also the frequency bands used to calculate the effective connectivity. Our results suggest that directional connectivity in the delta band (0-4 Hz), theta band (4-8 Hz) as well as oscillations in the alpha band (8-16 Hz). The theta band is related to the focal sub-cortical lesions, as typically observed in the temporal lobe. Able to identify the brain networks close to temporal lobe connections through our study.

The findings of connectivity have therefore been interpreted quite qualitatively utilizing the visualizations that neurophysiologists can generally interpret. In this context, attempts to develop a generalized quantitative evaluation scheme for EEG-based connectivity analysis and perhaps use the proposed dataset are encouraged. The overall estimate is divided into source localization and connectivity evaluation steps in precise source connectivity analysis and must, therefore, be assessed. We also quantified the accuracy of the source estimates by using the proposed inverse source reconstruction approach for synthetic data results. A fair quantitative evaluation is only feasible if the approximate sources are compared one-to-one to actual sources, which is not always possible. Because a method works well here, given the simplicity of the current simulation scenario, it does not, of course, guarantee that it does so with any other data set. But results obtained for several different methods indicate the preferred method.

5.4 Summary

The inverse and connectivity methods should be used jointly. Our findings indicate that the combination of particle filter and the functional, effective connectivity techniques used for focal epilepsy data and outcomes are significantly relative to the results in this same task. The particle filter was applied to extract the sources and their amplitudes and applied the multivariate model on estimated sources, using the correlation, coherence and imaginary coherence of the functional connectivity measures and Granger causality techniques to obtain the effective

connectivity measures of the given data. The simulated results show the directed flow among the sources by using Granger causality methods. Effective connectivity measures relying on Granger causality provide a correlation of specific frequency coupling in neural populations. Results showed that the effective connectivity at source level intensely depends on solving the EEG inverse problem and on the effective connectivity methods.

Chapter 6

Conclusions And Future Scope

6.1 Conclusions

A novel approach is proposed in this thesis to evaluate the scalp source EEG connectivity. The method proposed is based on an estimation of the time seriesof each neural source and its spatial characteristics using particle filters. Initially, each of these sources will be identified at a time by solving the inverse EEG problem from its raw scalp potential. This method avoids the prior constraints for localizing sources. Our studies found that current cerebral sources were distributed in conjunction with recent studies on EEG generators that support the idea that the novel approach is accurate.

The results which determine the positions of brain activity due to focal epileptic information is consistent with current knowledge about neuropsychology. The location of the source-reported focal epileptic activity in the cortex indicated the primary epileptic zone. The 3D location of the focal epileptic activity and the EEG data is available for identifying the location of the central epileptic region in the brain cortex, or the structure of the deeper temporal lobe. The results of the localization of a source can confirm that EEG measurements improve the correlation between epileptic localization and brain anatomy. Our findings indicate that the location of the expected seizure is near the temporal lobe, which is consistent with prior research.

In localization, the proposed approach can be utilized for resampling in the PF, in particular the minimum sampling variance resampling, which dependably produces the particle set characteristic of the sampling variance. Extensive simulations have conducted on both synthetic and real EEG experiments, to study the accuracy and robustness of the proposed algorithm. The optimality of the proposed procedure was exhibited in principle by using real data from estimating source locations in the cerebrum. Considering the outcomes regarding both location

and sampling variance, the proposed MSV resampling approach results in the smallest sampling variance among other resampling methods, which delivers a consistent number of equally weighted particles. This agrees with the theoretical justification. Next, the branching resampling algorithm is used in source localization to adaptively increase dynamic state estimation performance for tracking multiple neural dipole sources. Simulations demonstrated that the estimation performance is significantly improved, and the processing speed is faster due to the branching resampling in the particle filter.

The partial stratified resampling method is used in the particle filter for neural source localization and presented a comprehensive performance analysis of the resampling methods, namely multinomial, stratified, systematic, and partial stratified resampling methods in the particle filter. Our findings indicate that PSR's computational time is less than the traditional techniques of resampling, as only a few particles are resampled based on the defined threshold values. The PSR algorithm classifies weights according to a high threshold and low threshold. Nine separate threshold values are specified, with the interval between the two limits being increased progressively from 0.1 to 0.9 to estimate the position of the neural source for each situation. Our analysis demonstrated clearly that PSR is very reliable, and takes 65% less time than stratified resampling because only fewer particles are resampled. In particular, the PSR algorithm is time-efficient and can be used for estimating the location of the neural sources, as the computational complexity is low. In summary, using PSR, it is possible to achieve high speed for the location of the neural source than conventional methods of resampling.

If the number of neural dipole sources is not known, three methods of resampling for the particle filter have been suggested for both the number of dipole and its parameters to determine and demonstrate its output using computational simulations for synthetic as well as actual EEG data. In terms of MSE, relative accuracy and computer time, the method proposed achieves good performance with significantly less particles than the existing approaches.

For estimating the connectivity, both the source reconstruction and connectivity measures are used. Firstly, Particle filter is used for estimating the source locations, the time series. Secondly, MVAR modeling is applied on the time series and Functional, Effective connectivity measures are used to estimate connectivity. Granger Causality, DTF, and PDC are useful tools to investigate influences between neural groups. It can be applied to multivariate time series of different neural signal types. When applied to focal epilepsy data, it can be useful to non-invasively study inter-regional interactions with high spatial, temporal, and frequency precision in humans under normal physiological conditions.

6.2 Future Scope

There are still several issues that need to be addressed.

For neural dipole sources, the state evolution model is a random walk model. It is a general model that carries little knowledge about the evolution of neural dipoles over time. However, a more accurate model of state evolution is needed to improve the tracking performance further. For each type of disease, this model is likely to be different. Thus one method might be to use a set of training data to find the trajectory of the moving dipole and to build a model of state evolution for a specific trajectory-based brain disease.

These new connectivity indexes may be useful information on event-related brain potential mechanisms, which is a subject for further research. EEG source connectivity is considered to have great potential for brain research. This area is not yet established and the validation procedures have not been completed until now. This lack of validation, however, is not permanent and should not prevent us from stepping up our work in this field. In future developments, such as the simultaneous recording of intracerebral and scalp EEG data, which will be used further to assess the proposed algorithms, at least in epilepsy patients, this will undoubtedly make advances.

Selecting ROIs often also involves user intervention and certain criteria that are selected randomly. The collection of ROIs will preferably be substituted with an assessment of compatibility for all possible voxel combinations.

Appendix A

Pre-processing

A.1 Code for artiface removal from one channel using ICA

```
% Artifact removal using ICA
clc;
close all;
clear all;
Fs = 256;
load('D:\MATLAB\eegexdataset'); %Lode the data
Data= EEG.data; % nchan x time
Data=Data(1:10,5000:10000);
Data=double(Data);
Fnyq  = Fs/2;
F_notch = 50;
[b,a] = iirnotch(F_notch/Fnyq, F_notch/Fnyq/20);
Data  = filtfilt(b,a, Data);
F_cut = 4;
[b,a] = ellip(1, 0.5, 20, F_cut/Fnyq, 'high');
Data  = filtfilt(b,a, Data);
%Remove mean values from the channels and plot raw data
Data  = detrend(Data,'constant');
figure;
plot(Data);
title('EEG data');
%ICA
[weight, sphere] = runica(Data, 'verbose', 'off');
W = weight*sphere;    % EEGLAB --> W unmixing matrix
icaEEG = W*Data;      % EEGLAB --> U = W.X activations
figure;
```

```
plot(icaEEG);
xlabel('Time (s)')
title('Independent Components');
%Components to remove
ArtICs = [1 5 6];
icaEEG1 = icaEEG;
icaEEG1(ArtICs, :) = 0;          % suppress artifacts
Data_ICA = inv(W)*icaEEG1;       % rebuild data
figure;
plot(Data_ICA);
title('ICA cleaned EEG');
%for one channel across some time interval
```

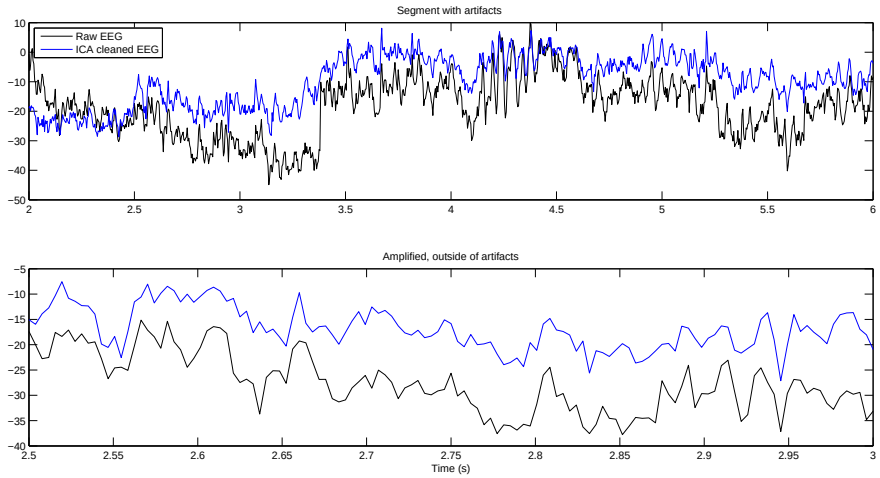

Figure A.1: ICA cleaned EEG for one channel with 4 time steps

```
figure
subplot(2,1,1);
T1 = 2; T2 = 6;
nT1 = T1*Fs; nT2 = T2*Fs;
plot((nT1:nT2)/Fs, Data(1,nT1:nT2),
'k',(nT1:nT2)/Fs, Data_ICA(1,nT1:nT2),'b');
legend({'Raw EEG','ICA cleaned EEG'},'Location','NorthWest');
title('with artifacts ');
subplot(2,1,2);
T1 = 2.5; T2 = 3;
```

```
nT1 = T1*Fs; nT2 = T2*Fs;
plot((nT1:nT2)/Fs,
Data(1,nT1:nT2),'k',(nT1:nT2)/Fs, Data_ICA(1,nT1:nT2),'b');
title('Amplified, outside of artifacts');
xlabel('Time (s)');
```

A.1.1 Image for the data before and after applying ICA for 5 channels

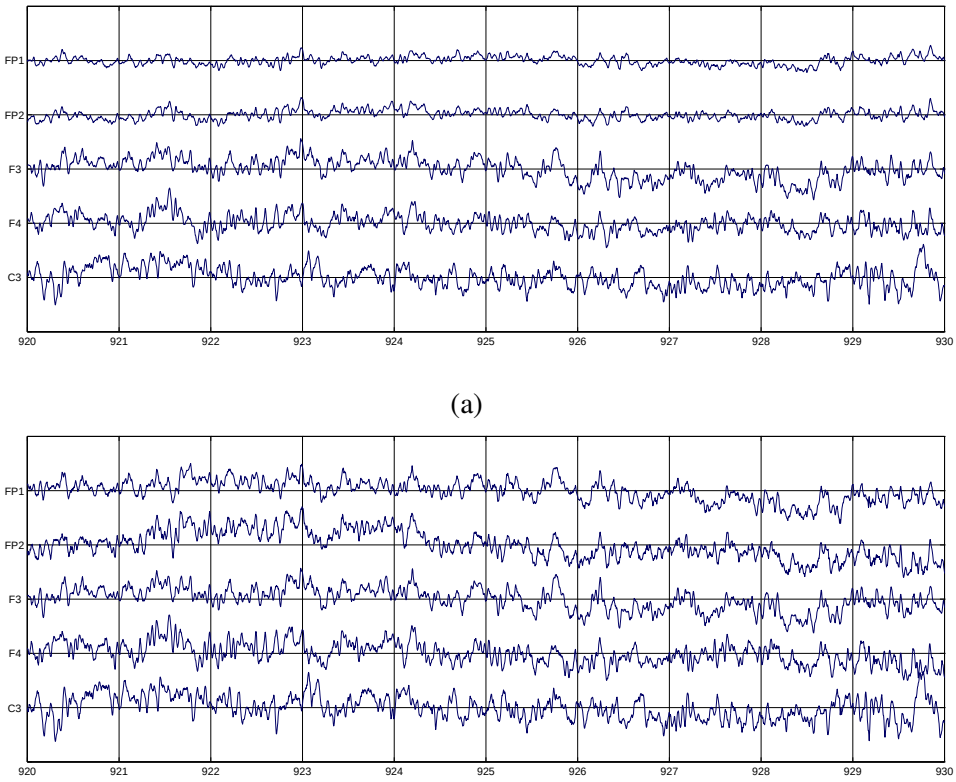

(a)

(b)

Figure A.2: (a) Before applying ICA to the data (b) data after ICA applied.

A.2 Image for DC removal

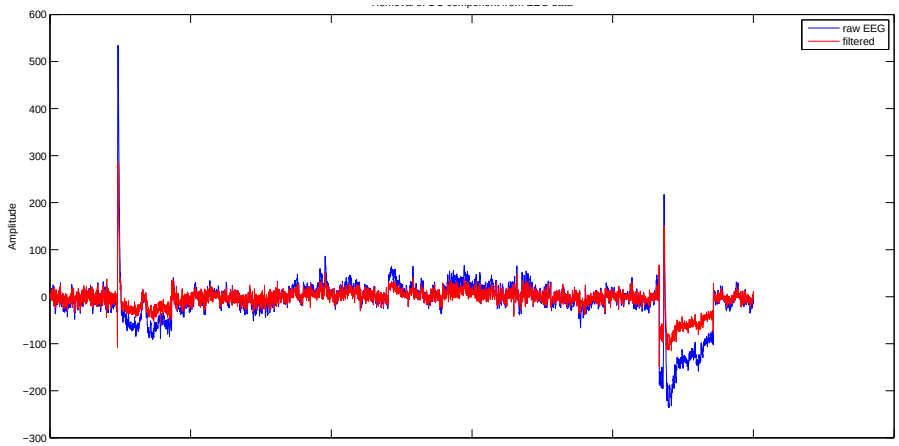

Figure A.3: Removal of DC component from EEG data

Appendix B

Localization

B.1 Particle filter for toy example

```
%Particle filter
T=0.4; %sampling period
A=[1 0 T 0;
    0 1 0 T;
    0 0 0 1;
    0 0 0 1];
F=[1 T T^2/2 T^3/3;
    0 1 T T^2/2;
    0 0 1 T ;
    0 0 0 1];
nt=100; %number of steps
x_r=zeros(4,nt); %state model
t=0:T:(nt-1)*T;
%state noise
w_s=[10^5 0 0 0;
0 10^3 0 0;
0 0 10^2 0;
 0 0 10^1 0]; %covariance matrix for process noise
w=sqrt(w_s); %square root of diagnol matrix
%measurement noise
v_s=10^6; %cov.
obs=sqrt(v_s);
error=zeros(4,nt);
rxe=zeros(4,nt);
x=[4000, 3000, 200, 400]; %initial state with [rx,ry,vx,vy],
error_x=x'; %error
Np=1000;  %number of particles
```

```
%reserve space
x_p=zeros(4,Np);  % initial particles
x_ap=zeros(4,Np);
y=zeros(4,Np); % measurements
y_d=zeros(4,Np);
x_l=zeros(4,Np); % likelihoods
noise_p=randn(4,Np); %noise
for i=1:Np,
x_p(:,i)=x'+(w.*noise_p(:,i));
end;
ux=randn(4,nt);
vy=randn(4,nt);
n=1;
while n<nt+1,
x_re(:,n)=error_x;
error(:,n)=x'-error_x;
x_r(:,n)=x';
x_rerror=A*x'+(w.*ux(:,n));
x=x_rerror';
y=F*x'+(obs*vy(n));
ym=y;
u_p=randn(4,Np);
v_ynoise=randn(1,Np);
for i=1:Np,
x_ap(:,i)=A*x';
x_ap(:,i)=x_ap(:,i)+(w.*u_p(:,i));
y(:,i)=F*x_ap(:,i)+(obs*v_ynoise(i));
y_d(:,i)=ym-y(:,i);
end;
v_state=max(abs(y_d(:,ip)))/4;
i=1:Np;
x_l(:,i)=exp(-((y_d(:,i)/v_state).^2));
normalize=sum(x_l(:,i));
x_l(:,i)=x_l(i)/normalize;
absolute=(max(x_ap')-min(x_ap'))';
sig=0.2*absolute*Np^(-1/3);
```

```
r_n=randn(4,Np);
%systematic Resampling
a=cumsum(x_l(:,ip));
c=linspace(0,1-(1/Np),Np)+(rand(1)/Np);
c(Np+1)=1;
m=1;
for i=1:Np
O=x_ap(:,m);
x_p(:,i)=O+(sig.*r_n(:,i));
i=i+1;
end;
error_x=sum(x_p,2)/Np;
n=n+1;
end;
figure
subplot(1,3,1)
plot(t,x_r(1,1:nt),'kx');
hold on;
plot(t,x_re(1,1:nt),'r');
title('position-x'); xlabel('seconds')
axis([0 nt*T 0 12*10^4]);
subplot(1,3,2);
plot(t,x_r(2,1:nt),'kx');
hold on;
plot(t,x_re(2,1:nt),'r');
title('position-y'); xlabel('seconds');
axis([0 nt*T 0 12*10^4]);

subplot(1,3,3)
plot(t,x_r(3,1:nt),'kx'); hold on;
plot(t,x_re(3,1:nt),'r');
title('velocity'); xlabel('seconds')
axis([0 nt*T 100 600]);

% axis([0 nt*T 0 12*10^4]);
% subplot(1,2,2);
```

```
% plot(t,x_r(4,1:nt),'kx'); hold on;
% plot(t,x_re(4,1:nt),'r');
% title('position-y'); xlabel('seconds');
% axis([[0 nt*T -6000 1000]]);
% figure;
% plot(t,x_r(3,1:nt),'kx'); hold on;
% plot(t,x_re(3,1:nt),'r');
```

References

[1] A. Zani and A. M. Proverbio, "Cognitive electrophysiology of mind and brain," in *The cognitive electrophysiology of mind and brain*. Elsevier, 2003, pp. 3–12.

[2] M. Teplan *et al.*, "Fundamentals of EEG measurement," *Measurement science review*, vol. 2, no. 2, pp. 1–11, 2002.

[3] F. Sharbrough, G. Chatrian, R. Lesser, H. Luders, M. Nuwer, and T. Picton, "American electroencephalographic society guidelines for standard electrode position nomenclature," *Journal of Clinical Neurophysiology*, vol. 8, pp. 200–202, 01 1991.

[4] M. Avoli, "Pierre gloor (1923–2003): an appreciation," *Epilepsia*, vol. 45, no. 7, pp. 882–886, 2004.

[5] A. M. Grass and F. A. Gibbs, "A fourier transform of the electroencephalogram," *Journal of neurophysiology*, vol. 1, no. 6, pp. 521–526, 1938.

[6] L. F. Haas, "Hans berger (1873–1941), richard caton (1842–1926), and electroencephalography," *Journal of Neurology, Neurosurgery & Psychiatry*, vol. 74, no. 1, pp. 9–9, 2003.

[7] J. Ward, *The student's guide to cognitive neuroscience*. Psychology Press, 2015.

[8] E. Niedermeyer and F. L. da Silva, *Electroencephalography: basic principles, clinical applications, and related fields*. Lippincott Williams & Wilkins, 2005.

[9] P. Olejniczak, "Neurophysiologic basis of EEG," *Journal of clinical neurophysiology*, vol. 23, no. 3, pp. 186–189, 2006.

[10] H. L. Atwood and W. A. MacKay, *Essentials of neurophysiology*. BC Decker, 1989.

[11] P. L. Nunez and B. A. Cutillo, *Neocortical dynamics and human EEG rhythms*. Oxford University Press, USA, 1995.

[12] W. O. Tatum, "Ellen r. grass lecture: Extraordinary EEG," *The Neurodiagnostic Journal*, vol. 54, no. 1, pp. 3–21, 2014.

[13] B. R. Cahn and J. Polich, "Meditation states and traits: EEG, ERP, and neuroimaging studies." *Psychological bulletin*, vol. 132, no. 2, p. 180, 2006.

[14] S. Ashwal and R. Rust, "Child neurology in the 20th century," *Pediatric research*, vol. 53, no. 2, pp. 345–361, 2003.

[15] G. Pfurtscheller, D. Flotzinger, and C. Neuper, "Differentiation between finger, toe and tongue movement in man based on 40 Hz EEG," *Electroencephalography and clinical neurophysiology*, vol. 90, no. 6, pp. 456–460, 1994.

[16] J. S. Ebersole and T. A. Pedley, *Current practice of clinical electroencephalography*. Lippincott Williams & Wilkins, 2003.

[17] B. J. Fisch and R. Spehlmann, *Fisch and Spehlmann's EEG primer: basic principles of digital and analog EEG*. Elsevier Health Sciences, 1999.

[18] S. Sanei and J. A. Chambers, *EEG signal processing*. John Wiley & Sons, 2013.

[19] L. Blumhardt, G. Barrett, and A. Halliday, "The asymmetrical visual evoked potential to pattern reversal in one half field and its significance for the analysis of visual field defects." *British Journal of Ophthalmology*, vol. 61, no. 7, pp. 454–461, 1977.

[20] R. Gilmore, "American-electroencephalographic-society guidelines in electroencephalography, evoked-potentials, and polysomnography," *Journal of Clinical Neurophysiology*, vol. 11, no. 1, pp. 1–142, 1994.

[21] S. Makeig, M. Westerfield, T.-P. Jung, S. Enghoff, J. Townsend, E. Courchesne, and T. J. Sejnowski, "Dynamic brain sources of visual evoked responses," *Science*, vol. 295, no. 5555, pp. 690–694, 2002.

[22] J. C. Mosher, P. S. Lewis, and R. M. Leahy, "Multiple dipole modeling and localization from spatio-temporal MEG data," *IEEE transactions on biomedical engineering*, vol. 39, no. 6, pp. 541–557, 1992.

[23] A. Galka, O. Yamashita, T. Ozaki, R. Biscay, and P. Valdés-Sosa, "A solution to the dynamical inverse problem of EEG generation using spatiotemporal kalman filtering," *NeuroImage*, vol. 23, no. 2, pp. 435–453, 2004.

[24] J. M. Antelis and J. Minguez, "Dynamic solution to the EEG source localization problem using kalman filters and particle filters," in *2009 Annual International Conference of the IEEE Engineering in Medicine and Biology Society*. IEEE, 2009, pp. 77–80.

[25] N. J. Gordon, D. J. Salmond, and A. F. Smith, "Novel approach to nonlinear/non-gaussian bayesian state estimation," in *IEE proceedings F (radar and signal processing)*, vol. 140, no. 2. IET, 1993, pp. 107–113.

[26] A. Sorrentino, L. Parkkonen, and M. Piana, "Particle filters: a new method for reconstructing multiple current dipoles from meg data," in *International congress series*, vol. 1300. Elsevier, 2007, pp. 173–176.

[27] B. D. Van Veen and K. M. Buckley, "Beamforming: A versatile approach to spatial filtering," *IEEE assp magazine*, vol. 5, no. 2, pp. 4–24, 1988.

[28] J. C. Mosher and R. M. Leahy, "Source localization using recursively applied and projected (rap) music," *IEEE Transactions on signal processing*, vol. 47, no. 2, pp. 332–340, 1999.

[29] H. R. Mohseni, E. L. Wilding, and S. Sanei, "Sequential monte carlo techniques for EEG dipole placing and tracking," in *2008 5th IEEE Sensor Array and Multichannel Signal Processing Workshop*. IEEE, 2008, pp. 95–98.

[30] A. Sorrentino, L. Parkkonen, A. Pascarella, C. Campi, and M. Piana, "Dynamical meg source modeling with multi-target bayesian filtering," *Human brain mapping*, vol. 30, no. 6, pp. 1911–1921, 2009.

[31] A. Doucet, S. Godsill, and C. Andrieu, "On sequential monte carlo sampling methods for bayesian filtering," *Statistics and computing*, vol. 10, no. 3, pp. 197–208, 2000.

[32] M. Arulampalam, S. Maskell, N. Gordon, and T. Clapp, "A tutorial on particle filters for online nonlinear/non-gaussian bayesian tracking," *IEEE Transactions on Signal Processing*, vol. 50, no. 2, pp. 174–188, 2002.

[33] R. D. Pascual-Marqui *et al.*, "Standardized low-resolution brain electromagnetic tomography (sloreta): technical details," *Methods Find Exp Clin Pharmacol*, vol. 24, no. Suppl D, pp. 5–12, 2002.

[34] S. Baillet, J. C. Mosher, and R. M. Leahy, "Electromagnetic brain mapping," *IEEE Signal processing magazine*, vol. 18, no. 6, pp. 14–30, 2001.

[35] M. Hassan, O. Dufor, I. Merlet, C. Berrou, and F. Wendling, "EEG source connectivity analysis: From dense array recordings to brain networks," *PLOS ONE*, vol. 9, no. 8, pp. 1–15, 08 2014.

[36] E. Bullmore and O. Sporns, "Complex brain networks: graph theoretical analysis of structural and functional systems," *Nature reviews neuroscience*, vol. 10, no. 3, pp. 186–198, 2009.

[37] P. L. Nunez, R. Srinivasan *et al.*, *Electric fields of the brain: the neurophysics of EEG*. Oxford University Press, USA, 2006.

[38] S. Haufe, *Towards EEG source connectivity analysis*. PhD thesis, Technische University at Berlin, 2012.

[39] W. Liao, J. Ding, D. Marinazzo, Q. Xu, Z. Wang, C. Yuan, Z. Zhang, G. Lu, and H. Chen, "Small-world directed networks in the human brain: multivariate granger causality analysis of resting-state fmri," *Neuroimage*, vol. 54, no. 4, pp. 2683–2694, 2011.

[40] M. J. Kaminski and K. J. Blinowska, "A new method of the description of the information flow in the brain structures," *Biological cybernetics*, vol. 65, no. 3, pp. 203–210, 1991.

[41] L. Barnett and A. K. Seth, "Granger causality for state-space models," *Physical Review E*, vol. 91, no. 4, apr 2015.

[42] S. Haufe and A. Ewald, "A simulation framework for benchmarking EEG-based brain connectivity estimation methodologies," *Brain Topography*, vol. 32, no. 4, pp. 625–642, jun 2016.

[43] S. Haufe, V. V. Nikulin, K. R. Müller, and G. Nolte, "A critical assessment of connectivity measures for EEG data: A simulation study," *NeuroImage*, vol. 64, pp. 120–133, jan 2013.

[44] M. Ding, Y. Chen, and S. L. Bressler, "Granger causality: Basic theory and application to neuroscience," in *Handbook of Time Series Analysis*. Wiley-VCH Verlag GmbH & Co. KGaA, pp. 437–460.

[45] L. Barnett and A. K. Seth, "The MVGC multivariate granger causality toolbox: A new approach to granger-causal inference," *Journal of Neuroscience Methods*, vol. 223, pp. 50–68, feb 2014.

[46] P. J. Uhlhaas and W. Singer, "Neural synchrony in brain disorders: Relevance for cognitive dysfunctions and pathophysiology," *Neuron*, vol. 52, no. 1, pp. 155–168, oct 2006.

[47] C. Brunner, M. Billinger, M. Seeber, T. R. Mullen, and S. Makeig, "Volume conduction influences scalp-based connectivity estimates," *Frontiers in Computational Neuroscience*, vol. 10, nov 2016.

[48] F. V. de Steen, L. Faes, E. Karahan, J. Songsiri, P. A. Valdes-Sosa, and D. Marinazzo, "Critical comments on EEG sensor space dynamical connectivity analysis," *Brain Topography*, vol. 32, no. 4, pp. 643–654, nov 2016.

[49] W. Pravdich-Neminsky, "An attempt to register electrical brain symptoms," *Zentralbl Physiol*, vol. 27, pp. 951–960, 1912.

[50] H. Berger, *About the human electroencephalogram*. Journal of Psychology and Neurology, 1930.

[51] L. Farwell and E. Donchin, "Talking off the top of your head: toward a mental prosthesis utilizing event-related brain potentials," *Electroencephalography and Clinical Neurophysiology*, vol. 70, no. 6, pp. 510–523, dec 1988.

[52] G. Pfurtscheller and F. L. da Silva, "Event-related EEG/MEG synchronization and desynchronization: basic principles," *Clinical Neurophysiology*, vol. 110, no. 11, pp. 1842–1857, nov 1999.

[53] O. G. Lins, T. W. Picton, P. Berg, and M. Scherg, "Ocular artifacts in recording EEGs and event-related potentials II: Source dipoles and source components," *Brain Topography*, vol. 6, no. 1, pp. 65–78, sep 1993.

[54] P. Berg and M. Scherg, "Dipole modelling of eye activity and its application to the removal of eye artefacts from the EEG and MEG," *Clinical Physics and Physiological Measurement*, vol. 12, no. A, pp. 49–54, jan 1991.

[55] N. Ille, P. Berg, and M. Scherg, "Artifact correction of the ongoing EEG using spatial filters based on artifact and brain signal topographies," *Journal of Clinical Neurophysiology*, vol. 19, no. 2, pp. 113–124, mar 2002.

[56] T.-P. Jung, S. Makeig, C. Humphries, T.-W. Lee, M. J. McKeown, V. Iragui, and T. J. Sejnowski, "Removing electroencephalographic artifacts by blind source separation," *Psychophysiology*, vol. 37, no. 2, pp. 163–178, mar 2000.

[57] S. Choi, A. Cichocki, H. M. Park, and S. Y. Lee, "Blind source separation and independent component analysis: A review," *Neural Information Processing-Letters and Reviews*, vol. 6, no. 1, pp. 1–57, 2005.

[58] S. Makeig, A. J. Bell, T. P. Jung, and T. J. Sejnowski, "Independent component analysis of electroencephalographic data," in *Advances in neural information processing systems*, 1996, pp. 145–151.

[59] C. A. Joyce, I. F. Gorodnitsky, and M. Kutas, "Automatic removal of eye movement and blink artifacts from EEG data using blind component separation," *Psychophysiology*, vol. 41, no. 2, pp. 313–325, 2004.

[60] M. Crespo-Garcia, M. Atienza, and J. L. Cantero, "Muscle artifact removal from human sleep EEG by using independent component analysis," *Annals of biomedical engineering*, vol. 36, no. 3, pp. 467–475, 2008.

[61] A. Flexer, H. Bauer, J. Pripfl, and G. Dorffner, "Using ICA for removal of ocular artifacts in EEG recorded from blind subjects," *Neural Networks*, vol. 18, no. 7, pp. 998–1005, 2005.

[62] X. Zhang, S. Qiu, Y. Ke, P. Li, X. Zhao, H. Qi, P. Zhou, L. Zhang, B. Wan, and D. Ming, "Stimulus artifact removal of semg signals detected during functional electrical stimulation," *Biomedical Engineering / Biomedizinische Technik*, jan 2013.

[63] K. J. Friston, W. Penny, C. Phillips, S. Kiebel, G. Hinton, and J. Ashburner, "Classical and Bayesian inference in neuroimaging: theory," *NeuroImage*, vol. 16, no. 2, pp. 465–483, 2002.

[64] A. M. Dale, A. K. Liu, B. R. Fischl, R. L. Buckner, J. W. Belliveau, J. D. Lewine, and E. Halgren, "Dynamic statistical parametric mapping: combining fMRI and MEG for high-resolution imaging of cortical activity," *Neuron*, vol. 26, no. 1, pp. 55–67, 2000.

[65] M. S. Hämäläinen, "Mne software user's guide," *NMR Center, Mass General Hospital, Harvard University*, vol. 58, pp. 59–75, 2005.

[66] A. Pascarella, , A. Sorrentino, C. Campi, and M. P. and, "Particle filtering, beamforming and multiple signal classification for the analysis of magnetoencephalography time series: a comparison of algorithms," *Inverse Problems & Imaging*, vol. 4, no. 1, pp. 169–190, 2010.

[67] C. Campi, A. Pascarella, A. Sorrentino, and M. Piana, "Highly automated dipole EStimation (HADES)," *Computational Intelligence and Neuroscience*, vol. 2011, pp. 1–11, 2011.

[68] R. E. Kalman, "A new approach to linear filtering and prediction problems," *Journal of Basic Engineering*, vol. 82, pp. 35–45, 1960.

[69] J. J. Riera, J. Watanabe, I. Kazuki, M. Naoki, E. Aubert, T. Ozaki, and R. Kawashima, "A state-space model of the hemodynamic approach: nonlinear filtering of BOLD signals," *NeuroImage*, vol. 21, no. 2, pp. 547–567, 2004.

[70] J. C. Jimenez and T. Ozaki, "Local linearization filters for non-linear continuous-discrete state space models with multiplicative noise," *International Journal of Control*, vol. 76, no. 12, pp. 1159–1170, 2003.

[71] R. C. Sotero, N. J. Trujillo-Barreto, J. C. Jiménez, F. Carbonell, and R. Rodríguez-Rojas, "Identification and comparison of stochastic metabolic/hemodynamic models (sMHM) for the generation of the BOLD signal," *Journal of Computational Neuroscience*, vol. 26, no. 2, pp. 251–269, oct 2008.

[72] T. Deneux and O. Faugeras, "Using nonlinear models in fMRI data analysis: model selection and activation detection," *NeuroImage*, vol. 32, no. 4, pp. 1669–1689, 2006.

[73] L. A. Johnston, E. Duff, I. Mareels, and G. F. Egan, "Nonlinear estimation of the BOLD signal," *NeuroImage*, vol. 40, no. 2, pp. 504–514, 2008.

[74] Z. Hu, X. Zhao, H. Liu, and P. Shi, "Nonlinear analysis of the BOLD signal," *EURASIP Journal on Advances in Signal Processing*, vol. 2009, no. 1, jun 2009.

[75] M. Chambers and C. Wyatt, "An analysis of blood-oxygen-level-dependent signal parameter estimation using particle filters," in *2011 IEEE International Symposium on Biomedical Imaging: From Nano to Macro*. IEEE, mar 2011.

[76] S. J. Kiebel, O. David, and K. J. Friston, "Dynamic causal modelling of evoked responses in EEG/MEG with lead field parameterization," *NeuroImage*, vol. 30, no. 4, pp. 1273–1284, 2006.

[77] B. Ristic, S. Arulampalam, and N. Gordon, *Beyond the Kalman Filter: Particle Filters for Tracking Applications*. Artech House, 2003.

[78] O. Cappe, S. J. Godsill, and E. Moulines, "An overview of existing methods and recent advances in sequential monte carlo," *Proceedings of the IEEE*, vol. 95, no. 5, pp. 899–924, may 2007.

[79] L. Murray and A. J. Storkey, "Continuous time particle filtering for fMRI," in *Advances in Neural Information Processing Systems*, 2008, pp. 1049–1056.

[80] S. Särkkä, A. Vehtari, and J. Lampinen, "Rao-blackwellized particle filter for multiple target tracking," *Information Fusion*, vol. 8, no. 1, pp. 2–15, jan 2007.

[81] N. Vlassis, B. Terwijn, and B. Krose, "Auxiliary particle filter robot localization from high-dimensional sensor observations," in *Proceedings 2002 IEEE International Conference on Robotics and Automation (Cat. No.02CH37292)*. IEEE.

[82] V. D. Merwe, D. R., D. F. A., N., and E. A. Wan, "The unscented particle filter," in *Advances in neural information processing systems*, 2001, pp. 584–590.

[83] C. Musso, N. Oudjane, L. Gland, and F., "Improving regularised particle filters," in *Sequential Monte Carlo methods in practice*, 2001, pp. 247–271.

[84] F. Hutter and R. Dearden, "The gaussian particle filter for diagnosis of non-linear systems," *IFAC Proceedings Volumes*, vol. 36, no. 5, pp. 909–914, 2003.

[85] J. Yun, F. Yang, and Y. Chen, "Augmented particle filters," *Journal of the American Statistical Association*, vol. 112, no. 517, pp. 300–313, 2017.

[86] N. Lingala, N. Perkowski, H. C. Yeong, N. S. Namachchivaya, and Z. Rapti, "Optimal nudging in particle filters," *Probabilistic Engineering Mechanics*, vol. 37, pp. 160–169, 2014.

[87] H. Zhou, Z. Deng, Y. Xia, and M. Fu, "A new sampling method in particle filter based on Pearson correlation coefficient," *Neurocomputing*, vol. 216, pp. 208–215, 2016.

[88] F. Wang, J. Zhang, B. Lin, and X. Li, "Two stage particle filter for nonlinear Bayesian estimation," *IEEE Access*, vol. 6, pp. 13 803–13 809, 2018.

[89] T. Li, M. Bolic, and P. M. Djuric, "Resampling methods for particle filtering: classification, implementation, and strategies," *IEEE Signal processing magazine*, vol. 32, no. 3, pp. 70–86, 2015.

[90] J. Carpenter, P. Clifford, and P. Fearnhead, "Improved particle filter for nonlinear problems," *IEE Proceedings-Radar, Sonar and Navigation*, vol. 146, no. 1, pp. 2–7, 1999.

[91] J. S. Liu and R. Chen, "Sequential Monte Carlo methods for dynamic systems," *Journal of the American statistical association*, vol. 93, no. 443, pp. 1032–1044, 1998.

[92] M. Bolic, P. Djuric, and S. Hong, "New resampling algorithms for particle filters," in *2003 IEEE International Conference on Acoustics, Speech, and Signal Processing, 2003. Proceedings. (ICASSP '03).* IEEE.

[93] L. Murray, "Gpu acceleration of the particle filter: the metropolis resampler," *arXiv preprint arXiv:1202.6163*, 2012.

[94] R. Douc and O. Cappe, "Comparison of resampling schemes for particle filtering," in *ISPA 2005. Proceedings of the 4th International Symposium on Image and Signal Processing and Analysis, 2005.* IEEE, 2005.

[95] J. D. Hol, T. B. Schon, and F. Gustafsson, "On resampling algorithms for particle filters," in *2006 IEEE Nonlinear Statistical Signal Processing Workshop*. IEEE, sep 2006.

[96] M. Bolić, P. M. Djurić, and S. Hong, "Resampling algorithms for particle filters: A computational complexity perspective," *EURASIP Journal on Advances in Signal Processing*, vol. 2004, no. 15, nov 2004.

[97] K. Pugalenthi and N. Raghavan, "A holistic comparison of the different resampling algorithms for particle filter based prognosis using lithium ion batteries as a case study," *Microelectronics Reliability*, vol. 91, pp. 160–169, 2018.

[98] L. Guo, Y. Peng, D. Liu, and Y. Luo, "Comparison of resampling algorithms for particle filter based remaining useful life estimation," in *2014 International Conference on Prognostics and Health Management*. IEEE, jun 2014.

[99] L. Miao, J. J. Zhang, C. Chakrabarti, and A. Papandreou-Suppappola, "Efficient Bayesian tracking of multiple sources of neural activity: Algorithms and real-time FPGA implementation," *IEEE Transactions on Signal Processing*, vol. 61, no. 3, pp. 633–647, 2012.

[100] A. Athalye, M. Bolic, Sangjin Hong, and P. M. Djuric, "Architectures and memory schemes for sampling and resampling in particle filters," in *3rd IEEE Signal Processing Education Workshop. 2004 IEEE 11th Digital Signal Processing Workshop, 2004.*, 2004, pp. 92–96.

[101] T. cheng Li, G. Villarrubia, S. dong Sun, J. M. Corchado, and J. Bajo, "Resampling methods for particle filtering: identical distribution, a new method, and comparable study," *Frontiers of Information Technology & Electronic Engineering*, vol. 16, no. 11, pp. 969–984, oct 2015.

[102] L. A. Baccalá and K. Sameshima, "Partial directed coherence: a new concept in neural structure determination," *Biological Cybernetics*, vol. 84, no. 6, pp. 463–474, may 2001.

[103] K. J. Friston, "Functional and effective connectivity in neuroimaging: A synthesis," *Human Brain Mapping*, vol. 2, no. 1-2, pp. 56–78, 1994.

[104] V. K. Jirsa and A. McIntosh, Eds., *Handbook of Brain Connectivity*. Springer Berlin Heidelberg, 2007.

[105] P. C. Lauterbur, "Image formation by induced local interactions: examples employing nuclear magnetic resonance," *nature*, vol. 242, no. 5394, pp. 190–191, 1973.

[106] M. E. Moseley, Y. Cohen, J. Kucharczyk, J. Mintorovitch, H. S. Asgari, M. F. Wendland, and D. Norman, "Diffusion-weighted MR imaging of anisotropic water diffusion in cat central nervous system," *Radiology*, vol. 176, no. 2, pp. 439–445, 1990.

[107] W. R. Adey, D. O. Walter, and C. E. Hendrix, "Computer techniques in correlation and spectral analyses of cerebral slow waves during discriminative behavior," *Experimental neurology*, vol. 3, no. 6, pp. 501–524, 1961.

[108] G. Pfurtscheller and C. Andrew, "Event-related changes of band power and coherence: methodology and interpretation," *Journal of clinical neurophysiology*, vol. 16, no. 6, 1999.

[109] D. Janzing and B. Scholkopf, "Causal inference using the algorithmic markov condition," *IEEE Transactions on Information Theory*, vol. 56, no. 10, pp. 5168–5194, oct 2010.

[110] M. Eichler, "On the evaluation of information flow in multivariate systems by the directed transfer function," *Biological Cybernetics*, vol. 94, no. 6, pp. 469–482, mar 2006.

[111] S. J. Kiebel, M. I. Garrido, R. J. Moran, and K. J. Friston, "Dynamic causal modelling for EEG and MEG," *Cognitive Neurodynamics*, vol. 2, no. 2, pp. 121–136, apr 2008.

[112] C. W. J. Granger, "Investigating causal relations by econometric models and cross-spectral methods," *Econometrica*, vol. 37, no. 3, p. 424, aug 1969.

[113] G. G. Supp, A. Schlögl, N. Trujillo-Barreto, M. M. Müller, and T. Gruber, "Directed cortical information flow during human object recognition: Analyzing induced EEG gamma-band responses in brain's source space," *PLOS ONE*, vol. 2, no. 8, pp. 1–11, 08 2007.

[114] K. Blinowska, R. Kus, M. Kaminski, and J. Janiszewska, "Transmission of brain activity during cognitive task," *Brain topography*, vol. 23, no. 2, pp. 205–213, 2010.

[115] R. Kus, M. Kaminski, and K. J. Blinowska, "Determination of EEG activity propagation: pair-wise versus multichannel estimate," *IEEE transactions on Biomedical Engineering*, vol. 51, no. 9, pp. 1501–1510, 2004.

[116] G. Varotto, P. Fazio, D. Rossi Sebastiano, D. Duran, L. D'Incerti, E. Parati, D. Sattin, M. Leonardi, S. Franceschetti, and F. Panzica, "Altered resting state effective connectivity in long-standing vegetative state patients: An EEG study," *Clinical Neurophysiology*, vol. 125, no. 1, pp. 63 – 68, 2014.

[117] E. M. Schumacher, T. A. Stiris, and P. G. Larsson, "Effective connectivity in long-term EEG monitoring in preterm infants," *Clinical Neurophysiology*, vol. 126, no. 12, pp. 2261–2268, 2015.

[118] F. Rotondi, S. Franceschetti, G. Avanzini, and F. Panzica, "Altered EEG resting-state effective connectivity in drug-naïve childhood absence epilepsy," *Clinical Neurophysiology*, vol. 127, no. 2, pp. 1130–1137, feb 2016.

[119] M. X. Cohen, "Effects of time lag and frequency matching on phase-based connectivity," *Journal of Neuroscience Methods*, vol. 250, pp. 137–146, jul 2015.

[120] V. Sakkalis, "Review of advanced techniques for the estimation of brain connectivity measured with EEG/MEG," *Computers in Biology and Medicine*, vol. 41, no. 12, pp. 1110–1117, dec 2011.

[121] K. J. Friston, "Functional and effective connectivity: a review," *Brain connectivity*, vol. 1, no. 1, pp. 13–36, 2011.

[122] G. Nolte, A. Ziehe, V. V. Nikulin, A. Schlögl, N. Krämer, T. Brismar, and K.-R. Müller, "Robustly estimating the flow direction of information in complex physical systems," *Physical Review Letters*, vol. 100, no. 23, jun 2008.

[123] G. Nolte and K.-R. Müller, "Localizing and estimating causal relations of interacting brain rhythms," *Frontiers in Human Neuroscience*, vol. 4, 2010.

[124] P. A. Valdes-Sosa, A. Roebroeck, J. Daunizeau, and K. Friston, "Effective connectivity: influence, causality and biophysical modeling," *Neuroimage*, vol. 58, no. 2, pp. 339–361, 2011.

[125] M. Eichler, "A graphical approach for evaluating effective connectivity in neural systems," *Philosophical Transactions of the Royal Society B: Biological Sciences*, vol. 360, no. 1457, pp. 953–967, 2005.

[126] G. Gómez-Herrero, M. Atienza, K. Egiazarian, and J. L. Cantero, "Measuring directional coupling between EEG sources," *NeuroImage*, vol. 43, no. 3, pp. 497–508, nov 2008.

[127] G. Nolte, A. Ziehe, N. Krämer, F. Popescu, and K. R. Müller, "Comparison of granger causality and phase slope index," in *Causality: Objectives and Assessment*, 2010, pp. 267–276.

[128] S. Haufe, R. Tomioka, G. Nolte, K.-R. Müller, and M. Kawanabe, "Modeling sparse connectivity between underlying brain sources for EEG/MEG," *IEEE Transactions on Biomedical Engineering*, vol. 57, no. 8, pp. 1954–1963, aug 2010.

[129] A. Omidvarnia, M. Mesbah, J. M. O'Toole, P. Colditz, and B. Boashash, "Analysis of the time-varying cortical neural connectivity in the newborn EEG: A time-frequency approach," in *International Workshop on Systems, Signal Processing and their Applications, WOSSPA*. IEEE, may 2011.

[130] L. Astolfi, F. Cincotti, D. Mattia, S. Salinari, C. Babiloni, A. Basilisco, P. M. Rossini, L. Ding, Y. Ni, B. He, and M. G. Marciani, "Estimation of the effective and functional human cortical connectivity with structural equation modeling and directed transfer function applied to high-resolution EEG," *Magnetic resonance imaging*, vol. 22, no. 10, pp. 1457–1470, 2004.

[131] L. Astolfi, F. Cincotti, D. Mattia, F. D. V. Fallani, A. Tocci, A. Colosimo, S. Salinari, M. G. Marciani, W. Hesse, H. Witte, and M. Ursino, "Tracking the time-varying cortical connectivity patterns by adaptive multivariate estimators," *IEEE Transactions on Biomedical Engineering*, vol. 55, no. 3, pp. 902–913, 2008.

[132] I. Hettiarachchi, S. Mohamed, and S. Nahavandi, "A marginalised markov chain monte carlo approach for model based analysis of EEG data," in *2012 9th IEEE International Symposium on Biomedical Imaging (ISBI)*. IEEE, may 2012.

[133] T.-P. Jung, S. Makeig, M. McKeown, A. Bell, T.-W. Lee, and T. Sejnowski, "Imaging brain dynamics using independent component analysis," *Proceedings of the IEEE*, vol. 89, no. 7, pp. 1107–1122, jul 2001.

[134] P. Comon, "Independent component analysis, a new concept?" *Signal Processing*, vol. 36, no. 3, pp. 287–314, apr 1994.

[135] J. Karhunen, S. I. M. O. N. A. MAIAROIU, and M. Ilmoniemi, "Local linear independent component analysis based on clustering," *International journal of neural systems*, pp. 439–451, 2000.

[136] G. D. Brown, S. Yamada, and T. J. Sejnowski, "Independent component analysis at the neural cocktail party," *Trends in neurosciences*, vol. 24, no. 1, pp. 54–63, 2001.

[137] K. A. Robbins, J. Touryan, T. Mullen, C. Kothe, and N. Bigdely-Shamlo, "How sensitive are EEG results to preprocessing methods: A benchmarking study," jan 2020.

[138] J. Onton, M. Westerfield, J. Townsend, and S. Makeig, "Imaging human EEG dynamics using independent component analysis," *Neuroscience & biobehavioral reviews*, vol. 30, no. 6, pp. 808–822, 2006.

[139] S. Makeig, T. P. Jung, A. J. Bell, D. Ghahremani, and T. J. Sejnowski, "Blind separation of auditory event-related brain responses into independent components," *Proceedings of the National Academy of Sciences*, vol. 94, no. 20, pp. 10 979–10 984, 1997.

[140] A. Delorme, T. Sejnowski, and S. Makeig, "Enhanced detection of artifacts in EEG data using higher-order statistics and independent component analysis," *Neuroimage*, vol. 34, no. 4, pp. 1443–1449, 2007.

[141] D. Mantini, M. G. Perrucci, S. Cugini, A. Ferretti, G. L. Romani, D. Gratta, and C., "Complete artifact removal for EEG recorded during continuous fMRI using independent component analysis," *Neuroimage*, vol. 34, no. 2, pp. 598–607, 2007.

[142] F. Grouiller, L. Vercueil, A. Krainik, C. Segebarth, P. Kahane, and O. David, "A comparative study of different artefact removal algorithms for EEG signals acquired during functional MRI," *Neuroimage*, vol. 38, no. 1, pp. 124–137, 2007.

[143] C. M. Michel, T. Koenig, D. Brandeis, L. R. R. Gianotti, and J. Wackermann, Eds., *Electrical Neuroimaging*. Cambridge University Press, 2009.

[144] M. Junghofer, T. Elbert, D. M. Tucker, and B. Rockstroh, "Statistical control of artifacts in dense array EEG/MEG studies," *Psychophysiology*, vol. 37, no. 4, pp. 523–532, jul 2000.

[145] J. S. Ebersole and S. Hawes-Ebersole, "Clinical application of dipole models in the localization of epileptiform activity," *Journal of Clinical Neurophysiology*, vol. 24, no. 2, pp. 120–129, 2007.

[146] V. Vivaldi and A. Sorrentino, "Bayesian smoothing of dipoles in magneto-/electroencephalography," *Inverse Problems*, vol. 32, no. 4, p. 045007, mar 2016.

[147] M. Hämäläinen, R. Hari, R. J. Ilmoniemi, J. Knuutila, and O. V. Lounasmaa, "Magnetoencephalography—theory, instrumentation, and applications to noninvasive studies of the working human brain," *Reviews of Modern Physics*, vol. 65, no. 2, pp. 413–497, apr 1993.

[148] N. Gordon, D. Salmond, and A. Smith, "Novel approach to nonlinear/non-gaussian bayesian state estimation," *IEE Proceedings F Radar and Signal Processing*, vol. 140, no. 2, p. 107, 1993.

[149] A. Doucet, N. Freitas, and N. Gordon, Eds., *Sequential Monte Carlo Methods in Practice*. Springer New York, 2001.

[150] R. D. Pascual-Marqui, "Review of methods for solving the EEG inverse problem," *International journal of bioelectromagnetism*, vol. 1, no. 1, pp. 75–86, 1999.

[151] G. Buzsáki, C. A. Anastassiou, and C. Koch, "The origin of extracellular fields and currents — EEG, ECoG, LFP and spikes," *Nature Reviews Neuroscience*, vol. 13, no. 6, pp. 407–420, may 2012.

[152] L. L. Glickfeld, J. D. Roberts, P. Somogyi, and M. Scanziani, "Interneurons hyperpolarize pyramidal cells along their entire somatodendritic axis," *Nature neuroscience*, vol. 12, no. 1, pp. 21–23, 2009.

[153] A. J. Trevelyan, "The direct relationship between inhibitory currents and local field potentials," *Journal of Neuroscience*, vol. 29, no. 48, pp. 15 299–15 307, 2009.

[154] P. L. Nunez and R. B. Silberstein, "On the relationship of synaptic activity to macroscopic measurements: does co-registration of EEG with fMRI make sense?" *Brain topography*, vol. 13, no. 2, pp. 79–96, 2000.

[155] L. Zhukov, D. Weinstein, and C. Johnson, "Independent component analysis for EEG source localization," *IEEE Engineering in Medicine and Biology Magazine*, vol. 19, no. 3, pp. 87–96, 2000.

[156] J. C. Mosher, R. M. Leahy, and P. S. Lewis, "EEG and MEG: forward solutions for inverse methods," *IEEE Transactions on Biomedical Engineering*, vol. 46, no. 3, pp. 245–259, 1999.

[157] J. Sarvas, "Basic mathematical and electromagnetic concepts of the biomagnetic inverse problem," *Physics in Medicine & Biology*, vol. 32, no. 1, 1987.

[158] D. Geselowitz, "On the magnetic field generated outside an inhomogeneous volume conductor by internal current sources," *IEEE Transactions on Magnetics*, vol. 6, no. 2, pp. 346–347, 1970.

[159] R. M. Leahy, J. C. Mosher, M. E. Spencer, M. X. Huang, and J. D. Lewine, "A study of dipole localization accuracy for MEG and EEG using a human skull phantom," *Electroencephalography and clinical neurophysiology*, vol. 107, no. 2, pp. 159–173, 1998.

[160] D. W. Shattuck, S. R. Sandor-Leahy, K. A. Schaper, D. A. Rottenberg, and R. M. Leahy, "Magnetic resonance image tissue classification using a partial volume model," *NeuroImage*, vol. 13, no. 5, pp. 856–876, 2001.

[161] J. J. Ermer, J. C. Mosher, S. Baillet, and R. M. Leahy, "Rapidly recomputable EEG forward models for realistic head shapes," *Physics in Medicine and Biology*, vol. 46, no. 4, pp. 1265–1281, mar 2001.

[162] C. Campi, A. Pascarella, A. Sorrentino, and M. Piana, "A rao–blackwellized particle filter for magnetoencephalography," *Inverse Problems*, vol. 24, no. 2, p. 025023, mar 2008.

[163] X. Chen, S. Särkkä, and S. Godsill, "A bayesian particle filtering method for brain source localisation," *Digital Signal Processing*, vol. 47, pp. 192–204, dec 2015.

[164] P. Georgieva, L. Mihaylova, N. Bouaynaya, and L. Jain, "Particle filters and beamforming for EEG source estimation," in *The 2012 International Joint Conference on Neural Networks (IJCNN)*. IEEE, jun 2012.

[165] B. Ebinger, N. Bouaynaya, P. Georgieva, and L. Mihaylova, "EEG dynamic source localization using marginalized particle filtering," in *2015 IEEE International Conference on Bioinformatics and Biomedicine (BIBM)*. IEEE, nov 2015.

[166] S. C. Jun, J. S. George, J. Paré-Blagoev, S. M. Plis, D. M. Ranken, D. M. Schmidt, and C. Wood, "Spatiotemporal bayesian inference dipole analysis for MEG neuroimaging data," *NeuroImage*, vol. 28, no. 1, pp. 84–98, oct 2005.

[167] B. . Vo, S. Singh, and A. Doucet, "Sequential monte carlo methods for multitarget filtering with random finite sets," *IEEE Transactions on Aerospace and Electronic Systems*, vol. 41, no. 4, pp. 1224–1245, 2005.

[168] D. Crisan, P. D. Moral, and T. Lyons, "Discrete filtering using branching and interacting particle systems," 1998.

[169] J. D. Hol, *Resampling in particle filters*. Linkoping University, Dissertation, 2004.

[170] V. S. Kumar and T. H. Rao, "Resampling schemes for rao-blackwellization particle filters," in *2016 International Conference on Computing, Analytics and Security Trends (CAST)*. IEEE, dec 2016.

[171] J. L. B. Claraco and M. Perception, "Development of scientific applications with the mobile robot programming toolkit," *The MRPT reference book. Machine Perception and Intelligent Robotics Laboratory, University of Málaga, Málaga, Spain*, vol. 40, 2008.

[172] G. Kitagawa, "Monte Carlo filter and smoother for non-Gaussian nonlinear state space models," *Journal of computational and graphical statistics*, vol. 5, no. 1, pp. 1–25, 1996.

[173] P. Fearnhead, *Sequential Monte Carlo methods in filter theory*, 1998.

[174] B. G. Sileshi, C. Ferrer, and J. Oliver, "Particle filters and resampling techniques: Importance in computational complexity analysis," in *2013 Conference on Design and Architectures for Signal and Image Processing*, 2013, pp. 319–325.

[175] D. J. Ballantyne, H. Y. Chan, and M. A. Kouritzin, "Novel branching particle method for tracking," in *Signal and Data Processing of Small Targets 2000*, O. E. Drummond, Ed., vol. 4048, International Society for Optics and Photonics. SPIE, 2000, pp. 277 – 287.

[176] M. A. Kouritzin, "Residual and stratified branching particle filters," *Computational Statistics & Data Analysis*, vol. 111, pp. 145–165, 2017.

[177] S. K. Veeramalla and V. K. H. R. Talari, "Multiple dipole source localization of EEG measurements using particle filter with partial stratified resampling," *Biomedical Engineering Letters*, vol. 10, no. 2, pp. 205–215, feb 2020.

[178] S. K. Veeramalla and V. H. R. Talari, "Neural source localization using particle filter with optimal proportional set resampling," *ETRI Journal*, feb 2020.

[179] R. Ling, "Cluster analysis algorithms for data reduction and classification of objects," *Technometrics*, vol. 23, pp. 417–418, 1981.

[180] S. Weerahandi, "Exact nonparametric methods," in *Exact Statistical Methods for Data Analysis*. Springer, 1995, pp. 77–107.

[181] C. Campi, A. Pascarella, A. Sorrentino, and M. Piana, "Highly automated dipole EStimation (HADES)," *Computational Intelligence and Neuroscience*, vol. 2011, pp. 1–11, 2011.

[182] S. Veeramalla and V. H. R. Talari, "Estimation of neural sources from EEG measurements using sequential monte carlo method," *Ingénierie des systèmes d information*, vol. 24, no. 4, pp. 411–417, oct 2019.

[183] S. K. Veeramalla and V. Talari, "Resampling schemes within a particle filter framework for brain source localization," *International Journal of Biomedical Engineering and Technology*, vol. **In press**, 2019.

[184] F. Tadel, S. Baillet, J. C. Mosher, D. Pantazis, and R. M. Leahy, "Brainstorm: A user-friendly application for MEG/EEG analysis," *Computational Intelligence and Neuroscience*, vol. 2011, pp. 1–13, 2011.

[185] A. M. Lascano, S. Vulliemoz, G. Lantz, L. Spinelli, C. Michel, and M. Seeck, "A review on non-invasive localisation of focal epileptic activity using EEG source imaging," *Epileptologie*, vol. 29, pp. 80–89, 2012.

[186] L. Koessler, C. Benar, L. Maillard, J. M. Badier, J. P. Vignal, F. Bartolomei, P. Chauvel, and M. Gavaret, "Source localization of ictal epileptic activity investigated by high resolution EEG and validated by SEEG," *Neuroimage*, vol. 51, no. 2, pp. 642–653, 2010.

[187] H. Stefan, S. Schneider, K. Abraham-Fuchs, J. Bauer, H. Feistel, G. Pawlik, U. Neubauer, G. Roohrlein, and W. J. Huk, "Magnetic source localization in focal epilepsy," *Brain*, vol. 113, no. 5, pp. 1347–1359.

[188] G. Ouyang, Y. Wang, Z. Yang, and X. Li, "Global synchronization of multichannel EEG in patients with electrical status epilepticus in sleep," *Clinical EEG and neuroscience*, vol. 46, no. 4, pp. 357–363, 2015.

[189] P. Nemtsas, G. Birot, F. Pittau, C. M. Michel, K. Schaller, S. Vulliemoz, V. K. Kimiskidis, and M. Seeck, "Source localization of ictal epileptic activity based on high-density scalp EEG data," *Epilepsia*, vol. 58, no. 6, pp. 1027–1036, 2017.

[190] P. Georgieva, N. Bouaynaya, F. Silva, L. Mihaylova, and L. C. Jain, "A beamformer-particle filter framework for localization of correlated EEG sources," *IEEE journal of biomedical and health informatics*, vol. 20, no. 3, pp. 880–892, 2015.

[191] A. Delorme and S. Makeig, "EEGLAB: an open source toolbox for analysis of single-trial EEG dynamics including independent component analysis," *Journal of neuroscience methods*, vol. 134, no. 1, pp. 9–21, 2004.

[192] M. C. Stevens, "The developmental cognitive neuroscience of functional connectivity," *Brain and cognition*, vol. 70, no. 1, pp. 1–12, 2009.

[193] M. K. Belmonte, G. Allen, A. Beckel-Mitchener, L. M. Boulanger, R. A. Carper, and S. J. Webb, "Autism and abnormal development of brain connectivity," *Journal of Neuroscience*, vol. 24, no. 42, pp. 9228–9231, 2004.

[194] B. P. Rogers, V. L. Morgan, A. T. Newton, and J. C. Gore, "Assessing functional connectivity in the human brain by fMRI," *Magnetic resonance imaging*, vol. 25, no. 10, pp. 1347–1357, 2007.

[195] O. David, D. Cosmelli, D. Hasboun, and L. Garnero, "A multitrial analysis for revealing significant corticocortical networks in magnetoencephalography and electroencephalography," *Neuroimage*, vol. 20, no. 1, pp. 186–201, 2003.

[196] F. Bartolomei, I. Bosma, M. Klein, J. C. Baayen, J. C. Reijneveld, T. J. Postma, J. J. Heimans, B. W. van Dijk, J. C. de Munck, A. de Jongh, and K. S. Cover, "How do brain tumors alter functional connectivity? A magnetoencephalography study," *Annals of neurology*, vol. 59, no. 1, pp. 128–138, 2006.

[197] F. Wendling, K. Ansari-Asl, F. Bartolomei, and L. Senhadji, "From EEG signals to brain connectivity: a model-based evaluation of interdependence measures," *Journal of neuroscience methods*, vol. 183, no. 1, pp. 9–18, 2009.

[198] J.-M. Schoffelen and J. Gross, "Source connectivity analysis with MEG and EEG," *Human Brain Mapping*, vol. 30, no. 6, pp. 1857–1865, jun 2009.

[199] L. Astolfi, F. Cincotti, D. Mattia, C. Babiloni, F. Carducci, A. Basilisco, P. Rossini, S. Salinari, L. Ding, Y. Ni, B. He, and F. Babiloni, "Assessing cortical functional connectivity by linear inverse estimation and directed transfer function: simulations and application to real data," *Clinical Neurophysiology*, vol. 116, no. 4, pp. 920–932, apr 2005.

[200] K. Hoechstetter, H. Bornfleth, D. Weckesser, N. Ille, P. Berg, and M. Scherg, "Besa source coherence: a new method to study cortical oscillatory coupling," *Brain topography*, vol. 16, no. 4, pp. 233–238, 2004.

[201] M. J. Brookes, J. R. Hale, J. M. Zumer, C. M. Stevenson, S. T. Francis, G. R. Barnes, J. P. Owen, P. G. Morris, and S. S. Nagarajan, "Measuring functional connectivity using MEG: Methodology and comparison with fcMRI," *NeuroImage*, vol. 56, no. 3, pp. 1082–1104, jun 2011.

[202] M. S. Hämäläinen and R. J. Ilmoniemi, "Interpreting magnetic fields of the brain: minimum norm estimates," *Medical & Biological Engineering & Computing*, vol. 32, no. 1, pp. 35–42, jan 1994.

[203] R. P. Marqui, C. M. Michel, and D. Lehmann, "Low-resolution electromagnetic tomography-a new method for localizing electrical activity in the brain," *International Journal of psychophysiology*, vol. 18, pp. 49–65, 1994.

[204] S. Haufe, V. V. Nikulin, A. Ziehe, K.-R. Müller, and G. Nolte, "Combining sparsity and rotational invariance in EEG/MEG source reconstruction," *NeuroImage*, vol. 42, no. 2, pp. 726–738, aug 2008.

[205] J. P. Owen, D. P. Wipf, H. T. Attias, K. Sekihara, and S. S. Nagarajan, "Performance evaluation of the Champagne source reconstruction algorithm on simulated and real M/EEG data," *Neuroimage*, vol. 60, no. 1, pp. 305–323, 2012.

[206] S. Castaño-Candamil, J. Höhne, J.-D. Martínez-Vargas, X.-W. An, G. Castellanos-Domínguez, and S. Haufe, "Solving the EEG inverse problem based on space–time–frequency structured sparsity constraints," *NeuroImage*, vol. 118, pp. 598–612, sep 2015.

[207] V. Veen, B. D., V. Drongelen, Y. W., M., and A. Suzuki, "Localization of brain electrical activity via linearly constrained minimum variance spatial filtering," *IEEE Transactions on biomedical engineering*, vol. 44, no. 9, pp. 867–880, 1997.

[208] A. Ewald, L. Marzetti, F. Zappasodi, F. C. Meinecke, and G. Nolte, "Estimating true brain connectivity from EEG/MEG data invariant to linear and static transformations in sensor space," *Neuroimage*, vol. 60, no. 1, pp. 476–488, 2012.

[209] F. Chella, L. Marzetti, V. Pizzella, F. Zappasodi, and G. Nolte, "Third order spectral analysis robust to mixing artifacts for mapping cross-frequency interactions in EEG/MEG," *NeuroImage*, vol. 91, pp. 146–161, may 2014.

[210] F. Shahbazi, A. Ewald, and G. Nolte, "Self-Consistent MUSIC: An approach to the localization of true brain interactions from EEG/MEG data," *NeuroImage*, vol. 112, pp. 299–309, 2015.

[211] L. Astolfi, F. Cincotti, D. Mattia, M. Marciani, L. Baccala, F. Fallani, S. Salinari, M. Ursino, M. Zavaglia, and F. Babiloni, "Assessing cortical functional connectivity by partial directed coherence: simulations and application to real data," *IEEE Transactions on Biomedical Engineering*, vol. 53, no. 9, pp. 1802–1812, sep 2006.

[212] M. J. Brookes, M. W. Woolrich, and G. R. Barnes, "Measuring functional connectivity in MEG: a multivariate approach insensitive to linear source leakage," *Neuroimage*, vol. 63, no. 2, pp. 910–920, 2012.

[213] T. Sasaki, M. Abe, E. Okumura, T. Okada, K. Kondo, K. Sekihara, W. Ide, and H. Kamada, "Disturbed resting functional inter-hemispherical connectivity of the ventral at-

tentional network in alpha band is associated with unilateral spatial neglect," *PLoS ONE*, vol. 8, no. 9, p. e73416, sep 2013.

[214] P. van Mierlo, M. Papadopoulou, E. Carrette, P. Boon, S. Vandenberghe, K. Vonck, and D. Marinazzo, "Functional brain connectivity from EEG in epilepsy: Seizure prediction and epileptogenic focus localization," *Progress in Neurobiology*, vol. 121, pp. 19–35, oct 2014.

[215] P. Barttfeld, A. Petroni, S. Báez, H. Urquina, M. Sigman, M. Cetkovich, T. Torralva, F. Torrente, A. Lischinsky, X. Castellanos, F. Manes, and A. Ibañez, "Functional connectivity and temporal variability of brain connections in adults with attention deficit/hyperactivity disorder and bipolar disorder," *Neuropsychobiology*, vol. 69, no. 2, pp. 65–75, 2014.

[216] R. K. Otnes, *Digital time series analysis*. John Wiley & Sons, ISBN: 0-471-65719-0, 1972.

[217] C. E. Shannon and W. Weaver, *The Mathematical Theory of Communication*. Urbana, IL: The University of Illinois Press, 1949.

[218] T. Kispersky, G. J. Gutierrez, and E. Marder, "Functional connectivity in a rhythmic inhibitory circuit using granger causality," *Neural Systems & Circuits*, vol. 1, no. 1, may 2011.

[219] Y. Liu and S. Aviyente, "Quantification of effective connectivity in the brain using a measure of directed information," *Computational and Mathematical Methods in Medicine*, vol. 2012, pp. 1–16, 2012.

[220] L. Bihan, M. D., J. F., C. Poupon, C. A. Clark, S. Pappata, N. Molko, and H. Chabriat, "Diffusion tensor imaging: concepts and applications," *Journal of Magnetic Resonance Imaging: An Official Journal of the International Society for Magnetic Resonance in Medicine*, vol. 13, no. 4, pp. 534–546, 2001.

[221] V. J. Wedeen, R. P. Wang, J. D. Schmahmann, T. Benner, W. Y. I. Tseng, G. Dai, D. N. Pandya, P. Hagmann, H. D'Arceuil, and A. J. de Crespigny, "Diffusion spectrum magnetic resonance imaging (DSI) tractography of crossing fibers," *Neuroimage*, vol. 41, no. 4, pp. 1267–1277, 2008.

[222] V. L. Towle, J. D. Hunter, J. C. Edgar, S. A. Chkhenkeli, M. C. Castelle, D. M. Frim, M. Kohrman, and K. E. Hecox, "Frequency domain analysis of human subdural recordings," *Journal of Clinical Neurophysiology*, vol. 24, no. 2, pp. 205–213, 2007.

[223] J. Cabral, M. L. Kringelbach, and G. Deco, "Exploring the network dynamics underlying brain activity during rest," *Progress in Neurobiology*, vol. 114, pp. 102–131, mar 2014.

[224] B. Horwitz, "The elusive concept of brain connectivity," *Neuroimage*, vol. 19, no. 2, pp. 466–470, 2003.

[225] C. C. French and J. G. Beaumont, "A critical review of EEG coherence studies of hemisphere function," *International Journal of Psychophysiology*, vol. 1, no. 3, pp. 241–254, 1984.

[226] L. G. Domínguez, J. Stieben, J. L. P. Velázquez, and S. Shanker, "The imaginary part of coherency in autism: Differences in cortical functional connectivity in preschool children," *PLoS ONE*, vol. 8, no. 10, p. e75941, oct 2013.

[227] F. Hohlefeld, C. Huchzermeyer, J. Huebl, G.-H. Schneider, G. Nolte, C. Brücke, T. Schönecker, A. Kühn, G. Curio, and V. Nikulin, "Functional and effective connectivity in subthalamic local field potential recordings of patients with parkinson's disease," *Neuroscience*, vol. 250, pp. 320–332, oct 2013.

[228] A. Schlögl and G. Supp, "Analyzing event-related EEG data with multivariate autoregressive parameters," in *Progress in Brain Research*. Elsevier, 2006, pp. 135–147.

[229] M. Kaminski and H. Liang, "Causal influence: Advances in neurosignal analysis," *Critical Reviews in Biomedical Engineering*, vol. 33, no. 4, pp. 347–430, 2005.

[230] H. Akaike, "A new look at the statistical model identification," *IEEE Transactions on Automatic Control*, vol. 19, no. 6, pp. 716–723, dec 1974.

[231] G. Schwarz, "Estimating the dimension of a model," *The Annals of Statistics*, vol. 6, no. 2, pp. 461–464, mar 1978.

[232] R. Oostenveld, P. Fries, E. Maris, and J.-M. Schoffelen, "FieldTrip: Open source software for advanced analysis of MEG, EEG, and invasive electrophysiological data," *Computational Intelligence and Neuroscience*, vol. 2011, pp. 1–9, 2011.

[233] J. Dauwels, F. Vialatte, T. Weber, T. Musha, and A. Cichocki, "Quantifying statistical interdependence by message passing on graphs—part II: Multidimensional point processes," *Neural Computation*, vol. 21, no. 8, pp. 2203–2268, aug 2009.

[234] D. Castle, S. Wessely, G. Der, and R. M. Murray, "The incidence of operationally defined schizophrenia in camberwell, 1965–84," *British Journal of Psychiatry*, vol. 159, no. 6, pp. 790–794, dec 1991.

[235] R. Q. Quiroga, A. Kraskov, T. Kreuz, and P. Grassberger, "Performance of different synchronization measures in real data: A case study on electroencephalographic signals," *Physical Review E*, vol. 65, no. 4, mar 2002.

List of Publications

Journal Papers

1. Veeramalla, S.K. and Talari, V.H.R. (2020), Neural source localization using particle filter with optimal proportional set resampling. **ETRI Journal**, 42, pp. 932-942. Available at: http://dx.doi.org/10.4218/etrij.2019-0020.

2. Santhosh Kumar Veeramalla, Hanumantha Rao T.V.K. (2020), Assessment of Directional Connectivity Between Neural Sources Using Effective Connectivity Measures and Particle Filters. **Journal of Circuits, Systems, and Computers**,0(0),pp.2150149. Available at: https://doi.org/10.1142/S0218126621501498.

3. Veeramalla, S.K. and Talari, V.K.H.R. (2020), Multiple dipole source localization of EEG measurements using particle filter with partial stratified resampling. **Biomedical Engineering Letters**, 10(2), pp.205–215. Available at: http://dx.doi.org/10.1007/s13534-020-00149-6.

4. Veeramalla, S.K. and Talari, V.H.R. (2019), Estimation of Neural Sources from EEG Measurements Using Sequential Monte Carlo Method. **Ingénierie des systèmes d information**, 24(4), pp.411–417. Available at: http://dx.doi.org/10.18280/isi.240408.

5. Veeramalla, S.K. and Talari, V.H.R. (2019), Resampling schemes within a particle filter framework for brain source localization, **International Journal of Biomedical Engineering and Technology**, (In press).

Conferences Papers

1. Kumar, V. Santhosh, and TVK Hanumantha Rao. (2016) Resampling schemes for Rao-Blackwellization Particle Filters. In *2016 International Conference on Computing, Analytics and Security Trends (CAST)*, pp. 377-382, IEEE, Pune.

2. Kumar, V. Santhosh, and TVK Hanumantha Rao. (2017) Functional Brain Connectivity analysis using Coherent Measures. In *EMBEC & NBC 2017, Finland*, IFMBE Proceedings, pp. 779-782. Springer, Singapore.

Book Chapter

1. Kumar, V. Santhosh, and TVK Hanumantha Rao. "Neural Source Connectivity Estimation Using Particle Filter And Granger Causality Methods." In Handbook of Artificial Intelligence in Biomedical Engineering, Apple academic press by CRC press, (In Production, March-2021). www.appleacademicpress.com/handbook-of-artificial-intelligence-in-biomedical-engineering-/9781771889209